Check for updates

ADVANCED MATERIALS TECHNOLOGIES
www.advmattechnol.de

Research and Development on Coatings and Paints for Geothermal Environments: A Review

Francesco Fanicchia and Sigrún Nanna Karlsdottir*

Geothermal power plants are complex systems, where the interplay between different metallic components transforms the enthalpy of hot brine in the form of electricity or usable heated water. The naturally occurring variety in brine chemistry, linked to the presence of specific key species, and its thermo-physical properties, leads to the development of different power plant configurations. Key species and power plant configuration in turn determine the extent of damage experienced by each component in the power plant: erosion, corrosion, and/or scaling, often acting combined. Paints and coatings, compared to changing the component alloy, have represented a preferred solution to mitigate these issues due to advantages in terms of costs and repairability. This is reflected in the large number of publications on research and development in this area within the past ≈50 years, with even an increasing trend in the past 10–20 years, indicating the strong interest to develop this clean and sustainable energy source. Therefore, in this work, the first of its kind after 1980, an in-depth review of all published work on research performed on paints and coatings for geothermal applications, subdivided by the material system, is provided.

1. Introduction

It is estimated that the amount of heat within 10 km of the earth's surface contains 50 000 more energy than all oil and gas resources worldwide.[1] Geothermal energy is the energy harnessed from this heat and can be used directly for heating or transformed into electricity. Due to its complete day- and year-round availability, geothermal power production can play a fundamental role in the mitigation strategy for climate change compared to other renewable energy sources such as solar and wind energy.[2] The potential for growth of geothermal energy is immense. However, according to the International Energy Agency (IEA), the technology is currently not on track with the Net Zero Emissions by 2050 Scenario, which requires a 13% annual increase in its power generation over the 2021–2030 period.[3] Clearly, the wide development of geothermal energy is currently prevented by some technological barriers which led, up to now, to its economical use only in a few regions with particularly favorable geological conditions, such as volcanically active areas.[4] Although the costs for geothermal electricity generation have decreased during the years, in fact, the development of geothermal energy is often hindered by the high capital costs (i.e., exploration, power plant and well construction, injection system, and capital costs) and operation and maintenance (O&M) costs (i.e., management labor, insurance, consumables and equipment) connected to the development of a geothermal power plant.[4–7] An in-depth economic analysis performed by Sanyal et al.,[5] on a range of 5 to 150 MW-sized geothermal power plants, provided an estimated minimum achievable power cost of 3.4¢ kWh^{-1}. According to the authors, this cost is most sensitive (in decreasing order of sensitivity) to unit O&M costs, unit capital costs, interest rate, and inflation rate. An independent report by the U.S. Energy Information Administration (EIA)[8] calculates, for a 50 MW binary cycle geothermal plant, total capital, and O&M costs at 2,521$ kW^{-1} and 128.54$ kW^{-1} $year^{-1}$, respectively. It is therefore clear that technological advances leading to the reduction in both capital and O&M costs would lower development barriers for the utilization of geothermal energy.

Material degradation, due to corrosion, erosion, and scaling phenomena, is one of the main contributors to the overall O&M costs for a geothermal power plant.[9–12] These material degradation phenomena are driven by the chemical, mechanical, and thermodynamic properties of the geothermal fluid, which can generate an extremely severe environment for the materials of the power plant components. A major effect of the degradation phenomena is either a reduced energy generation efficiency and/or a shorter component lifetime, leading in both cases to

F. Fanicchia
Surface Engineering and Precision Centre
School of Aerospace Transport and Manufacturing
Cranfield University
Bedford MK43 0AL, UK
E-mail: francesco.fanicchia@cranfield.ac.uk
S. N. Karlsdottir
Faculty of Industrial Engineering
Mechanical Engineering, and Computer Science
University of Iceland
Hjardarhagi 2-6, Reykjavík 107, Iceland

The ORCID identification number(s) for the author(s) of this article can be found under https://doi.org/10.1002/admt.202202031

© 2023 The Authors. Advanced Materials Technologies published by Wiley-VCH GmbH. This is an open access article under the terms of the Creative Commons Attribution License, which permits use, distribution and reproduction in any medium, provided the original work is properly cited.

DOI: 10.1002/admt.202202031

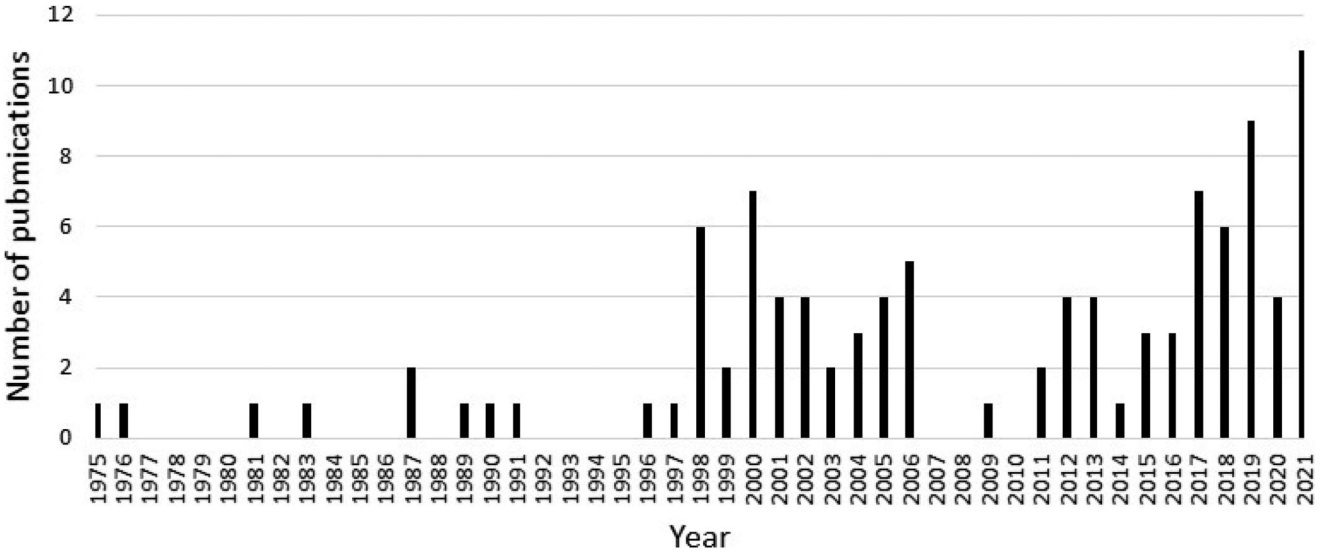


Figure 1. Breakdown of the 103 publications identified on coatings for geothermal applications per year (including peer-reviewed journal papers, conference transactions and reports), showing an increasing trend to date.

the need for maintenance on the affected components.[13] Due to the low cost and easy fabrication of carbon steel in the construction of geothermal power plants, it is commonly used despite its low resistance against corrosion. Due to this, maintenance is often needed quite frequently since geothermal power plants are expected to have long lifetime (>25–30 years). In the most aggressive geothermal environments corrosion-/erosion-resistant alloys such as stainless steel, titanium- and nickel-based alloys thus must be used as materials to increase the components' lifetime.[9] However, the selection of such resistant alloys has two major drawbacks: a) cost, translating into increased capital cost and b) the strong affinity to scale formation of the passive layer that forms on their surface after exposure to geothermal fluid.[14]

Significant reductions in both capital and O&M costs can instead be achieved by replacing some (or all) of the most expensive component materials with more economical ones coated with corrosion-, erosion, and scaling-resistant coatings.[15] In this way, together with a reduction in material cost, improved component lifetime and maintenance schedule can be achieved. The renewed interest of the research community about coatings for geothermal applications is confirmed by the significant number of published studies. However, to the authors' knowledge, the only comprehensive review available to date on coatings for geothermal applications is the work of Reeber,[16] published in the year 1980, who identified the main geothermal coating systems, both already used in production or still in the research phase, investigated up to that year. The value of the review is significant, especially considering the limited availability of published literature on the subject in those years. No other such review has been identified by the authors.

Therefore, to fill this literature gap, the aim of this review is to provide a comprehensive overview of the published work performed on the topic of coatings for geothermal energy production. An in-depth literature review on the subject has highlighted a total of 103 accessible publications specifically focused on the testing and analysis of coatings and paints for geothermal applications (including peer-reviewed journal papers, conference transactions, and project reports) in a time span from 1975 to December 2021. The breakdown of these publications per year is presented in **Figure 1**.

Figure 1 clearly shows an increasing tendency in the years reported. It is worth noting that the publications identified here only include work aimed at developing coatings tested specifically in geothermal conditions, either simulated or in field tests. Although in fact coatings developed for other harsh environments (e.g., hydrothermal power resources, biomass power production, etc.) could also represent promising candidates to mitigate degradation in geothermal systems, these have not been included in this review. The lack of papers up to the late 1990 s is observed since a significant amount of research in this area was performed privately within industrial research programs, with the consequence that novel developments would not be made publicly available. A deviation from this trend is observed from the early 2000s, where the global trend for geothermal energy development has triggered an increase of public investment in technologies facilitating the development of this renewable energy source. The present review paper is broadly subdivided into two sections: a first theoretical overview of the material degradation phenomena linked to material interaction with geothermal fluid (Section 2) and the actual review on coatings for geothermal applications (Section 3).

2. Material Degradation in Geothermal Power Plants

The selection of a coating system for a specific component in the geothermal power plant depends on the degradation mechanism developed due to the interaction of the geothermal fluid and the material of which the components of the geothermal

© 2023 The Authors. Advanced Materials Technologies published by Wiley-VCH GmbH

Table 1. List of the main key species found in geothermal fluids which can cause corrosion, erosion, and scaling degradation mechanisms.

Species name	Chemical formula	Main effects in geothermal plants
Hydrogen ion	H^+	Determines the fluid pH level and thus corrosion potential.
Chloride ion[a)]	Cl^-	Accelerates corrosion (especially pitting or crevice in stainless steel).
Hydrogen Sulfide	H_2S	Promotes corrosion in steels, particularly hydrogen damage.
Carbon Dioxide	CO_2	Accelerates corrosion in steels
Ammonia	NH_3	Accelerates corrosion (especially in mild steels and copper alloys).
Sulfate ion	SO_4^{2-}	Generates very acidic fluids if in significant amount, thus highly corrosive.
Oxygen	O_2	Only present due to ingress of atmosphere and generally at low temperatures and pressures.Does not originate in geothermal fluid. Increases corrosion if present.
Silica	SiO_2	Generates silica scales.
Calcium ion	Ca^{++}	Generates calcium carbonate scales ($CaCO_3$).
Magnesium ion	Mg^{++}	Generates magnesium silicate ($MgSiO_3$) scales.
Metal ions	Fe^{++}, Zn^{++}, Cu^+, Pb^{++}	Generates metal silicate and sulfide deposits, which are very hard.

[a)] When dry steam containing HCl gas cools to its acid dew point, the solution becomes highly corrosive.

power plant are made of. The specific type and severity of the degradation mechanism depend on two main factors: a) geothermal fluid chemistry, dictated by the geographical area and thus specific geology of the geothermal reservoir, and b) power plant configuration (cycle type), e.g., direct steam, flash, double-flash, binary, etc., affecting variability in geothermal fluid flow and chemistry within a specific power generation cycle.

2.1. Geothermal Fluid Chemistry and Classification

2.1.1. Geothermal Fluid Chemistry

The term geothermal fluids refer to the fluids in the geothermal reservoir independent of the state and composition of the fluid (i.e. steam, liquid, gas). Depending on the reservoir temperature, geothermal fluids can be composed of a liquid phase with dissolved solids and gas or can be a mixture of liquid, steam, and gas. The chemistry of the geothermal fluid is the result of the equilibrium reached with the rocks/formation in the reservoir. Geothermal fluids thus generally contain numerous dissolved and/or free components such as minerals, salts, and gases.[6,9–12,17–19] Corrosion, scaling, and erosion (often combined), as later described, represent the three main degradation mechanisms in geothermal systems.[18] The occurrence of corrosion and scaling is directly related to the presence of specific "key species" within the fluid, while erosion is connected to the mechanical action of the geothermal fluid and hard particles in the fluid, traveling at high flow speed.[17,18] A list of the most common key species that have been identified in geothermal fluids, together with their main effects, is summarized in **Table 1**.

The presence of one or more key species within the geothermal fluid can vary greatly between geothermal fields. This reflects in variability of degradation mechanisms encountered in service. It is worth noting that, although not mentioned in the table, some of the solid particulates present in the fluid may also contribute to erosive wear. As this type of damage mechanism highly depends on the geometry of the component (e.g., pipe bends, elbows, etc.,) and the geothermal fluid flow rate, it is related to the specific power plant configuration rather than the fluid chemistry. For this reason, erosion wear damage is not captured in Table 1 but is discussed in the following sections of this work.

A summary of the species analyzed/used within the natural/simulated brines of 103 publications identified in this work is presented in **Figure 2**.

It is worth noting that the table is roughly subdivided into two, a first part (from As to Zn) listing ions and pure elements and a second part related to compounds (from $BaCl_2$ to *Thiobacillus Ferroxidans*). This is due to the different ways species were reported by different papers and on whether natural or simulated brines were used. Pure or ionic species are generally listed in papers using natural brines (from their analysis) while compounds are used when simulated brines were prepared. Oxidation states for pure metallic elements are not listed in those cases where multiple oxidation states were identified from different works. From the figure, the species in Table 1 are among the ones appearing most frequently, thus confirming the great concern of the scientific community over their negative effect on materials. It is worth noting that care must be taken in analyzing the data in the figure, and that the table in the Supplementary Information, together with the referenced papers, must be consulted for a statistically correct analysis. In fact, data in the figure only list species specifically analyzed or introduced in the testing brines, which might be misleading for some species. For instance, O_2 would be naturally present in all brines performed in open vessels, even though its presence is not often specified (e.g., in all electrochemical tests using only NaCl in solution); therefore the actual height of the O_2 bars is expected to be substantially higher than presented in the figure. Other effects are due to experimental reasons. For instance, NaCl is by far the most used species, likely due to its widespread use as standard in electrochemical corrosion measurement methods. H_2S instead, although its negative influence on corrosion mechanisms is well known, does not appear as often as expected, due to health and safety concerns within research labs.

© 2023 The Authors. Advanced Materials Technologies published by Wiley-VCH GmbH

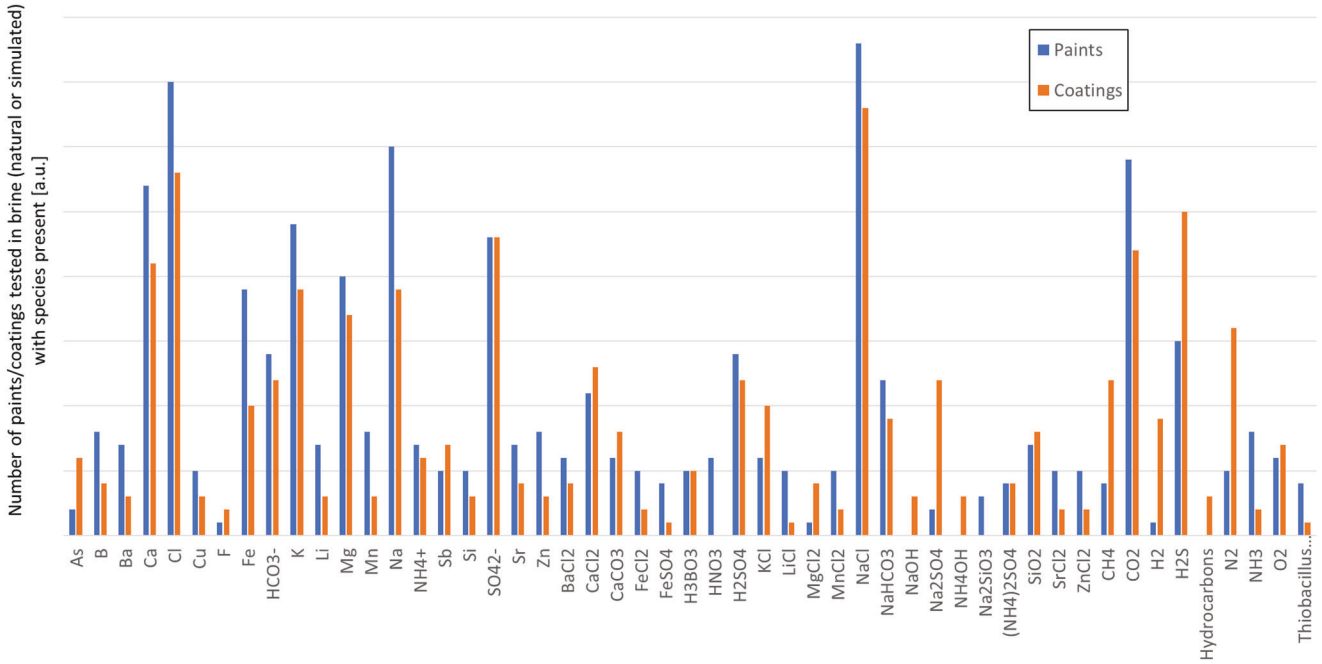


Figure 2. Number of paints and coatings tested in brine where a specific species was present, as summarized from 103 publications identified in this work. Only species appearing more than twice have been presented in the graph. A complete list of all the species can be found in the table in Supplementary Information.

2.1.2. Classification Methods for Geothermal Environments

Generic Classification: No specific standard is available to categorize geothermal environments. A classification of generic corrosive environments can however be found in standard EN ISO 12944-2 that deals with the definition of corrosive environments for corrosion protection by means of paint systems. The standard defines two classes of corrosive environments: "atmospheric corrosion," "corrosion in water/soil," and "special cases." Atmospheric corrosion is defined as corrosion with the earth's atmosphere (i.e., mixture of gases, aerosols, and particles surrounding a given object), at ambient temperature as the corrosive environment. In the standard, several categories of corrosivity are proposed, from C1 (very low) to CX (extreme) depending on the atmospheric humidity and chemistry. Corrosion in water and soil instead considers structures partly immersed in water or buried in soil where corrosion is therefore restricted to a small part of the structure. Special cases include environments where specific chemical species, high temperature, and mechanical stress act, also combined, to define the overall corrosion mechanism. The above classification could be broadly applied to geothermal power plants. The most severe instances of degradation in geothermal power plants are found in components in contact with the geothermal fluid (e.g., internal surface of pipelines, steam turbine components, etc.). These can involve enclosed atmospheres at elevated temperature, pressure, mechanical loads, and a variety of corrosive chemical species depending on the specific location within the plant cycle and location of the geothermal region. Atmospheric corrosion is instead relevant to the outside surface of components not experiencing high temperature, but in contact with the atmosphere. In this case, corrosion can be observed both in components enclosed within a building structure or exposed to the external atmosphere. Examples of components affected by atmospheric corrosion include cooling towers, electricity transmission lines, and transformers.[18]

Specific Geothermal Fluid Classification: Although not covered by any standard, attempts to classify the chemistry of geothermal fluids have been made by three main research studies.[6,10,20] In the classification by Ellis et al.,[6] geothermal fluids are ranked based on classes of a corrosivity index. The classification, based on samples from 45 geothermal sites from El Salvador, Iceland, Italy, Japan, Mexico, New Zealand, and the United States, assumes that the concentration of key species (Total Key Species (TKS), in ppm) defined as total chloride, sulfate, carbon dioxide species, sulfide species, and ammonia species, in the fluid determines its corrosion potential. The classes identified by the study are summarized in **Table 2**, where Corrosivity Class I leads to the highest corrosion rates (CR) of carbon steel and CR decreases with increasing number, except for Class VI where limited data were available.[5]

Another classification was proposed by Sanada et al.,[20,21] where chemical data from a range of deep and acidic geothermal wells was collated and organized with the scope of providing guidelines for corrosion control and materials selection. As a result, five main types of geothermal fluid were identified: 1) Near-neutral to alkaline pH fluid, 2) Acid sulfate (chloride) fluid, 3) acid chlorine (sulfate) fluid, 4) hypersaline fluids, and 5) superheated steam with high HCl concentrations. More recently, a comprehensive classification method has been proposed in the work of Nogara et al.[10] Their proposed harmonized corrosivity classification aims at incorporating knowledge from previous classifications and more recent geothermal fluid analyses to provide a more comprehensive classification framework (**Table 3**).

© 2023 The Authors. Advanced Materials Technologies published by Wiley-VCH GmbH

Table 2. Summary of geothermal resource corrosion classification as proposed by Ellis et al.[6]

Corrosivity Class	Total Key Species (TKS) [ppm]	Resource type [liquid/vapor]	pH (un-flashed)	pH (flashed)	Plant inlet temperature [°C]
I	>100 000 (mainly Cl^-)	Liquid	5–6	>6	>199
II	1000–10 000	Liquid	<4.5	<4.5	120–177
III	10 000–20 000	Liquid	5–6	>6	149–191
IV	500–10 000	Liquid	≥5	>7	121–199
V	<5000	Liquid	>6.5	n/a	50–105
VI	<5 wt.% (NCG)	Vapour	n/a	n/a	160–180

It is worth noting that, compared to previous works, the classification in Table 3 now contains several sub-classes: II-A and II-B for liquid-dominated acid fluids (acid sulfate (chloride) and acid chloride (sulfate), respectively) and VI-A, B, and C for vapor-dominated steams (without traces of HCl (VI-A), and with HCl (VI-B and C)).

The above classifications suggest that degradation mechanisms of materials in contact with the geothermal fluid can vary based on the specific chemistry of the geothermal reservoir. In a power plant however, the properties of the geothermal fluid exiting the wellbore will show significant variation in process parameters such as temperature, pressure, and flow rate depending on the thermodynamic cycle used to produce power. This of course effects the potential degradation mechanism, including erosive wear mechanisms related to geothermal fluid flow and specific components geometrical configuration. These variations are characteristic of the specific power plant configuration.

2.2. Power Plant Configuration

The chemical and flow properties of the geothermal fluid as it is drawn from the wellbore varies considerably within the geothermal energy production cycle. Consequently, the specific type of damage mechanism varies according to the specific location within the power generation cycle. Geothermal power plants can be subdivided into three main groups[22,23]: "steam" (including dry-steam, single-flash, and double-flash, **Figure 3**a–c), "binary" (Figure 3d), and "hybrid cycles." Steam cycles are generally employed for wells with higher enthalpies while binary cycles are used for lower enthalpies wells, whereas hybrid systems represent a custom-built combination of the first two. In the steam cycles, either direct steam from the reservoir (dry steam) or steam from boiled geothermal fluid is expanded through a turbine, thus generating electrical power. In binary cycles, instead, the thermal energy from the geothermal fluid is employed to evaporate a secondary working fluid; it is this latter then, and not the geothermal fluid that expands through the turbine to generate power.

The "dry steam" configuration is depicted in Figure 3a. This configuration is mainly used in reservoirs where vapor (or dry steam) represents the main phase.[24] The steam from the production well (PW), transported via steam pipelines (SP), is then used directly to drive the turbine/generator (T/G). Exhaust steam from the turbine is then condensed by means of ad-hoc condensers (C) and cooling towers (CT). The excess of condensate, usually available at the end of the cycle, is generally re-injected into the reservoir at the injection wells (IW). The steam from the production wells generally carries particulates (e.g., minerals) and moisture for which, between the wellhead valve (WV) and

Table 3. Harmonized geothermal corrosivity classification, as proposed by Nogara et al.[10]

Class	Resource type [Liquid (L)/Vapor (V)]	Total Key Species (TKS) [ppm]	Chloride fraction in TKS [%]	pH (un-flashed/flashed)	Volume of gas in steam [%]	Plant inlet temperature [°C]	$CaCO_3$ content [ppm]
I[a)]	Liquid	>100 000	99	<5/5–6	<2.5	199	–
II-A[b)]	Liquid	1000–60 000	15–99	>3/<5	Not established	Not established	–
II-B[c)]	Liquid	500–40 000	20–99	<3	Not established	Not established	–
III[d)]	Liquid	10 000–20 000	45–99	5–6/>6	Not established	149–191	–
IV[e)]	Liquid	500–10 000	45–99	≥5/>6	<2.5	121–199	–
V-A[f)]	Liquid	<5000	3–72	6.7–7.6/n.a.	n.a.	49–96	207–1239
V-B[g)]	Liquid	<5000	3–72	7.8–9.85/n.a.	n.a.	120–205	<210
VI-A[h)]	Vapour	<1	–	n.a.	<5	177–250	–
VI-B[i)]	Vapour	–	–	–	–	–	–
VI-C[j)]	Vapour	–	–	–	–	–	–

[a)] Salton Sea (USA); [b)] acid sulfate (chloride) – 4 sites (Philippines), 5 sites (Japan), Miravalles (Costa Rica), Soultz-sous-Forets (France), Tatun (Taiwan); [c)] acid chlorine (sulfate) – Pinatubo (Philippines), Alto Peak (Philippines), 3 sites (Japan), Miravalles (Costa Rica), Lahendong (Indonesia), Los Humeros H4 (Mexico); [d)] Cerro Prieto (Mexico), East Mesa (USA); [e)] Ahuachapan (El Salvador), HTA (Iceland), Hatchobaru (Japan), Otake (Japan), Broadlands (New Zealand), Wairakei (New Zealand), Baca (USA), Heber (USA), Brady (USA), Raft River (USA); [f)] Madison Aquifer (USA), Pagosa Spring (USA), Marlin (USA); [g)] 15 sites (Iceland), Klamath Falls (USA); [h)] 10 sites (Italy), The Geysers (USA), Kamojang (Indonesia); [i)] (High NCG concentration) – Kizildere (Turkey); [j)] (HCL gas production) – Krafla-IDDP1 (Iceland), The Geysers (USA).

© 2023 The Authors. Advanced Materials Technologies published by Wiley-VCH GmbH

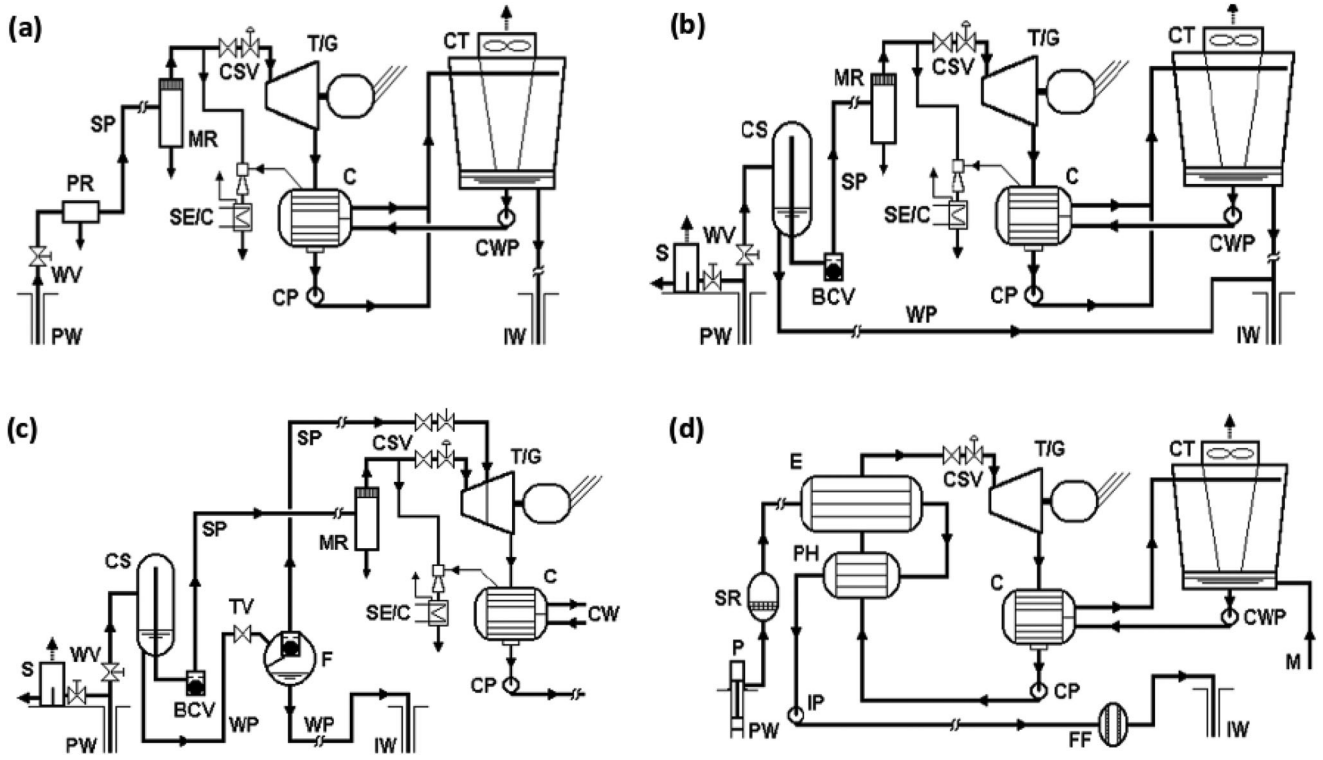


Figure 3. Schematics of geothermal power plant configurations: a) dry steam, b) single-flash, c) double-flash, and d) binary. In the figure: BCV (ball check valve), CP (condensate pump), CSV (control and stop valve), CW (cooling water), E (evaporator), FF (final filter), IW (injection wells), MR (moisture remover), PH (preheater), R (recuperator), SE/C (steam ejector/condenser), SP (steam piping), T/G (turbine/generator), WP (water piping), C (condenser), CS (cyclone separator), CT (cooling tower), CWP (cooling water pump), F (flasher), IP (injection pump), M (make-up water), P (well pump), PR (separator), PW (production wells), S (silencer), SH (superheater), SR (sand remover), TV (throttle valve), WV (wellhead valve). Reproduced with permission.[23] Copyright 2011, Geo-Heat Digital Library, Oregon Institute of Technology Library. Klamath Falls, Oregon.

the turbine, several particulate removal systems are placed (e.g., separators, (PR)) together with moisture removal systems (MR). Moreover, due to the common presence of non-condensable gases (NCG) within the steam, steam ejectors with pre-and after-condenser systems (SE/C) are generally used. The "single-flash" configuration is depicted in Figure 3b. This represents the most common type of geothermal power plant as most reservoirs are liquid-dominated.[24] In this case, the steam necessary to drive the turbine/generator is separated from the liquid geothermal fluid by a rapid evaporation (i.e., flash). This latter operation is performed by the cyclone separator (CS). The separated brine from the cyclone separator is generally re-injected within the reservoir, carried via a water piping system, (WP). Ball check valve (BCV) and moisture removal systems are placed after the cyclone separator to insure against any possible slug entering the steam line. The after-turbine system in this type of plant essentially mirrors the one for the dry-steam one. The "double-flash" configuration is depicted in Figure 3c. The cycle is fundamentally like the single-flash plant, with the exception that the brine obtained from the cyclone separator is not directly re-injected back into the reservoir but withstands further flashing within a second flasher (F). The low-pressure steam ejected from the secondary brine is then fed either into a separate low-pressure turbine or to a separate stage of the main turbine. The re-usage of the primary brine generally allows for 20–25% more power to be generated as compared to single-flash plants.[24]

Within "binary" configurations (Figure 3d), the geothermal fluid is not directly employed to rotate the turbine, but its thermal energy is transferred instead, via a heat exchanger, to a secondary working fluid. The working fluid can be a mixture of hydrocarbons (e.g., isopentane and isobutene) or water and ammonia. The geothermal fluid is generally maintained in the liquid state throughout the cycle, maintained below its flash level by down-hole pumps (P) to raise its pressure. The working fluid steam required to rotate the turbine is generated at the evaporator (E) as opposed to the cyclone separator typical of flash plants. A pre-heater (PH) is also present prior to the evaporator to provide the working fluid with additional thermal energy, possibly still available from the geothermal fluid. The preheater-evaporator ensemble is generally referred to as a heat exchanger. Finally, *hybrid* systems (not depicted in Figure 3), are composed of combinations of the above-described four basic systems. In fact, a hybrid plant is designed to achieve an optimized efficiency to suit the specific set of working conditions experienced by the plant site (in terms of pressure, temperature, NCGs, dissolved solids, pH, scaling. and corrosion potential). Examples of this type of plant are dry-steam/binary,[25] single-flash/binary,[25] single-/double-flash,[26,27] and hybrid fossil-geothermal systems.[28] Additionally, geothermal combined heat and power (GCHP) plants exists (e.g., additions to single and double flash) which include additionally heat exchangers to the systems to heat up cold water with the geothermal fluid (liquid) from the separators. The heated water

© 2023 The Authors. Advanced Materials Technologies published by Wiley-VCH GmbH

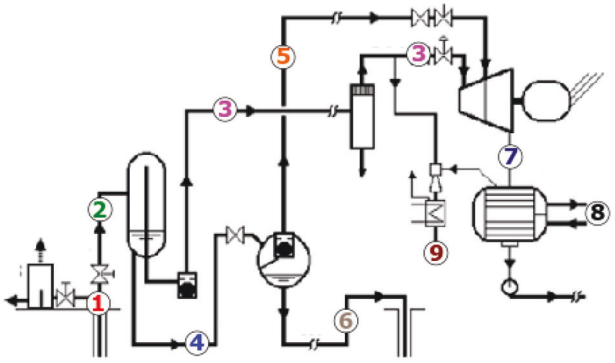


Figure 4. The schematic diagram of the double-flash power plant configuration from Figure 3c[23] adapted with areas of significant geothermal fluid properties variation highlighted with numbers. These properties are reported, for a class III fluid (according to the classification in Table 3), in Table 4. Reproduced with permission.[23] Copyright 2011, Geo-Heat Digital Library, Oregon Institute of Technology Library. Klamath Falls, Oregon.

can then be used e.g., in district heating systems to make more efficient use of the geothermal resource and improving the economics of the system. Further description of these complex systems is beyond the scope of this review and will thus not be further described.

Irrespective of the configuration, the above analysis demonstrates that the geothermal fluid originally drawn off the production well is subject to variations in both chemistry and thermodynamic properties during the energy production cycle. To quantify this variation, we refer to a detailed analysis performed as part of the Horizon 2020 collaborative project Geo-Coat.[29] **Figure 4** from the work shows a schematic diagram of a generic double-flash power plant configuration of Figure 3c where different areas have been numbered.

These areas represent regions where significant changes in the properties of the geothermal fluid are measured. This configuration was selected in this review as single- and double-flash configurations which give the highest share distribution in terms of installed capacity.[30] Considering the Hellisheiði geothermal power plant in Iceland, which has a class III geothermal fluid (from Table 3) at the plant inlet, a variation in the geothermal fluid properties corresponding to the numbered areas in Figure 4, is given in **Table 4**, together with the corresponding degradation mechanisms and affected components.

In Table 4, the term Corrosion (C) includes all possible forms of corrosion observed in geothermal energy production (uniform corrosion, stress corrosion cracking, etc.) which will be described in detail in Chapter 2.3. Moreover, Erosion-Corrosion (EC) is here considered to include all the mechanisms from pure erosion to corrosion accelerated by erosive damage. The analysis in the table clearly highlights the effect of the variation in geothermal fluid properties in the degradation mechanisms. For instance, it is known that scaling (S) and Erosion-Corrosion (EC) are damage mechanisms typical of steam turbine components. This corresponds in the transition from area 3 to 7 in Figure 4 and Table 4. An analysis of the geothermal fluid in these two areas shows that a decrease in all thermodynamic properties occurs in the transition. Consequently, condensation of the inlet steam will occur, leading to the formation of liquid droplets acting as an erosive medium. Moreover, since the solubility of silica (SiO_2) is proportional to the fluid temperature, a decrease in fluid temperature leads to the precipitation of silica and the growth of silica scales in the region. Further analysis of the degradation mechanisms and the relationship to the properties of the geothermal fluid is required before an informed decision is made on appropriate coating material selection for different components used in geothermal power production.

2.3. Degradation Mechanisms

Depending on the power plant configuration, the class of geothermal fluid, and its interaction with the component materials, several degradation mechanisms can be experienced. The most common ones identified to date, have been summarized in **Table 5** and subdivided between corrosion and mineral precipitation;[31,9,10] however, a different classification could have been used instead.

It is worth noting that, although the classes of degradation have been clearly separated in the table, they normally act combined in-service conditions, such as the combined effect of scaling and erosion-corrosion in turbine components, i.e., due to

Table 4. Geothermal fluid properties for the Hellisheiði geothermal power plant, assumed in the generic double-flash power plant configuration in Figure 4.

Area	State (liquid, steam, 2-phase)	Pressure [high/low]	Temperature [°C]	pH	Bulk velocity [high/low]	NCG concentration [high/low]	Degradation mechanism[a)]	Equipment affected[b)]
1	Liquid/2-phase	high	160–200	5–8	High	High	S, EC, C	P, SC, V
2	2-Phase	high	160–200	5–8	High	High	EC, S	PS, VS, HX
3	Steam	high	155–200	n/a	n/a	High	C, EC, S	PS, T
4	Liquid	n/a	100–155	5–6	Low	Low	EC, C	PS
5	Steam	low	100–130	>6	n/a	Low	C	PS, V
6	Liquid	low	100–130	>6	n/a	Low	S, C	P, PS,
7	Steam/2-phase	low	30–130	<6	Low	High	C	PS
8	Liquid/2-phase	low	30–60	<6	Low	High	S	SN
9	Steam	low	30–60	n/a	Low	High	n/k	PS

[a)] Degradation mechanisms – Corrosion(C); Scaling (S), Erosion-Corrosion (EC); [b)] Equipment affected – Pump (P), Surface casing (SC), Valves (V), Pipelines (PS), vessel (VS) Heat exchanger tube (HX), Turbine (T), spray nozzles (SN).

© 2023 The Authors. Advanced Materials Technologies published by Wiley-VCH GmbH

Table 5. Common degradation mechanisms experienced in geothermal systems.[9,10,31]

Type	Description	Sub-types	Affected materials (Metals, Inorganic, Organic)[a]	Affected components
Corrosion				
General	Uniform thinning of the whole exposed surface	Uniform corrosion	Metals	Casing, fluid transportation pipe
		Galvanic corrosion	Metals	Air conditioning unit coil, production well casing, weld area
		Microbiologically induced corrosion[c]	Metals, Inorganic	Cooling tower, condenser
		Polymer degradation	Polymers	Bearings, protective coatings
Localized	Rapid penetration/dissolution of metal at specific sites	Pitting corrosion	Metals	Heat exchanger, bellow absorber, reinjection well
		Crevice corrosion	Metals	Heat exchanger
Mechanically assisted	Attack enhanced by mechanical load	Erosion-corrosion[b]	Metals, Inorganic, Organic	Pipe bend, turbine
		Corrosion Fatigue	Metals	Pipe, turbine
Environmentally induced cracking	Corrosion-induced cracking	Stress Corrosion Cracking	Metals	Drill string, casing, turbine, steam transportation pipe, heat exchangers
		Hydrogen Embrittlement (Hydrogen Induced Cracking (HIC), Sulfide Stress Corrosion Cracking (SSC))	Metals	Steam transportation pipe, well liner, control board, mist/droplet eliminator
Metallurgically influenced	Preferential attack of specific phases or grain boundaries due to elemental segregation	Intergranular corrosion	Metals	Casing, fluid transportation pipe
		Dealloying	Metals	Solder
Mineral precipitation				
Scaling	Precipitation of dissolved minerals	Silica (SiO_2)	All materials	Production/reinjection well, steam/water pipe, separator, turbine
		Silicates (Fe, Mg)		
		Carbonate ($CaCO_3$)		
		Metal Sulfides (mainly Zn and Fe)		

[a] In this context, inorganic systems relate to concrete used in geothermal cooling towers and organic systems to polymeric coatings; [b] Includes any degradation mechanism between pure erosion and erosion-enhanced corrosion. Thus, also non-metallic systems are included under this category in cases of pure erosion degradation type; [c] Microbial corrosion has been here considered under the uniform corrosion type, however, forms of localized microbial corrosion are also possible.

the precipitation of silica and formation of water droplets in the lower pressure side of the turbine.

Although a clear distinction has been made among the above degradation mechanisms, these are often found acting combined in-service. This is revealed by the results in **Figure 5**, a summary of a recent survey performed as part of the Horizon 2020 project Geo-Coat on 12 power plant operators from different geological regions worldwide.[32] The survey was part of a comprehensive failure mode and effect analysis (FMEA), and the result presents a list of the critical components, principal degradation mechanisms, and the effect on the component operational behavior.

In the following, a description of the degradation mechanisms in Table 5 is provided.

2.3.1. Corrosion

Metal corrosion is a naturally occurring phenomenon where the material deteriorates due to a chemical or electrochemical reaction with its environment.[33] Irrespective of the type of corrosion (i.e., uniform, localized, etc.), a metal that is corroding is characterized by both anodic and cathodic sites, where

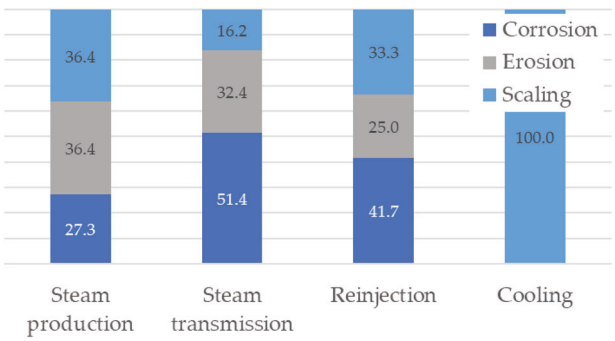


Figure 5. Probability (%) of occurrence of corrosion, erosion, and scaling mechanisms in the main four systems of a geothermal power plant, obtained as a summary of the table in ref. [32], where critical components, principal damage mechanisms and their effects compiled from FMEA analysis from 12 different geothermal power plants were analyzed.

© 2023 The Authors. Advanced Materials Technologies published by Wiley-VCH GmbH

oxidation (i.e., loss of electrons) and reduction (i.e., gain of electrons) reactions take place respectively.[34] It is the nature of the anodic and cathodic sites, together with the additional presence of environmental factors (e.g., load) that defines the type of corrosion as listed in Table 5. Irrespective of the corrosion type, because of metal oxidation, all reactions produce corrosion products at the anodic sites, such as oxides, hydroxides, carbonates, etc. It is important to differentiate between corrosion products and the films that form due to a drop in solubility of mineral species dissolved in the aqueous medium. The latter process is referred to as *scaling* within the geothermal community. These products can be porous and loosely adhered to the surface, dense and tightly and adhered to the surface, soluble or insoluble in the electrolyte (i.e., the geothermal fluid). Therefore, depending on the nature of the corrosion product, corrosion can be classified as either active (soluble corrosion products) or passive (insoluble corrosion products).[9]

General Corrosion: General corrosion is active when the geothermal fluid has access to the entire metal surface. The resulting mechanism is a uniform loss of metal, which can be therefore quantified in mm per year. This form of corrosion is preferred to localized types (e.g., pitting) as it is predictable and thus acceptable for design through corrosion allowances.[35]

The uniform corrosion sub-type is defined as general corrosion where the metal degrading is not in contact with other metals of different corrosion potential or the corrosion mechanism itself is not enhanced by microbial activity.[36] If these latter phenomena are active, general corrosion is then defined as either galvanic corrosion or microbiologically induced corrosion respectively. *Galvanic corrosion* occurs when two dissimilar metals are in contact in aqueous environment.[34,37] Due to the difference in corrosion potential between the metals, a potential difference is generated which creates a current between the components. Due to oxygen diffusion generally being the rate-determining factor in aqueous corrosion, large ratios of cathode area to anode area will generally correspond to galvanic attack of higher intensity.

"Microbiologically induced corrosion" is defined as material deterioration affected by the presence and/or activity of microorganisms.[38] The bacteria provide this corrosive action by two main means: a) their adsorption onto the material surface with formation of biofilms accelerating electrochemical reactions and b) formation of acidic species such as sulfuric and nitric acid. Although this category of corrosion has here been considered under the general type of corrosion, localized attack (e.g., pitting) has also been detected in geothermal systems. This type of corrosion is common in geothermal condensers and cooling towers.[39]

"Polymer degradation," unlike other forms of corrosion described here, describes the change in properties of polymer systems under the influence of environmental factors. In geothermal systems, this mechanism has been observed in the form of hydrothermal oxidation in fluoroelastomer bearings[40,41] and protective paints.[42,14] Degradation is in this case due to the attack of oxygen to the primary polymer chain structure, with consequent formation of components of lower molecular weight, acting as sites for cracks initiation/propagation.

Localized Corrosion: Unlike general corrosion, localized corrosion can be described as the degradation of a small portion of the material at a significantly higher rate than the rest of the surface.[34] Due to its localized nature, this form of corrosion is difficult to detect and is therefore less desirable than uniform corrosion. Two sub-types of this category have been proposed: pitting and crevice corrosion.

"Pitting" corrosion is associated with the breakdown of a passive film that forms on the metal surface. Alloys such as stainless steels, Ni-alloys, and titanium are therefore more susceptible to this type of corrosion.[43] The specific pit nucleation site is determined by a combination of factors: a) discontinuities in the passive film (e.g., at screw dislocations, slip planes, etc.), b) material-specific metallurgical defects (e.g., grain boundaries, intermetallics, etc.), and c) external factors, such as localized settlement of deposits. This type of localized corrosion is enhanced by the presence of aggressive ions such as Cl^- or SO_4^- and low pH environments. The driving force for "crevice" corrosion is instead differential aeration, i.e., where some form or restricted access to oxygen occurs.[34,44,45] Due to this restricted access, small differences in potential are generated, resulting in high concentrations of anions. Forms of restricted areas can be generated, in geothermal environments, by scale deposits, mill scales, or crevices under bolts or rivet heads.

Mechanically Assisted Corrosion: Mechanically assisted corrosion can be defined as corrosion processes accelerated by the action of mechanical load. If the mechanical load is of erosive nature, the phenomenon is termed erosion-corrosion, while corrosion fatigue is used when a cyclic stress is operational. In passivating systems, mechanically assisted corrosion processes are thought to cause rupture of the protective passive film, thus accelerating corrosion. In erosion-corrosion, the corrosion phenomenon is accelerated by the relative motion between corrosive media and metallic surface.[46] The corrosive media can be either a fluid (often carrying suspended solid particles and/or bubbles), steam, or a combination of the two. This relative motion accelerates the corrosion mechanisms by continuously removing passive film or corrosion products, thus exposing fresh surface to the corrosive medium. Hence, the rate of erosion-corrosion is accelerated in areas of increased flow velocity. In geothermal systems, these are commonly encountered in pipe elbows, valves, turbine blades, nozzles, and other structural features that alter the fluid flow direction and velocity. Corrosion fatigue is enhanced by the combined action of alternating stresses and corrosive environment.[47,48] This type of mechanism is prevalent in passivating metals, as stresses can facilitate the formation of pits, which act in turn as stress raisers and sites of fatigue crack initiation. It should be noted that since this class of corrosion is characterized by crack propagation, could also be classified under the environmentally induced cracking class. Corrosion fatigue generally leads to brittle fracture through the growth of transgranular cracks. In geothermal systems, sources of cyclic stress have been identified in steam turbine vibrations, and periodic expansion/contraction of pipelines due to varying temperature of the carried steam or fluid.

Environmentally Induced Cracking: Environmentally induced cracking is defined as cracking induced by the action of specific corrosive species, in the presence of stress. Sub-types of this corrosion category have been defined to differentiate based on the

© 2023 The Authors. Advanced Materials Technologies published by Wiley-VCH GmbH

corrosive species involved in the crack initiation and their interaction with the specific component material: stress corrosion cracking, hydrogen cracking, and environmental stress cracking. The three mechanisms all rely on the preferential initiation of cracks on areas of lower energy within the component (e.g., corrosion products, brittle phases, etc.). The difference between corrosion sub-types is then defined by the specific formation mechanism of these lower energy areas. "Stress corrosion cracking" occurs because of stress being applied while a material is in a corrosive environment.[49,50] The load can be either applied or residual, but it must have a surface tensile component. The specific corrosion process leading to crack initiation is highly material specific. For instance, stainless steels have shown cracking in the presence of chlorides, while copper alloys are susceptible to traces of ammonia in geothermal environments. It is the combination of stress, component material and its interaction with chemical species in the corrosive environment that determine the extent of this type of corrosion mechanism. Although hydrogen cracking could be thought as a sub-ensemble of stress corrosion cracking, the difference between the two mechanisms is that while the former relies on cathodic polarization (inducing hydrogen production), the latter relies on anodic dissolution (for at least a part of the propagation process).[34] It should be noted, however, that often a clear distinction between the two types is difficult to perform. It is worth noting that, although not specified in Table 5, stress corrosion cracking is referred to as "environmental cracking" when occurring on polymers. "Hydrogen cracking" instead occurs when hydrogen ions (H^+), either generated by manufacturing operations or as a by-product of corrosion reactions, diffuse into the metal lattice structure.[51,52] Hydrogen ions can eventually recombine to form molecular hydrogen (H_2), many times larger in volume than ions causing local areas of high stress and possibly cracking. In the presence of tensile stress, these cracks can propagate and eventually lead to brittle failure. Hydrogen cracking can be accelerated by the presence of hydrogen sulfide (H_2S) or arsenic compounds. These substances can delay the formation of molecular hydrogen and thus increase the residence time of atomic hydrogen on the metal surface. When this occurs in H_2S wet environment then it is generally termed Sulfide Stress Cracking (SSC). As above, it should be noted that it is not always possible to distinguish between hydrogen cracking and stress corrosion cracking as the crack initiation mechanism is often difficult to unequivocally determine.

Metallurgically Influenced Corrosion: Metallurgically Influenced corrosion includes degradation mechanisms driven by local elemental segregation in the material. In "intergranular corrosion," the grain boundary region of the material is corroded preferentially due to the presence, in these regions, of phases with lower corrosion potential.[53] These less-noble phases allow the formation of galvanic couples with the main grain phase, thus driving localized accelerated corrosion. The high rate of corrosion is further enhanced by the high area ratio between phases at the grain boundaries and matrix. "Dealloying" is instead observed in alloys forming solid solutions when one or more of the elements are preferentially corroded.[10] This occurs when some of the elements in the alloy are less noble than others. This form of corrosion has been observed in low-temperature geothermal components: brass de-zinsification, cast iron graphitization, and de-plumbification (lead removal) from lead-tin solder.

2.3.2. Mineral Precipitation (Scaling)

Mineral precipitation occurs in geothermal environments due to changes in geothermal fluid thermodynamic properties (temperature and pressure) and pH during the energy production cycle. The term *scaling* is used to define this mechanism, although this latter denomination is also used in corrosion engineering to define to the formation of corrosion products. In the review paper, however, scaling is only considered in the context of mineral precipitation. Minerals in the reservoir rocks are in fact in equilibrium with the geothermal fluid in the reservoir until a modification in the abovementioned properties generates a chemical unbalance. Scaling is highly undesirable in geothermal systems as it leads to constriction of geothermal brine flow, with subsequent decrease in production efficiency and need for equipment cleanup maintenance. To date, the most encountered forms of scales in geothermal environments are silica (SiO_2), silicates (Fe-, Mg-based), carbonates ($CaCO_3$), and sulfides.[9]

Silica scales are common in all geothermal systems, especially in high-temperature reservoirs.[54] The driving force for silica scale formation is the dependency of its solubility with temperature. Silica scale is formed in two main scenarios: (a) at an increase in silica concentration within the fluid and (b) at a drop in fluid temperature. The former case often occurs at flashing of the fluid, which increases the concentration of silica within the remaining fluid portion. As a result of the increased silica concentration, its solubility decreases and an increase in temperature is therefore required to avoid precipitation. It is important therefore, to avoid the formation of silica, to maintain the fluid temperature above a certain threshold and to control the amount of steam produced. This latter generally corresponds to a maximum of 25% of the fluid.[9]

Fe silicate scales forms if there is a significant concentration of Fe within the geothermal fluid.[55] Fe can be generated, for instance, as by-products of corrosion reactions of plant metallic components.[7] These forms of scale are generally found together with sulfide scales in saline geothermal fluids and do not form at pressure higher than 16–18 bar. For this reason, their formation can be avoided by maintaining the wellhead pressure above this limit. Mg silicate scales form when geothermal fluid and fresh water are mixed. The solubility of these scales has been observed to decrease at higher temperature and pH.

Calcium *carbonate* represents most of the carbonate types encountered in geothermal plants and, together with silica scales, accounts for most of the scale species in geothermal applications.[17,9,56] This form of scaling is common in wells with reservoir temperatures of 140–240 °C and is primarily found at the location where the fluid starts to boil. Boiling causes stripping of the CO2 species and an increase in pH, which favors $CaCO_3$ deposition. The solubility of $CaCO_3$ is observed to be inversely proportional to the fluid temperature for which, at temperatures >260 °C its deposition does not generally represent a problem.

Sulfide scales, i.e., PbS, ZnS, CuS, FeS, etc., are generated by the reaction of metals with H_2S. These are generally formed at high temperatures but are also found in low-/medium-temperature wells.[57] ZnS scale, for instance, is more common in higher temperature wells 250 °C and is a very hard compound. Sulfide scales often form at high temperatures but are also found in wells with low/medium temperature resources, form when the

© 2023 The Authors. Advanced Materials Technologies published by Wiley-VCH GmbH

temperature decreases due to super-saturation of the sulfide minerals in the fluid. Sulfide scales are known to cause plugging of two-phase flow pipelines carrying brine from production wells e.g., in wells in the Reykjanes geothermal area (Iceland).[58]

3. Review of Paint and Coating Systems

3.1. Adopted Terminology

Standard terminology related to coatingand paint systems can be found in standards EN ISO 12944 Parts 1 to 8 (general for both coating and paint systems, EN ISO 14713 Parts 1 and 2 (specific for zinc coatings not applied by thermal spray, and EN ISO 2063 Parts 1 and 2 (specific for thermal spray of Zn/Al alloys. In these standards, the definition of coat, paint, protective paint system and protective coating system is provided. *Coat* defines a continuous layer of metal material or a continuous film of *paint*, resulting from a single application; *paint* refers to pigmented coating material which, when applied to a substrate, forms an opaque dried film having protective, decorative or specific technical properties; *protective coating system* is the sum total of the *coats* of metal materials and/or *paints* or related products which are to be applied or which have been applied to a substrate to provide corrosion protection and *protective paint system* is the sum total of the *coats* of *paints* or related products which are to be applied or which have been applied to a substrate to provide corrosion protection. Therefore, *coat* is the generic term used to define a continuous film from a single application, irrespective of the type (e.g., metallic, organic, etc.), while *paint* is a coat specifically made of pigmented material. The final systems used for protection of the components of a geothermal system can be either be made of a single coat, however they are more often composed of multiple overlapped layers. This is summarized by the terms *protective coating system*, where metallic coating is present (also in combination with paints), and *protective paint system*, in reference to overlapped paints. It is worth mentioning, however, that paints and coatings are often offered under brand names for which an unequivocal classification under the above classes is often nontrivial.[59] Nevertheless, some features characteristic to protective coating and paint systems can be identified.

Due to the significant diversity in type of materials identified from the background literature review of this work, it was identified that the above nomenclature could not be easily employed. Instead, to allow an efficient classification, it was decided to employ a simplified terminology:

- **Paint** – Single- or multi-layer made of a *polymer* material,
- **Coating** – Single- or multi-layer made of metals, ceramics or their combination.

The classification is not meant to be of absolute validity and a different terminology could have been equally effective. In some instances, in fact, an overlapping in categories was identified. For instance, in cases where a multi-layer was identified composed of combined paint and coating materials, the whole system is given the category of the upper layer in contact with the environment (e.g., an organic sealant applied onto a thermally sprayed coating is considered a paint). In cases where a phase is dispersed within a matrix of a different category, the overall system is given the category of the matrix (e.g., electroless plated Ni-P with dispersed PTFE is considered a coating). With regards to nomenclature for each paint and coating system, the following methodology was employed. Traditional names[60] have been adopted, in most cases, for the paint systems as we believe this would make the review more accessible to a wider community. The only exception are the self-assembled monolayers, where the name of the spatial configuration of the molecule is adopted, rather than the name of the specific polymers composing them. For coatings, the name of the principal element is used for alloys, while systematic and common names are used for all other categories: ceramic fused basalt, cermet, high-entropy alloys, oxides, polymer concrete.

3.2. Identified Paint and Coating Systems

In this section, the result of the literature review is reported for the 23 paint and coating systems, by listing the identified materials in alphabetical order. The review only includes systems specifically intended for geothermal application and thus excludes other systems that, although potentially performing well in geothermal environments, were tested for other purposes (e.g., oil & gas, hydrothermal, etc.). The protective coating and paint systems identified in this work are summarized in **Table 6**. In total, 23 and 20 categories were identified for paint and coatings respectively.

Hereafter, a summary of the above systems is presented. A comprehensive list of all the identified systems, including layer properties, application methods, substrate type, testing conditions, etc., can be found in the table in the Supplementary Information. It is worth noting that the table present a summarized overview of al of the systems: if multiple systems of the same category, and deposited by the same technique, are assessed in a specific work, only one row would be presented in the table for that specific category. Additionally, some systems in the table could not be easily assigned to a specific category due to being

Table 6. Protective coating and paint systems identified in this review, listed in alphabetical order.

Class	Systems identified
Paints	Acrylic, Alkyd, Coal Tar and Bitumen, Epoxy, Fluoropolymer, Phenol, Polyamide, Polyaromatic, Polybenzimidazole, Polybutadiene, Polyetheretherketone, Polyethersulfone, Polyimide, Polyphenylenesulfide, Polysiloxane, Polysiloxane Organometallic Polymers, Polyurethane, Polyvinilalcohol, Self-Assembled Monolayers, Thiol, ST-TMP[a)], Vinyl Esther
Coatings	Aluminum, Antimony, Arsenic, Boron Phosphide, Bulk Metallic Glass, Calcium Carbonate, Ceramic Fused Basalt, Cermet, Chromium, Cobalt, Copper, Gold, High-Entropy Alloys, Iron, Nickel, Oxides (Al, Si, Ti, Y, Zr), Polymer concrete, Titanium, Tungsten, Tantalum, Zinc

[a)] Trimethilpropane trimethacrylate cross-linked Styrene/Methyl Methacrylate Copolymer.

© 2023 The Authors. Advanced Materials Technologies published by Wiley-VCH GmbH

a commercial product or only being given a generic name in the paper (e.g., "polymer"); these systems have been marked as "*not disclosed*". A summary from the table of the number of papers identified for each paint and coating system is presented in **Figure 6**a,b respectively.

As in many papers more than one class of coating system was studied, to avoid repetition, a mode in-depth description of that work is only presented in the first class of coating where that paper appears; only a briefer summary for that paper is then presented in other coating classes.

3.2.1. Paints

Acrylic: The effect of acrylic and epoxy paint systems onto the corrosion of carbon steel for pipeline applications was studied by Batis et al.,[61] by testing in simulated geothermal fluid from the Sousaki field (Greece). Among the paint systems tested, water-based acrylic paints were employed as both primers, undercoat, and finish layers, while a two-component epoxy system was also tested as finish layer for a total thickness in the range 60–80 µm. Acrylic systems included different types of pigment such as tannin, chromate, iron oxide, micaceous iron oxide and titania. In the study, corrosion performance was evaluated by means of electrochemical measurements (i.e., half-cell potential and potentiodynamic polarization) and weight loss analysis over a period of 450–160 days and temperatures between 20 and 60 °C. Results demonstrated that a superior protection is provided by the systems with epoxy as finish coat compared to all the other acrylic systems tested. The good performance of these coatings was further confirmed by a better rusting degree and blistering size/density factor after potentiodynamic polarization experiments. Differences in performance between paint systems AC/E (Acrylic primer containing Chromate pigment) and WT/E (Water-based Tannin-containing primer) (the former was generally tested to perform better than the latter) was attributed by the authors to the superior corrosion inhibition characteristic of the former. The authors however specify that the results obtained might differ from those obtained from field tests because the velocity of the real fluid, not present in simulated tests, would have a detrimental effect on the overall corrosion performance. At the same time however, the low concentration of oxygen in real pipeline networks would contribute to a lower corrosion rate if compared to the aerated conditions experienced in simulated tests.

A thermally sprayed ethylene methacrylic acid copolymer (EMAA) protective paint system was also tested by Allan et al.,[62] for corrosion protection of mild steel in biochemical processing of chemical residues. In the work, the EMAA, ceramic-filled epoxy (applied by brushing) and ethylene tetrafluoroethylene (ETFE) paints (also applied by thermal spray methods), were tested in both hypersaline geothermal brine and medium containing Sulfur oxidizing bacteria (*Thiobacillus ferroxidans*). The mechanical strength of the systems was also assessed by means of peel strength test in both the unexposed and exposed states. Post-exposure results demonstrated that corrosion products form at the substrate/paint interface for both EMAA and ETFE systems suggesting their inadequacy in the environments tested. The formation of corrosion products is linked, according to the authors, to the permeation of water and oxygen favored by the hydrophilic carboxylic acid groups in EMAA. The detrimental effect of water-sensitive groups in stability to geothermal environments has been also reported elsewhere.[63] Conversely, the brushable ceramic-filled epoxy paint system showed no visible signs of deterioration with only a limited amount of corrosion products formed (**Figure 7**).

A hydrothermally self-advancing hybrid paint, prepared by blending styrene acrylic latex (SAL, matrix) and calcium aluminate cement (CAC, filler containing aluminum and calcium oxide) was also tested by Sugama for corrosion mitigation of carbon steel in contact with CO_2-laden 250 °C geothermal brine.[64] The paints were prepared at different SAL/CAC ratios, to thicknesses ranging from 0.9 to 1.2 mm and exposed for up to 21 days. AC electrochemical impedance spectroscopy (EIS) and DC polarization testing were used to evaluate the coating performance in the simulated geothermal brine. The paints were analyzed after the tests for phase and microstructural changes. Results demonstrated that the paint system successfully reduced the uptake of corrosive electrolytes, thus inhibiting the corrosion of the steel substrate. This was related, according to the authors, to the continuous growth of crystalline calcite and bohemite phases, together with Ca-CCG-SAL, i.e., Ca-complexed carboxylate groups. The growth led to the densification of the originally porous coating microstructure, already after only 7 days of exposure (Figure 7).

The performance of a commercial acrylic paint, together with other proprietary paints such as epoxy, silicone, zinc-modified and CVD coatings, were evaluated by Belas-Dacillo et al.[65] for corrosion mitigation in acidic geothermal brine. The paints/coatings were deposited onto different substrates, R46 carbon steel, Type 316 stainless steel (UNS 31600) and K55 carbon steel (UNS C70250), which were also assessed as bare specimens for corrosion performance. Corrosion performance was evaluated by electrochemical methods in a geothermal brine sampled from a well in the Greater Tongonan Geothermal Field (GTGF, Leyte, Philippines), with a measured pH = 3.78 at 22.4 °C and a significant concentration of Cl^- and Na^+ ions. Tests were conducted at three different conditions of temperature/pressure/exposure time: (a) room temperature, atmospheric pressure for 30 days, (b) 70 °C, atmospheric pressure for 7 days and (c) 250 °C, 3.97 MPa pressure for 4 h. Microstructural and phase changes were examined after the exposure tests. Results revealed that all coatings demonstrated corrosion protection performance in the tested environment at room temperature and pressure. At high temperatures, in fact, a 20 to 50% decrease in protection efficiency was measured, together with appearance of visible coating defects, such as wrinkles and pinholes. At these higher temperatures, only one of the CVD coatings performed adequately, although even in this case, deposition of silica, inorganic salts and oxide scales was measured which could hinder its utilization.

Alkyd and Polyaniline (PANi): The addition of PANi and silicon dioxide (SiO2) into an alkyd binder as a paint system for corrosion protection of carbon steel was studied by Aristia et al.[66] Four different systems were tested: carbon steel (CS), alkyd binder only (Binder), Binder + SiO_2 (Si15) and Binder + SiO_2 + PANi (PS). The binder used was an alkyd commercial marine coating containing $CaCO_3$. The systems were exposed

© 2023 The Authors. Advanced Materials Technologies published by Wiley-VCH GmbH

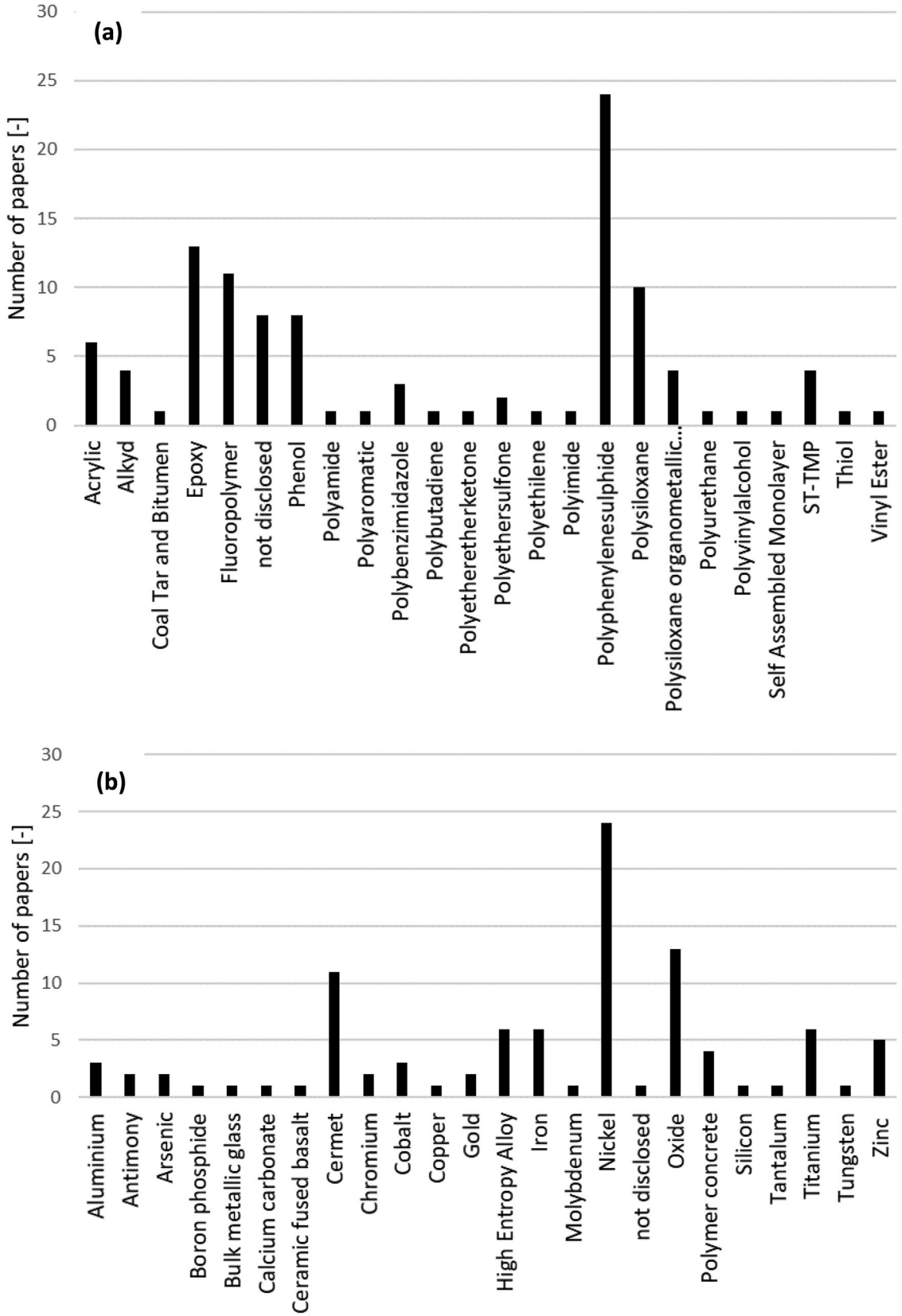


Figure 6. Number of papers, identified in this work, reporting the testing of a) paint and b) coating systems for mitigation of damage in geothermal components. Summarized from the table in the Supplementary Information.

© 2023 The Authors. Advanced Materials Technologies published by Wiley-VCH GmbH

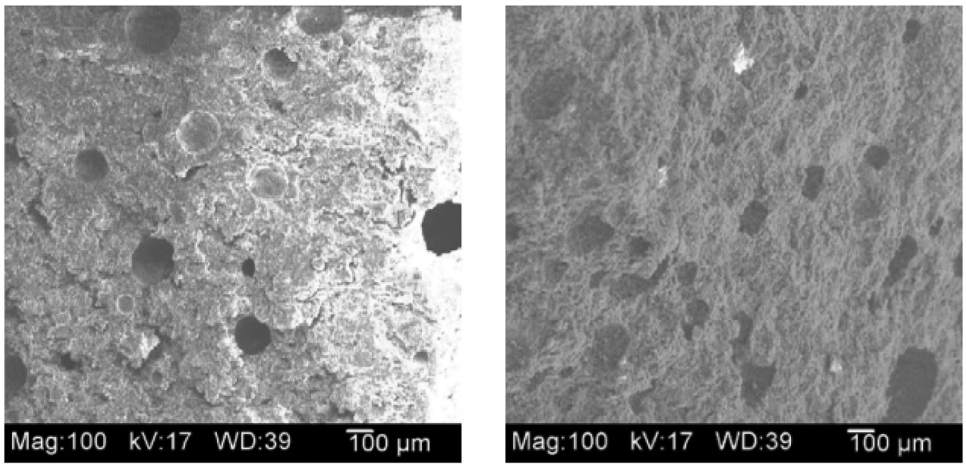


Figure 7. SEM micrographs of fractured surfaces for styrene acrylic latex(SAL)/calcium aluminate cement(CAC) at 30/70 ratio in (left) non-exposed and (right) exposed to 21 days simulated geothermal conditions. Pores originally identified on the as-deposited specimen (left) were observed to be filled with boehmite and calcite phases during the exposure (right). Reproduced with permission.[64] Copyright 2006, Brookhaven National Laboratory.

in artificial geothermal water simulating the conditions found in Sibayak (Indonesia), at 150 °C and 1 MPa for 7 days. Results were evaluated by visual assessment, in-depth microstructural characterization techniques and electrochemical test after exposure to quantify the corrosion behavior. A visual assessment of the specimens after exposure is reported in **Figure 8**.

The photographs show that carbon steel (Figure 8a) suffered from pitting (likely due to Cl^- ions present in solution). Dark spots were also observed in the binder-only paint system (Figure 8b), suggesting that degradation of this system has taken place. Some dark spots were also observed, focused on the edges of the specimen, are also observed in the Si15 system (binder + SiO_2, Figure 8c), even though the system seems overall better than the binder-only one. Finally, the best performances were obtained with the PS paint system (binder + SiO_2 + PANi, Figure 8d) with no dark spots observed. Additional thickness loss measurement after the exposure tests showed 23 and 7% average losses for S115 and binder-only paint systems respectively, which confirmed the beneficial effect of SiO_2 in enhancing mechanical properties. Furthermore, electrochemical measurements showed a more positive free corrosion potential for the paint systems compared to bare CS both at room temperature and 150 °C environment. However, the authors also specify that the significant improvement in corrosion protection obtained by the paint systems compared to bare carbon steel tested at room temperature is reduced at higher temperature (150 °C).

A similar experimental procedure (i.e., materials, exposure parameters, chemistry, and analysis) was employed by the same author one year later[67] however with a different PANi synthesis chemistry. In fact, one of the disadvantages of using polyaniline is that some polyaniline types synthesized by inorganic acid, e.g., phosphoric acid, sulfuric acid, or hydrochloric acid, exhibit properties of particles which are not easily processable, due to the stiffness in its polymeric backbone. The authors therefore decided to chemically synthesize PANi by using two different dopants, i.e., phosphoric acid and dodecylbenzenesulfonic acid (only phosphoric acid was used in ref. [66]). Visual assessment of the specimens after exposure tests revealed that specimens PS1 and PS1 performed better than both Pani-1 and −2 and Binder only, which the authors ascribe to an improvement in thermal degradation given by the SiO_2 phase. Further electrochemical tests performed on paint systems PS1 and PS2 are reported in **Figure 9**. The results from the first two hours of experiment (Figure 9a) show a lower OCP for carbon steel (i.e. ≈720 mV) compared to PS1 and PS2, which show no significant difference between them. After an increase in exposure time (Figure 9b), the carbon steel specimen shows an initial spike in potential, likely due to the formation of iron oxide or salt layer on the surface. Both paint systems also show an initial increase in OCP, followed by a plateau, higher for PS1 compared to PS2. Although this could suggest better corrosion resistance of the paint PS1 compared to PS2, a visual assessment of the coupons' surface reveals extensive degradation for both systems. The authors therefore conclude that the modification in PANi synthesis chemistry did not significantly affect the corrosion performance of the overall paint systems.

An electrochemically deposited PANi paint system was also tested by the same group the same year.[68] Cyclic voltammetry in a 200 ml electrolyte consisting of 0.1 M oxalic acid and 0.05 M aniline was employed, onto carbon steel, for the electrochemical deposition and the same testing conditions employed in previous works[66,67] were also used to assess the system performance. The authors report a stable and adherent coating after deposition, of a green coloration corresponding to the synthesis of PANi in the emeraldine state. Results from electrochemical corrosion tests reveal a better performance of PANi-coated carbon steel compared to bare carbon steel at room temperature. Moreover, a higher impedance of PANi-coated carbon steel coupons compared to bare carbon steel was also measured at 150 °C, thus again suggesting an improvement in corrosion protection provided by the new paint system.

More recently,[69] the same group presented results from the exposure of four different coatings: an alkyd + $CaCO_3$ paint, a SiO_2-modified alkyd paint, a PANi-modified alkyd paint and a PANi/SiO_2-modified alkyd paint. The coatings were applied onto carbon steel and tested by exposure and electrochemical tests in a deaerated geothermal brine simulating the one found in Sibayak,

© 2023 The Authors. Advanced Materials Technologies published by Wiley-VCH GmbH

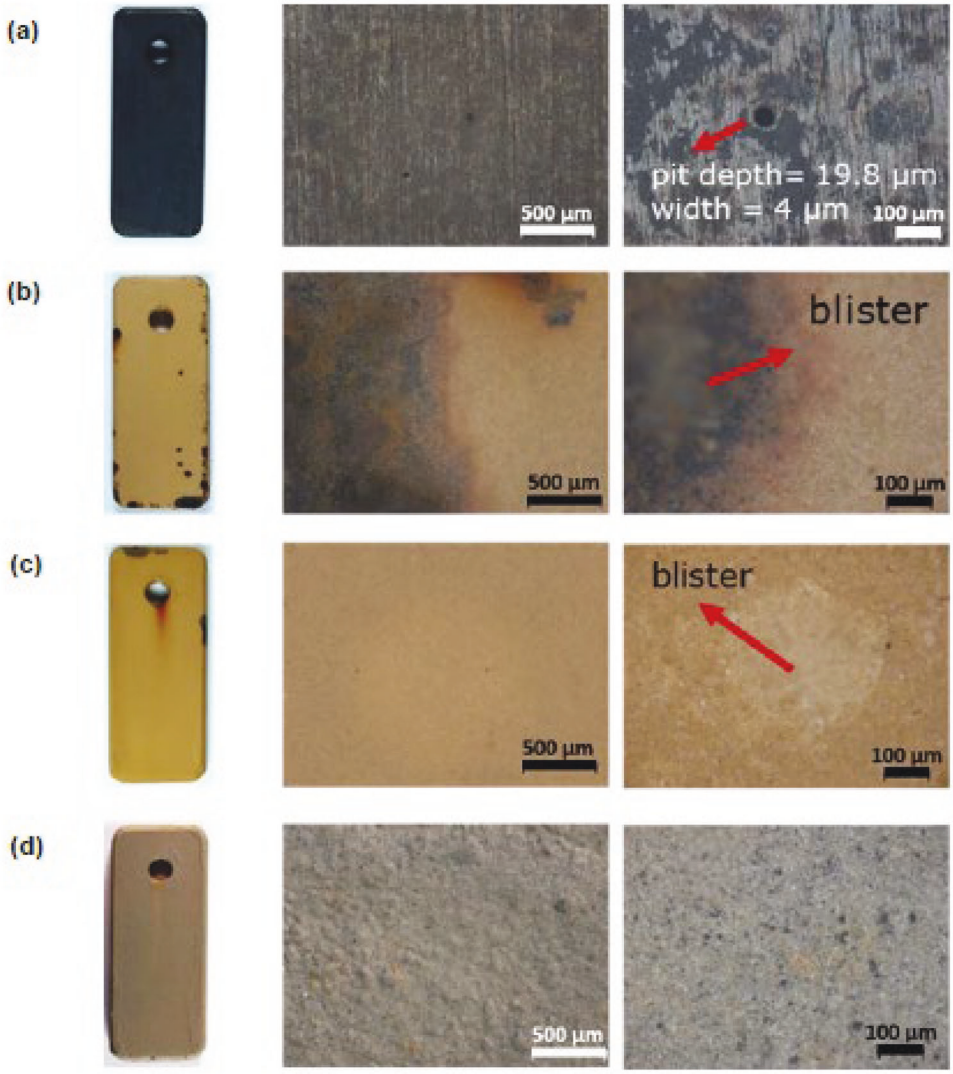


Figure 8. Overview (left), stereo picture (center), and light microscope images (right) of specimens exposed at 150 °C and 1 MPa for 7 days of a) carbon steel, b) binder, c) Si15, and d) PS. Reproduced with permission.[66] Copyright 2018, Association for Materials Protection and Performance.

Indonesia. Exposure tests were performed for 7, 28 and 168 days at 150 °C and 1 MPa pressure, while electrochemical tests were run both at 25 and 150 °C at both ambient and 1 MPa pressure. Mass loss, visual and chemical characterization of the specimens' surface after exposure were used to characterize the results. Results showed that the addition of individual pigments (i.e., only SiO_2 or PANi) to the alkyd binder was not sufficient to protect carbon steel, even after a short exposure time. However, a successful protection of carbon steel was observed for the PANi/SiO_2 modified paint, as confirmed after the 6 months exposure at 150 °C.

Coal Tar and Bitumen: Coal tar is a viscous material formed by hydrocarbons and free carbon, obtained from coal as a byproduct of coke production. Coal tar enamel has a long history of use in corrosion protection of geothermal steel and cement structures in contact with water.[70,71] Recent scientific literature on the use of this class of materials for geothermal applications is, to the author knowledge, not available.

Bitumen (or asphalt) is another viscous material formed by hydrocarbons and obtained from petroleum. An interesting recent utilization of this material in paint form can be found in the recent paper by Cadelano et al.[72] The group compared the thermal resistance of six pipes made of different materials: HDPE plastic, carbon steel, stainless-steel type 304 (UNS S30400), stainless-steel type 316 (UNS S31600), carbon steel S235JRH, carbon stee S235JRH with bitumen paint and carbon steel S235JRH with alkyd-based primer paint resembling ground heat exchangers for shallow geothermal systems. Results revealed that commonly used HDPE pipes have the lowest thermal conductivity among all systems tested, while the lowest was measured for the stainless steels, followed by the carbon steel-coated specimens. Although the coated tubes result therefore promising for the intended application, the authors suggest that a selection between stainless- and coated carbon steel components must be performed according to costs and characteristics of the subsoil.

© 2023 The Authors. Advanced Materials Technologies published by Wiley-VCH GmbH

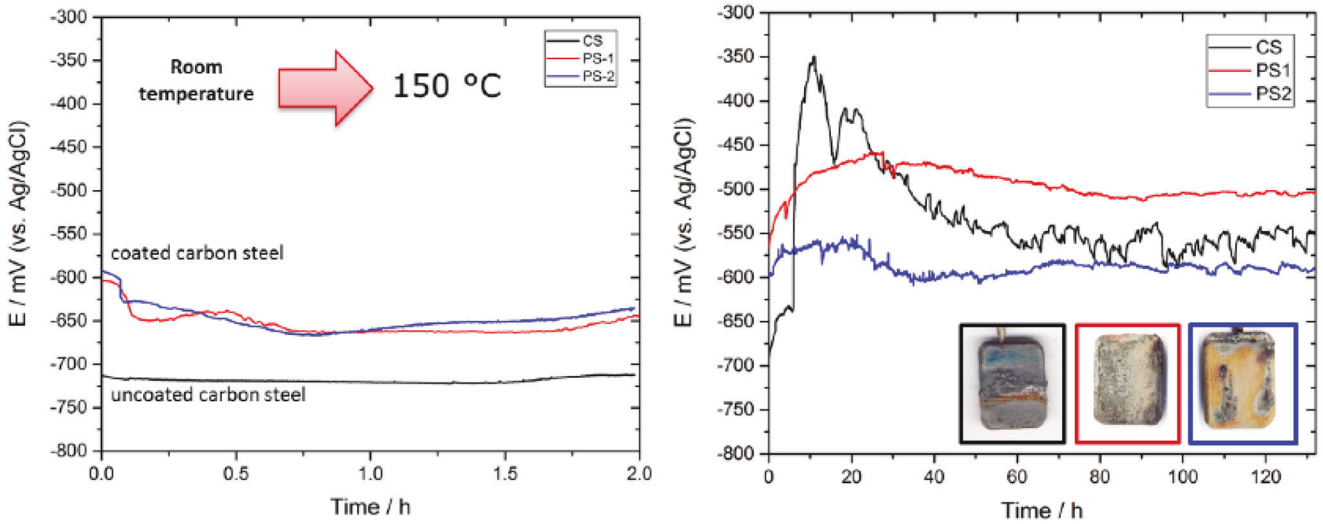


Figure 9. Open Circuit Potential (OCP) of carbon steel, PS1, and PS2 paint systems in artificial geothermal water and oxygen free environment at 150 °C and 1 MPa for 132 hours. Reproduced with permission.[67] Copyright 2019, Association for Materials Protection and Performance.

Epoxy: A comprehensive study on several protective paint systems, including one epoxy, has been originally reported by Lorensen et al.[63] in 1975. The study was part of an effort to develop protective coating systems for pipes, nozzles, turbine, and condenser components resistant to hot, pressurized geothermal brine for what the authors called "Total Flow" energy production process.[73] In the work, among other tests, the weight loss of 30 selected commercial paint systems was measured during exposure to synthetic hypersaline (24 wt.% NaCl) geothermal brine at 300 °C for 72 h. An epoxy/carbon fiber composite system is also present among the tested systems. However, it demonstrated a significant −43% weight loss after 72 h exposure, with a predicted −100% weight loss if a full epoxy system was assumed. This system was therefore not deemed suitable for the environment targeted in the work (**Figure 10**).

One fused powdered epoxy and several commercial phenolic epoxies were also tested, together with other non-metallic materials, by Jacobson et al.[74] Exposure tests were conducted for 58 days in the harsh environment of the Magnamax 1 Salton Sea brine. Among the tested epoxy systems, mixed results were obtained, with the best performance given by the Tuboscope TK-2 and TK-7 phenolic epoxies.

A custom-made epoxy paint system was also tested by Bai et al.[75] for corrosion and wear mitigation of well pump shafts in the Tianjin geothermal area. The paint was applied with 5 coats to a final thickness of 150–200 μm over Grade 35 carbon steel shafts and tested in an experimental loop connected to a geothermal well for 18 months. Qualitative visual assessments of the shafts post exposure revealed adequate protection provided by the coating system, although in-depth chemical analysis was not provided.

Epoxy was later tested by Batis et al.,[61] as finish coat in protective paint systems employing acrylic primers as primer and applied onto low carbon steel substrates. These paint systems were found to provide better corrosion protection than other paint systems with acrylic systems as finish coat. This superior performance was also demonstrated by lower weight loss and corrosion current densities measured during potentiodynamic polarization, coupled with visual examination for degree of rusting (ASTM D610) and blistering (ASTM D714). In fact, the degree of rusting for the epoxy finish coat systems was assessed to be very low (ranking number >8 even for long immersion times) and the blistering present but with small density compared to the other systems tested, even at higher testing temperatures.[61] Two systems with epoxy finish coat were tested, having the same type of two-component epoxy finish coat but differing in the type of primer: AC/E (two-component acrylic primer containing chromate pigment) and WT/E (water based acrylic primer with

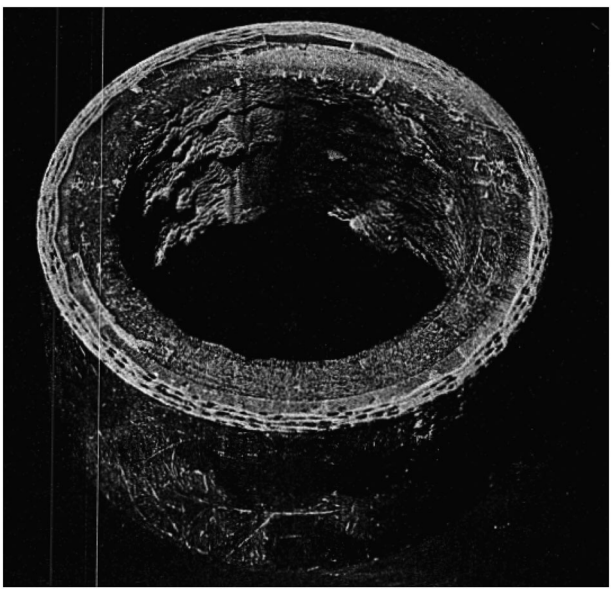


Figure 10. Epoxy fiberglass pipe after 72 h exposure to a synthetic hypersaline brine (24 wt.% NaCl) at 300 °C, showing clear presence of scale on the internal diameter. Reproduced with permission.[63] Copyright 1975, Lawrence Livermore National Laboratory.

© 2023 The Authors. Advanced Materials Technologies published by Wiley-VCH GmbH

dispersed tannin). The authors report that for the higher testing temperatures, the blister size in the AC/E system was smaller than in WT/E, result that was ascribed to the higher hydrophilicity of the water-based primer in this latter (as the finish coat was the same in the two systems). The protective performance of the two epoxy systems was attributed to different reactions. For the WT/E system (water-based primer containing tannin), the following reaction is thought to take place at primer application:

$$\left[A_2Fe-\right] + [-O-] + \left[-FeA_2\right] \rightarrow A_2Fe-O-FeA_2 \quad (1)$$

With A being the tannin anion. The reaction is confirmed by the blue appearance of the primer layer after its application. It is then postulated that a protective Fe_3O_4 layer is produced at contact of the A_2Fe-O-FeA_2 complex in the presence of oxygen. In the AC/E system instead, it is thought that the chromate ions leach out from the pigment to provide corrosion inhibition through the formation of $Fe(OH)_2 \cdot 2CrOOH$ on the steel surface.[76]

A later study by the same author,[77] focused only on the best performing epoxy paint systems from the previous work (AC/E and WT/E in ref. [61], renamed PC and RC respectively in ref. [77]), assessed the effect of sandblasting onto the corrosion protection performance of the protective paint systems. In the study, three surface preparation methods were employed prior to paint deposition: immersion in strong HCl solution containing corrosion inhibitor (ID), acetone degreasing (DA) and sandblasting followed by acetone degreasing (SB). The protective paint systems were deposited to a final thickness of 58 ± 3 µm. Earlier mass loss measurements results demonstrated that the acetone degreasing (DA) and sandblasting (SB) preparation methods led to the lowest and highest corrosion rate among the surface preparation methods tested respectively. The negative effect of surface roughness (provided by the sandblasting method) on the corrosion performance was also observed by immersion tests in low enthalpy geothermal fluid, although all the systems treated with protective paint system were deemed superior to the uncoated substrate. Moreover, in agreement with their previous study, the authors also reported a better performance for the paint system with chromate pigment-containing primer (PC) compared to the one with tannin-containing water-based primer (RC).

A ceramic-filled epoxy paint system for corrosion protection in a biochemical process to treat geothermal residues was tested by Allan et al.[62] The system was tested, together with ethylene methacrylic acid (EMAA) and ethylene tetrafluoroethylene (ETFE), in both hypersaline geothermal brine and medium containing Sulfur oxidizing bacteria *Thiobacillus ferroxidans* by partial immersion exposure. The two-component brushable epoxy was applied onto grit blasted mild steel substrates to a final thickness of 1072 ± 180 µm according to the authors. Among the paint systems tested, the ceramic-filled epoxy performed the best, with no visible signs of deterioration other than surface staining. Corrosion in the underlying substrate was evaluated by mechanically removing the epoxy paint system at the end of the test. Slight corrosion was then observed in the upper half of the liquid zone for the panels exposed to *Thiobacillus ferroxidans*, with no corrosion observed in the lower half of the liquid zone nor in the vapor zone. A similar behavior was observed in the specimens exposed to hypersaline brine with only slight corrosion observed in the liquid zone. The epoxy protective paint system was therefore deemed suitable for the application of interest and further tests under field conditions were recommended by the authors for future work.

The adverse effect of bacteria and microscopic fungi on microbially influenced corrosion of concrete is well known (see for instance[78,79]). Among the bacteria, sulfur oxidising bacteria (SOB, such as *Thiobacillus ferroxidans*) act to produce sulfuric acid (H_2SO_4) by oxidising hydrogen sulfide (H_2S) in the presence of oxygen (**Figure 11**a). The bacteria can form a wet bio film on the surface of the concrete structure, therefore generating an area of high localized concentration of sulfuric acid. The sulfuric acid causes sulfate attack on the concrete leading to the formation of hydrated compounds such as *gypsum* ($CaSO_4 \cdot H_2O$) and *ettringite* ($3CaO \cdot Al_2O_3 \cdot 3CaSO_4 \cdot 32H_2O$) among others (Figure 11b). The larger volume of these compounds compared to the parent material eventually leads to cracking and disintegration.

Improvement of resistance of concrete in cooling towers from MIC induced by *Thiobacillus ferroxidans* sulfur oxidizing bacteria, by means of paints and coatings, has also been later investigated by Berndt et al.[80,81] In the study, several commercial epoxies

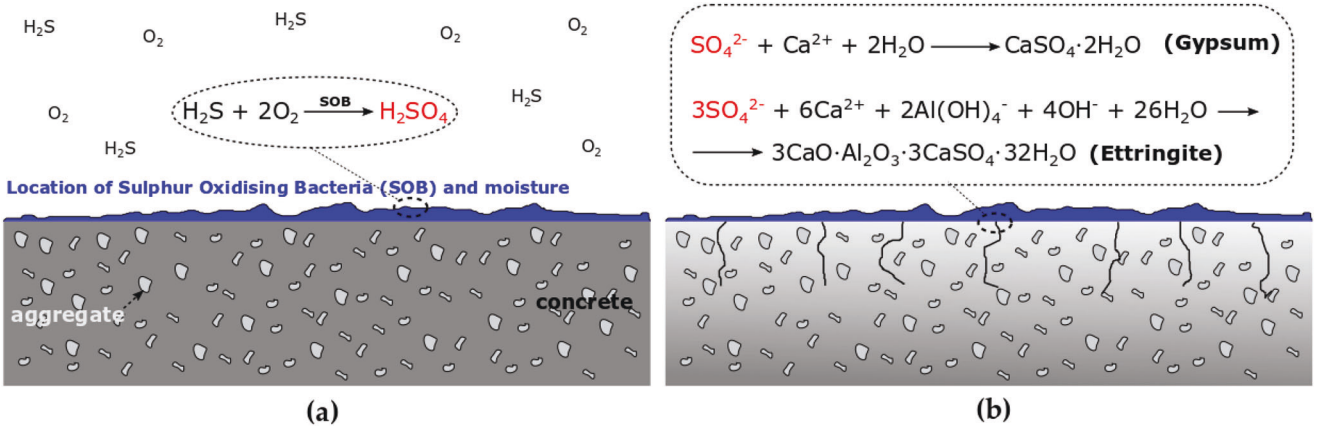


Figure 11. Microbiologically Induced Corrosion (MIC) of concrete due to sulfur oxidising bacteria (SOD) is due to the formation of a) sulfuric acid (H_2SO_4) from hydrogen sulfide (H_2S) and oxygen (O_2) in the atmosphere and b) sulfuric acid attack with formation of hydrated gypsum and ettringite compounds, causing substrate cracking and disintegration.

© 2023 The Authors. Advanced Materials Technologies published by Wiley-VCH GmbH

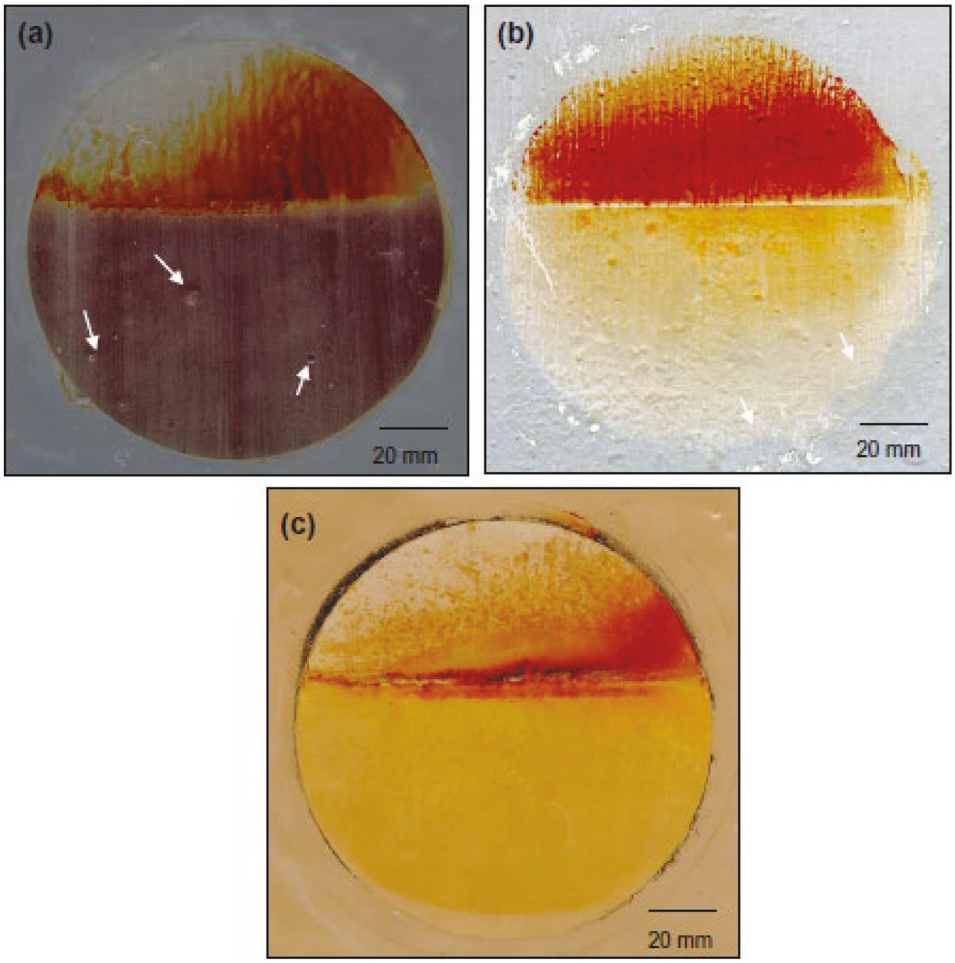


Figure 12. Appearance of a) Amercoat 351, b) Amercoat 385, c) Sikagard 62 after 60-day exposure to *T. ferrooxidans*. All the epoxy coatings show good condition, except for Amercoat 351 where blisters were observed (white arrows). Reproduced with permission.[80] Copyright 2011, Elsevier.

were tested alongside modified mortars and tested in both lab-based immersion tests (60 days in Atlas cell arrangement ASTM C 868) and field tests in a cooling tower basin for a geothermal plant in Indonesia. The surface of the epoxy-coated coupons after 60 days lab immersion test was free of biofilm (**Figure 12**). The formation of brown stains in the vapor zone was observed in all cases and attributed to the formation of iron salts. All coatings showed good post-exposure condition, except for Amercoat 351, where small blisters (1–2 mm in diameter, indicated by arrows in Figure 12a) and discoloration of the immersed zone were observed. Although a slight discoloration was also observed in paint systems Amercoat 385 and Sikagard 62, these paints were considered satisfactory post-exposure. A different outcome was recorded from the field tests, with excellent durability demonstrated by all paints except Sikagard 62, due to an excessive deviation from the manufacturer's recommended thickness according to the authors.

Interestingly, none of the paints exposed in the work showed a significant reduction in bond strength. The Sikagard 62 after field test represented the only exception. In this case, the reduction in mechanical properties was attributed to the excessive thickness (compared to the manufacturer's recommended thickness) which was addressed as the cause for the formation of blisters during the test.[80,81] The recorded bond strengths, generally higher than 3 MPa, are considered acceptable for coatings/mortars on concrete.

Several commercial organic-inorganic epoxy paint systems have also been tested by Knudsen et al.[82] with the aim of finding systems that could withstand temperatures of 225 °C or higher in a simulated wellbore environment. In the study, preliminary tests performed by the group on commercial epoxies Green Mountain DEG, Cotronics 868, Cotronics 863 and Cotronics 4525 in air and argon atmospheres showed significant degradation. For this reason, the paints were not selected for further tests. A new paint system was then tested, Cotronics 4538, whose mechanical properties can be tuned by varying the mixing ratio of resin to hardener. The paints were then tested in three different atmospheres containing argon, a mixture of hydrogen (5%) + argon and water (100 ppm) + argon for 500, 240 and 280 h respectively. According to the authors, the best results were obtained with the combination prepared from 5 g of resin and 15 g of hardener (sample 4538S-300) where no cracks was observed throughout the tests. Conversely, sample 4538S-80 (5 g resin and 4 g hardener) was deemed too brittle for the application.

© 2023 The Authors. Advanced Materials Technologies published by Wiley-VCH GmbH

More recently, numerous research studies have investigated utilizing epoxy-based paints to limit scaling. For instance, a composite epoxy-silicone paint with embedded Ni, Cu and Al powders were tested by Wang et al.[83] to limit $CaCO_3$ scaling in geothermal pipelines. The composite paint system was tested by immersion in simulated geothermal water at 50 °C for 72 h and 168 h, alongside epoxy-silicone paint only (i.e. no embedded Ni, Cu and Al) and 304 stainless steel. The simulated geothermal water contained supersaturated Ca^{2+} and HCO_3^- ions, whose reactions leads to the nucleation of $CaCO_3$ both in bulk solution and on the component's surface. According to the authors, the formation of Ni^{2+}, Cu^{2+} and Al^{3+} ions, and their release in bulk solution would slow down the nucleation and crystal growth rate of $CaCO_3$. An analysis of the tested surfaces after testing indeed revealed a reduced amount of $CaCO_3$ of needle-like shape on the surface of the composite paint compared to both stainless steel and pure epoxy-silicone. According to the authors, Ni^{2+}, Cu^{2+} and Al^{3+} ions combine with CO_3^{2-} to form complex carbonates such as $[Ni(CO_3)_2]^{2-}$, which can work as nucleation sites for $CaCO_3$ in the bulk solution as opposed to the component's surface. This was further demonstrated by monitoring the variation in Ca^{2+} concentration with time in the simulated geothermal water for the 72 h exposure tests on bare stainless steel and composite paint system.

A comprehensive analysis in the fundamental mechanisms of $CaCO_3$ scaling is also addressed by Boersma et al.[84] by testing several paint and coating systems applied over steel substrates. The authors demonstrate that the scaling is the result of the contributions of three surface properties: surface energy, roughness, and bulk modulus. These parameters were embedded into a single equation for the scale pull-off force (F):

$$F \sim \frac{K}{\gamma_{13} + \gamma_{23} \cdot r_2 - \gamma_{12} r_1} \tag{2}$$

where $K = E/(3 \times (1\text{-}\nu^2))$ is the bulk modulus, obtained from elastic modulus E and Poisson's ratio ν, γ is surface tension, r_2 is the increase in surface area due to roughness, r_1 is the area of contact between the crystals and the surface and the digit indexes 1,2 and 3 for the surface tensions refer to scale, substrate, and water respectively. The authors derived this equation by testing the several paint systems alongside un-coated steel surfaces of different roughness and a glass fiber reinforced epoxy substrate. Results show a clear demarcation value at approximately 6 GPa/(mN/m) above which the scale formation is considerably enhanced. The best results were obtained for the coatings of low surface energy (i.e. Fluoroacrylate, Fluorolink F10 and SmartCoat) deposited over the GFR epoxy substrate. The Araldite epoxy systems were found to perform the worst among the paint systems tested, due to their higher surface energy compared to other systems tested.

Results of the application of a polymeric paint system (not specified of what nature) for the scaling protection of Organic Rankine Cycles (ORC) heat exchangers was presented by Scheiber et al.[85] In the study, although specifics on the type of coating material are not given, results from its application in the period from 2008 to 2012 to an ORC unit of the Soultz-sous-Forêts EGS power plant are provided. Although the paint system showed great potential in terms of scaling reduction directly after the first application, first signs of paint blistering and spallation were observed in 2012. Chemical analysis of delaminated paint fragments showed different chemistries on the side in contact with the geothermal fluid and with the underlying steel substrate. On the former surface, strontium rich barite (Ba1- xSrxSO4), galena (PbS) and minor fractions of mixed sulfides ((Fe,Sb,As)Sx) were detected, while a mixture of iron oxides, hydroxides and/or carbonates were found, indicating that corrosion of the underlying substrate is taking place. The authors therefore concluded that paint systems have potential for scaling and corrosion protection, but their chemistry must be specifically optimized to the service environment. For this reason, the work reports on a set of new thermosetting and thermoplastic paint systems intended to be exposed at geothermal fluid at 160 °C and 20 bar for 6 months, including an epoxy mixed with PTFE. However, results from these tests are not reported in the paper.

Commercial paint systems, including epoxy/sol-gel coatings, were also tested by Losada et al.[86] and Freire et al.[87] for scaling and corrosion protection in heat exchanger applications. In the study, fluoropolymer-based, phenolic-based, and composite epoxy/sol-gel paint systems were applied onto carbon and stainless steel and tested into a synthetic brine resembling the composition found at the Balmatt power plant (Belgium). Tests were run for 570 h at 130 °C and 40 bar pressure and the performance was evaluated by visually assessing adhesion, rusting, and blistering, together with electrochemical impedance spectroscopy (EIS) to measure the corrosion protection. Although the commercial name of the exact paint systems employed is not disclosed in the work, the authors describe that the tested epoxy paint systems EP1 is a multilayer where the first layer is a Zn-rich two-component epoxy primer, the second an amine cured two-component epoxy with pigments including iron mica, the third layer is an amine cured two-component epoxy with pigments (not specified) and the fourth layer is a low surface energy hybrid organic-inorganic sol-gel coating (this latter described in ref. [88]). The system EP2 is the same as EP1 with the difference that the primer layer 1 is missing. A low surface tension (<30 mN/m) was measured on all the tested coatings in the as-deposited condition. The results demonstrate that the paint systems EP1 (epoxy/sol-gel) on carbon steel and F2 (fluoropolymer based)/EP2 (epoxy/sol-gel) on stainless steel effectively protect the system against corrosion, while maintaining a low surface tension. Additional calculations performed by the authors show that the best performing paint systems have a low impact on the overall thermal conductivity of the heat exchanger system.

Two commercial epoxy paints deposited onto carbon steel substrates were also tested, together with other proprietary paints and CVD coatings, for corrosion mitigation in acidic geothermal brine by Belas-Dacillo et al.[65] The study reported acceptable corrosion mitigation performances at room temperature for all coatings tested (including the epoxy paints). The corrosion performance was however observed to decrease at the higher exposure temperatures and pressure, with only one of the CVD coatings showing satisfactory performance among the tested systems.

Fluoropolymers: Teflon TFE (Polytetrafluoroethylene, PTFE) and PFA (Perfluoroalkoxy) systems showed the best performance among all the paint systems tested by Lorensen et al,.[63] In fact, together with the lowest weight change recorded after 72 h exposure test in 300 °C synthetic brine, the fluoropolymer

© 2023 The Authors. Advanced Materials Technologies published by Wiley-VCH GmbH

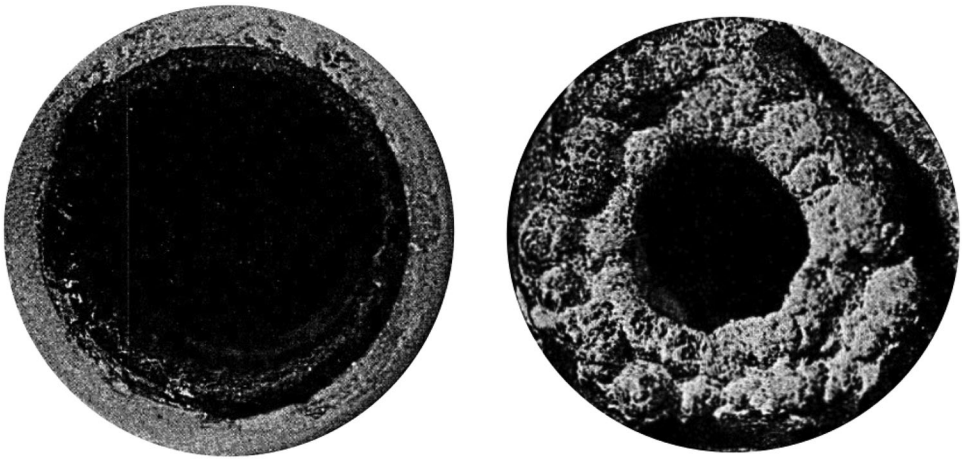


Figure 13. Teflon PFA (left) and Ploy phenylquinoxaline (right) nozzle exits after field tests showing considerable difference in amount of mineral scaling. The Teflon PFA paint system demonstrated the least scaling and highest resistance to erosive wear among the tested systems by Lorensen et al. Reproduced with permission.[63] Copyright 1975, Lawrence Livermore National Laboratory.

systems also demonstrated a limited scaling tendency and high erosion resistance in field tests compared to the other paint systems tested (**Figure 13**).

The ability of the tested paint systems to withstand the aggressive environments was connected to the polymer chemistry. Hydrolyzable bonds were proven prone to degradation, as demonstrated by the poor performance of polyimide, polyamide, carborane and aromatic polyester paint systems. This also applies to some of the epoxy systems, where some of the crosslinking phenomena are reversible at high temperature in aqueous environments. In contrast, a high degree of aromaticity and the presence of hydrophobic molecules led to superior chemical resistance and reduced mineral nucleation (i.e. scaling) for PBI, H-resins, PPQ, phenolic and fluoropolymers tested.[63]

Several fluoropolymers were tested, among other non-metallic systems, by Jacobson et al.,[74] by exposure for 58 days in the Magnamax-1 Salton Sea brine. Among the tested systems, only the Teflon PFA and a generic Fluoropolymer were considered satisfactory, with reduced amount if silica scaling also observed. However, as noted by the authors, the system was also found difficult to bond to large carbon steel vessels with nozzles.

A chlorosulfonate polyethylene paint was also tested, alongside a custom-made epoxy paint, by Bai et al.[75] for corrosion and wear mitigation of well pump shafts in the Tianjin geothermal area. The paint was applied with 5 coats to a final thickness of 150–200 μm over Grade 35 carbon steel shafts and tested in an experimental loop connected to a geothermal well for 18 months. Qualitative assessments post exposure showed a remarkable corrosion resistance improvement in the coated shafts compared to the uncoated ones.

Thermally sprayed ethylene tetrafluoroethylene (ETFE) paint systems were also tested, alongside ceramic-filled epoxy and ethylene methacrylic acid (EMAA), for corrosion protection of mild steel in synthetic hypersaline brine and *Thiobacillus ferroxidans* bacteria by Allan et al.[62] The test results after exposure (both in brine and *Thiobacillus ferroxidans*) of the ETFE paint system shows the formation of blisters and formation of corrosion products at the substrate/paint interface. The coating was therefore deemed of insufficient long-term durability at the conditions tested.

Several Viton fluoropolymer paint systems were also tested, alongside others, by Bratt et al.,[89] for protection of geothermal steam turbine blade roots suffering from stress corrosion cracking (SCC). The targeted paint systems were selected with the target of withstanding a 350°F temperature, low pH ≈2 (representing early condensate regime) and moisture containing sulfides, chlorides, ammonia, and boron. These target properties were selected to mimic the conditions found in plants at the western side of The Geysers Geothermal Steam Field. A few details the tested systems are provided, with generic denominations "Polymer", abbreviations "DMCE" and "PSE" and N/A proposed, with no further specifications provided on the chemistry of these systems apart from measured thermo-mechanical properties. The paint systems were tested against penetrability performance, flexibility performance, and strength/durability and exposure performance via test apparatuses specifically designed for the scope. Results from the different tests highlighted the following scenarios: a) the Viton paint systems performed best in penetrability among the tested systems (possibly due to their higher viscosity compared to the other systems), b) the Viton system #1 and the "Polymer" system #7 performed best in flexibility both pre- and post-exposure, c) both "Polymer" and "PSE" paint systems performed best in strength test. Therefore, the mixed nature of the results emphasized that none of the tested paint systems would be suitable for the environment under analysis in this work.

An interesting study on the corrosion protection and hydrothermal oxidation properties of the Poly(tetrafluoroethylene)/(hexafluoropropylene) paint system exposed for 20 days in 200 °C synthetic brine (20 000 ppm CO_2 and 13 wt.% NaCl) deposited onto carbon steel was later proposed by Sugama et al.[90] The paint system was applied onto 1010 carbon steel panels by dipping and curing for 24 h at room temperature, thanks to the presence of an organic silicon oligomer catalyst. The average thickness of the film so deposited was 0.185 mm. Electrochemical corrosion techniques were employed to evaluate the degradation, with phase changes and

© 2023 The Authors. Advanced Materials Technologies published by Wiley-VCH GmbH

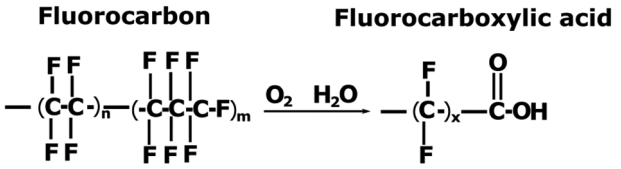


Figure 14. Mechanism of hydrothermal oxidation of the polyfluorocarbon, possibly leading to the formation of fluorocarboxylic acid fragments.

surface energy properties monitored before and after the tests. The results demonstrate that indeed the coating underwent hydrothermal oxidation, involving substitution of fluorine atoms with oxygen atoms and scission of backbone carbon-carbon linkages and eventually formation of fluorocarboxylic acid (**Figure 14**).

The presence of these oxidation-induced fragmented derivatives is also held responsible for the measured uptake of water by the coating, together with decrease in contact angle and transformation from semi-crystalline polyfluorocarbon into amorphous fluorocarboxylic acid derivatives. However, no corrosion products, nor layer delamination was observed after exposure, indicating that the coating successfully acted as a barrier at the test conditions employed. Similar results were also obtained by the same authors on commercial fluoroelastomer bearings exposed in synthetic brine at 150 °C for 120 days.[40]

Several fluoropolymer-based paint systems were also tested by Scheiber et al.,[85] applied as multilayers over pipes for corrosion and scaling protection, and tested in the high temperature skid designed for the Soultz-sous-Forêts geothermal power plant. The tested paint systems were a combination of perfluoroalkoxy (PFA), fluorinated ethylene propylene (FEP), polytetrafluoroethylene (PTFE), and polyetheretherketone (PEEK) and the coated pipes were damaged by scratching before the test. Unfortunately, no publication could be found detailing the results of these tests.

Encouraging results from the use of Fluoroacrylate and Fluorolink F10 fluoropolymers used to reduce scaling were obtained by Boersma et al.[84] The paint systems were tested in a solution containing $CaCO_3$ at room temperature for 1 h and the scaling tendency was measured by specular light reflection and adhesive tape removal. Results demonstrated that the lowest amount of scale was formed on the two fluoropolymers paints and the SmartCoat (SiO_2 based), due to their low surface energy compared to the other paint systems tested. Results demonstrate that a lower surface energy, γ_{total} = 5.3, 8.9, and 14.1 mN m^{-1} for SmartCoat, Fluoroacrylate, and Fluorolink F10, respectively, has the effect of reducing the amount and adhesion strength of scale deposited onto the substrate.

Two fluoropolymer-based paints were also tested together with phenolic and epoxy/sol–gel systems by Losada et al. and Freire et al.[86,87] The paint systems were applied on both carbon (P265G) and stainless steel (316L) with the aim of reducing corrosion and scaling in heat exchanger tubes and were tested for 570 h at 130 °C and 40 bar in synthetic brine resembling the chemistry of the Balmatt power plant. The EP1 epoxy/sol–gel system on carbon steel and F2 fluoropolymer and EP2 epoxy sol-gel systems on stainless steel were found to effectively protect against corrosion, together with possessing a low surface energy (ideal for scaling reduction). Additionally, for the best-performing paint systems F2, EP1, and EP2, the thermal transfer resistance was calculated. The measured thermal resistance is similar or lower than the brine-side fouling factor (i.e., the thermal resistance introduced by a fouling layer) of the heat exchangers used in the Balmatt power plant (i.e. R_f = 0.0004 m^2 K W^{-1}). These results suggested that these coatings could be a viable option for corrosion and scaling reduction in heat exchangers applications.

PTFE fluoropolymers were also used as filler phase (i.e., pigment) within a matrix of polymers of different chemistry. For instance, Gawlik et al.,[91,92] tested a PTFE-blended polyphenylenesulfide (PPS) system with a zinc phosphate (ZnPh) undercoat/primer over steel for heat exchanger corrosion, erosion, and fouling protection.

A commercial fluoride compound tetra deca-flouro hexane paint (TDFH, Chemguard, Sigma–Aldrich) was also prepared by Covelo et al.[93] by sol–gel synthesis and spin-coating deposition to enhance hydrophobicity and corrosion protection to aluminum heat exchangers. Different paint samples were prepared by varying the proportions of the TDFH compound incorporated during sol-gel synthesis (10%, 20%, and 30%). The paints were tested alongside perfluoro ethyl trioxi sylane $\{CF_3(CF_2)_5(CH_2)_2\text{-}Si(OCH_2CH_3)_3\}$ (PTES) paint deposited by dip technique and 3-glycyloxypropyltrimethoxysilane (GPTMS) paint, deposited by spin-coating. The aluminum substrates were prepared by electrochemical etching prior to paint application. The performance of the systems was evaluated by microstructural characterization, surface energy, and thermal conductivity measurements after electrochemical impedance spectroscopy in simulated geothermal fluid (3580 ppm Na and 6693 ppm Cl) for 1000 h. Water contact angle measurements showed that hydrophobic surfaces were obtained by both TDFH (20% and 30%) and PTES paints. The authors also reported an enhanced thermal conductivity compared to bare aluminum substrate (although this was only measured on the PTES paint, the thickest among the paints produced). Finally, EIS measurements demonstrate a good corrosion resistance for both TDFH (20%) and PTES paint systems, which however appears to decrease after ≈720 h exposure time.

An interesting recent development by Zhang et al.,[94] has seen the introduction of graphene oxide (GO) into a commercial Xylan G5844 fluoropolymer paint to develop advanced coating solutions for drilling components. The paper only presents the initial microstructural and mechanical characterization of these paints and other coating, including WCCoCr and CrC-NiCr cermets, self-fluxing NiCrFeSiB, a nanocrystalline/amorphous coating and a HEA $CoCrFeMo_{0.85}Ni$ coating. Reported analysis involved metallographic examination, hardness sliding wear tests. The PTFE-based paints were prepared by mixing different loading levels of GO from 0.5 to 5 wt.% and applied onto carbon steel substrates. Interestingly, the group observed the formation of cracks at the higher loading levels (i.e., 2.5 and 5 wt.%) and a significant reduction in friction coefficient from 0.55 to 0.13 compared to carbon steel, as measured by sliding wear test (**Figure 15**).

The same PTFE-based paints developed by Zhang et al. were also exposed to simulated geothermal conditions by Straume et al.[95] In the study, a High-Pressure High Temperature (HPHT) autoclave was employed to test the graphene oxide (GO)-PTFE based paints with loading levels of 0, 0.5 and 2.5 wt.% GO deposited onto carbon steel substrates. The tests were performed

© 2023 The Authors. Advanced Materials Technologies published by Wiley-VCH GmbH

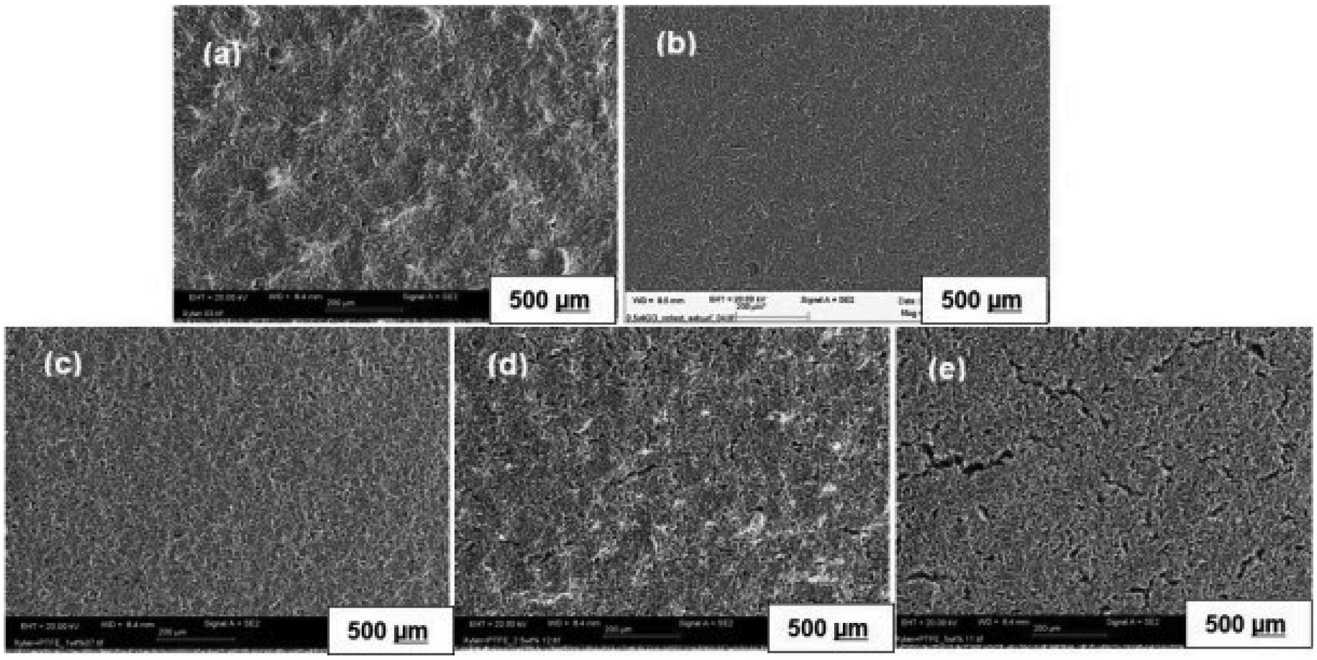


Figure 15. SEM micrographs of the surface of Xylan-based coatings a) pure Zylan, b) Xylan+0.5 wt.%Graphene Oxide(GO), c) Xylan+1 wt.%GO, d) Xylan+2.5 wt.%GO, e) Xylan+5 wt.%GO. Reproduced with permission.[94] Copyright 2021, International Geothermal Association.

in a CO_2- and H_2S-containing brine, at 250 °C, 50bar for 7 days. Apart from weight loss, microstructural characterization was performed, post-exposure, to characterize the specimens. The authors report the lowest and highest weight gain for the specimens containing 0.5 and 2.5 wt.% GO respectively, which was linked to the formation of FeS scale. Then authors therefore conclude that a maximum optimum loading level exists for these paints.

Phenol: Phenolic-based paint systems were tested by Lorensen et al.,[63] together with 28 other systems, and exposed to 24 wt.% NaCl synthetic brine at 300 °C. The phenol-based systems tested, polyphenylquinoxaline/carbon fiber and phenolic/fiberglass composites (60% and 70% estimated carbon fiber and fiberglass loading respectively), were amongst the paint systems showing less than 10 wt.% change after the test (0 and −3 wt.% respectively). One of the two paint systems, the polyphenylquinoxaline/carbon fiber composite, was therefore selected and exposed to geothermal brine from the well in a nozzle configuration from 110 to 130 hours, followed by visual inspection. Unfortunately, a significant amount of scaling was observed after the test compared to the other fluoropolymers tested in the study (see Figure 13).

A commercial baked-on phenolic was also tested, as exposed for 58 days in the Magnamax-1 Salton Sea geothermal brine, by Jacobson et al.,[74] together with other non-metallic paint systems. Unfortunately, the system was observed to be chipped after the test. However according to the authors this system, together with the vinyl ester paints, is considered promising if applied as thick paint (i.e. $t > 1.5$ mm).

Resole-type phenolic paint systems (i.e. systems made with a formaldehyde to phenol ratio greater than one) were later tested by Sugama et al.[96] The paint system, applied onto AISI 1008 carbon steel to a total thickness of140–150 µm, was exposed for up to 15 days in synthetic brine (pH = 1.6, 1 wt.% H_2SO_4, 13 wt.% NaCl) at temperatures ranging from 150 °C and 200 °C and pressures between 0.5 and 1.6 MPa. The oxidative mechanisms (or hydrothermal oxidation) occurring in the paint system was then characterized by means of standard microstructural and phase change analysis techniques, while and EIS was employed to quantify corrosion phenomena. Changes in the chemical state of the paint surface, obtained by XPS analysis, led the authors to the conclusion that hydrothermal degradation of resole-type phenolic paint systems indeed occurs with the transition methylene → benzlhydrol → benzophenone → salicylic acid. According to the authors, the breakage of C-C-C linkages in the polymer structure increases the paint susceptibility to moisture. This was confirmed by contact angle measurements (a 29.5% decrease in contact angle from the initial 88.5° was measured for the system exposed to 200 °C), TGA (3.7% weight loss for the system exposed to 200 °C attributed to water evaporation), EIS (decline in pore resistance measured for the system exposed to 200 °C) and SEM-EDS (revealing coating crack due to stresses generated by formation of iron oxides at the paint/substrate interface). Iron oxides were found at the paint/substrate interface for the systems tested at both 175 °C and 200 °C, leading in some cases to paint delamination and blistering. For this reason, the authors suggest a 150 °C as upper limit of useful temperature for these systems.

A phenolic-based paint system was also tested, together with two fluoropolymer-based paints and epoxy/sol-gel systems by Losada et al.[86] The paint systems were applied on both carbon (P265G) and stainless steel (316L) for corrosion and scaling mitigation in heat exchanger tubes and tested for 570 h at 130 °C and 40 bar in synthetic brine. The phenolic-based paint system showed great adhesion and limited presence of defects (i.e. blisters and rusting), however, its surface energy was measured to

© 2023 The Authors. Advanced Materials Technologies published by Wiley-VCH GmbH

rise from 30 to 44 mN/m after exposure, indicating the possibility of a reduction in scaling mitigation capability. Moreover, from electrochemical corrosion tests, the paint system was found to allow electrolyte permeation through the paint system, which would make it inadequate for corrosion mitigation applications. Nevertheless, no corrosion products at the paint/substrate interface were found. The coating was therefore not deemed promising for the specific application, and only the EP1 (epoxy-based) and F1, F2 (fluoropolymer-based) paint systems were considered suitable.

More recently, interesting results have been obtained by Espartero et al.,[97] by testing a polybenzoxazine (PBZ) and rubber-modified (PBZ-R)/montmorillonite (MMT) nanoclay composite paint system in acidic geothermal brine (pH = 3). Polybenzoxazines are polymers formed as condensation products between a phenol, formaldehyde and amine and have been used due to their excellent properties such as near-zero shrinkage upon polymerization, low surface free energy, low water absorption, good thermal stability and good mechanical properties.[98–100] Moreover, in the work, MMT was added, at various loading levels (i.e. 0, 1, 3, 5 and 7 wt.%), with the aim of improving the thermos-mechanical and corrosive medium permeation resistance properties compared to the PBZ-only paint system. Although technically polybenzoxazines do not fall under the phenols class, they have been included under this category within this review.

The paint system was applied onto carbon steel and tested for phase changes, mechanical properties, microstructural modifications, and corrosion performance after 1 and 7 days immersion in simulated geothermal brine. Results demonstrated that an improvement in thermal stability and mechanical properties (but not adhesion strength) was obtained by incorporation of MMT in the PBZ matrix compared to the PBZ-only paint system. Interestingly, also the corrosion performance is improved by the addition of MMT, as extrapolated by 1 and 7 days electrochemical corrosion tests. Results showed a higher 7 days corrosion rate for the PBZ-R-7%MMT paint system (i.e. 0.007 mm $year^{-1}$) compared to the PBZ-R-5%MMT system (i.e. 0.005 mm $year^{-1}$), thus suggesting the existence of an optimum amount of MMT loading. The promising performance of the PBZ-R-5%MMT paint system was confirmed by SEM analysis, showing no signs of corrosion damage after the 7 days immersion test (**Figure 16**).

Two commercial phenolic paint systems, Si 14 E and Heresite formulation 4403 were also tested by Gawlik et al, in both field and laboratory accelerated tests for cost reduction, corrosion and scaling mitigation in heat exchanger application.[91,92] The systems were applied, on carbon steel tubes, by using a "fill and drain" technique repeated 6 to 8 times, followed by post curing at 200 °C. Field tests were performed at the Hoch power plant (Salton Sea geothermal area), exposed to hypersaline brine for a minimum of 45 days at temperatures up to 110 °C. The laboratory-based accelerated tests were performed in low pH, hypersaline brine (1 wt.% H_2SO_4, 13 wt.% NaCl, and 86 wt.% water) at 200 °C for 40 days. The performance of the paint systems was evaluated by hydroblasting tests, calculation of fouling coefficient and chemical analysis through pyrolysis mass spectroscopy. Results showed that no degradation occurred when the phenolic paint systems were exposed to field tests, but a noticeable change in composition was observed after exposure to accelerated conditions. These chemical changes were linked to elimination of the phenolic hydroxyl group. Moreover, the scale formed on the component after field test could be removed even at the lower water pressures with no apparent degradation of the underlying paint surface. The results led then authors to conclude that the coatings could represent a viable solution for cost-effective heat exchangers in contact with hypersaline brine.

A phenolic-based commercial paint was also reported by Losada et al. and Freire et al.[86,87] for scaling and corrosion protection in heat exchanger applications. The paints were applied onto carbon and stainless steel and tested into a synthetic brine resembling the composition found at the Balmatt power plant (Belgium). Results demonstrated acceptable performance for this system.

Polyamide: The only reference to the use of a polyamide paint system in geothermal applications was found in the work of Lorensen et al.[63] The system, a DuPont-KS Polyamide, was tested alongside several other paints in 24 wt.% NaCl synthetic brine at 300 °C for 72 h, showing 100% weight loss after the test. Further field tests were conducted by applying the paint onto a nozzle and exposing it for 110 to 130 hrs. Results showed partial flow blockage due to growth of scale products and areas of severe erosion.

Polyaromatics: Since many polycyclic aromatic hydrocarbon (PAH) have been tested carcinogenic, mutagenic and/or toxic for reproduction, their use has been widely limited. The only study found that uses PAH as paint systems for geothermal application is the one from Lorensen et al. in 1975,[63] for application in steam turbines. Four PAH paints and one polyaromatic polyester paint were tested in the study. Among the PAHs, three of them were applied with different dispersed pigments Al_2O_3 (40 wt.%) and graphite (50 wt.%). Exposure tests in 300 °C synthetic brine for 72 hours showed that the pure PAH and the PAH with graphite pigment performed best among all the PAH systems tested (both 0 wt.% weight loss). It is worth nothing however, that a good performance was also recorded for the other PAHs paint systems tested, except for the polyaromatic polyester, for which a significant 69 wt.% weight loss was measured. Due to the good performance recorded, two PAH systems were further exposed to 250 °C synthetic brine, again showing adequate performance. The conclusion was drawn that a high degree of aromaticity, combined with water-insensitive linkages, confer stability to the paint system in the tested environment.

Polybenzimidazole (PBI): Some polybenzimidazole (PBI) systems were already tested in 1975 by Lorensen et al.[63] Their performance, evaluated after 72 h exposure to 300 °C synthetic brine, was evaluated satisfactory as these materials showed a less than 10 wt.% weight loss after the test. The good performance of the systems was attributed to the high degree of aromaticity and absence of hydrolyzable linkages. One of the systems was further tested for 202 h at both 250 °C and 300 °C with results comparable to what obtained at 72 h in 300 °C artificial brine, demonstrating good resistance in the tested medium. However, the material was not selected for further field tests.

A more recent application by Sugama[101] aimed at evaluating the thermal stability of PBI paint system deposited onto carbon steel after exposure to brine at 300 °C. Factors evaluated included thermal degradation, the degree of surface's energy and hydrothermal oxidation, the changes in chemical compositions and states for the coatings' surfaces before and after exposure

© 2023 The Authors. Advanced Materials Technologies published by Wiley-VCH GmbH

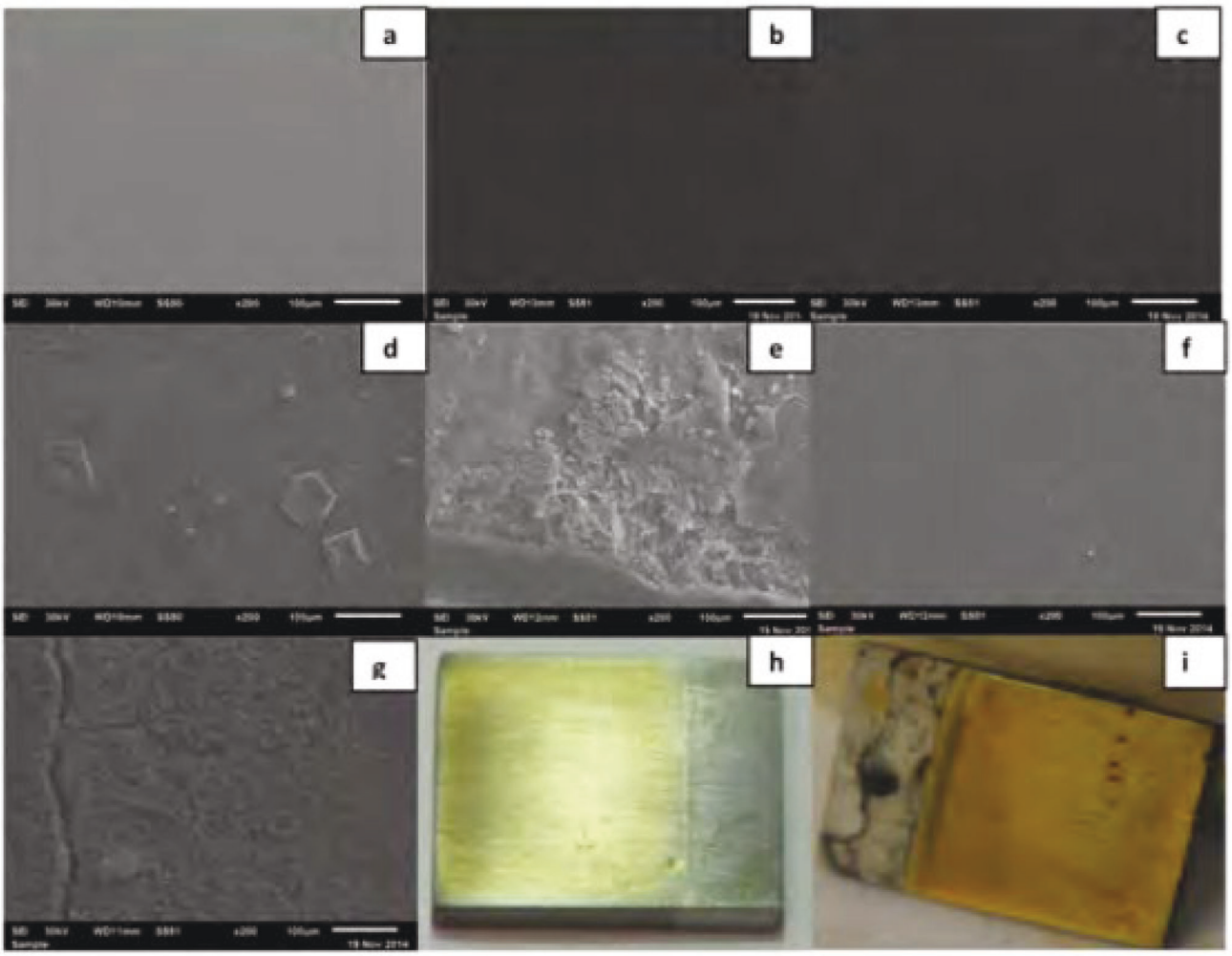


Figure 16. SEM micrographs before and after exposure tests of polybenzoxazine (PBZ) and rubber-modified (PBZ-R)/montmorillonite (MMT) nanoclay composites: a) bare carbon steel, b) PBZ-R, c) PBZ-R-5MMT before immersion in geothermal brine, d) bare steel immersed in 0.5 M NaCl, e) bare steel, f) PBZ-R, g) PBZ-R-5MMT immersed in geothermal brine for 7 days, and optical images of PBZ-R-5MMT, h) before immersion, i) after immersion in simulated geothermal brine for 7 days. The smooth surface appearance of the sample PBZ-R-5MMT in panel (i) shows no clear signs of corrosion or damage. Reproduced with permission.[97] Copyright 2019, Association for Materials Protection and Performance.

and the ionic conductivity of corrosive electrolyte species through the exposed layer. Results demonstrated that exposure to 300 °C brine led to hydrolysis of the = N = C and ≡C-N = bonds in the structure of the PBI's imidazole rings, with consequent formation of hydrolyzate derivatives biphenyl tetra-amine and benzodicarboxylic acid. The formation caused a decline in the polymer thermal stability and an increase in wetting. This increase in wetting eventually led to the uptake of corrosive electrolyte during exposure, with the result that the paint system was completely delaminated from the carbon steel substrate after 14 days. The paint system was therefore considered inadequate for application in the environment tested.

Polybutadiene: The only reference to polybutadiene paint systems being tested in geothermal environment was found in the work of Lorensen et al. in 1975.[63] Four different commercially available polybutadiene types (Dienite, manufactured by Firestone) were tested, with and without the addition of chopped glass filler. The polymers were tested first in 300 °C synthetic brine for 72 h and the weight loss measured. Interestingly, all the tested polybutadiene systems measured a weight loss lower than 10 wt.% after the test, which suggested promising performance. Two of the Dienite systems were therefore further tested by exposure to 250 °C and 300 °C for 202 h together with a few other selected polyaromatic and PBI organic systems to test the potential suitability to low-temperature geothermal brine. Results showed a low weight loss (up to 2.3%) for the two systems, which the authors considered promising due to the inexpensive nature of the polybutadiene materials.

Polyetheretherketone (PEEK): The only reference to the use of a PEEK paint system for geothermal application was found in the work of Scheiber et al.[85] In the study, a PEEK/PFA multilayer paint system was developed and applied as over pipes for corrosion and scaling protection and tested in the high temperature skid designed for the Soultz-sous-Forêts geothermal power plant. The system was tested together with others, including combinations of perfluoroalkoxy (PFA), fluorinated ethylene

© 2023 The Authors. Advanced Materials Technologies published by Wiley-VCH GmbH

propylene (FEP) and polytetrafluoroethylene (PTFE). Unfortunately, no publication could be found detailing the results of these tests.

Polyethersulfone (PES): The only reference to the use of polyethersulfone (PES) was found in the work of Sugama[102] for corrosion and scaling mitigation in joint areas of carbon steel pipelines and heat exchanger units. In the work, the PES paint systems were produced by using N-methyl pyrrolidone (NMP) as precursor at several PES/NMP weight ratios: 5/95, 10/90, 15/85 and 20/80, thus obtaining layers of ≈25, 48, ≈74, and ≈100 μm thickness respectively. The systems were evaluated by means of electrochemical impedance spectroscopy (EIS, in aerated 0.5 M NaCl solution at 25 °C) for corrosion mitigation, water contact angle measurement for wetting behavior, and X-ray photoelectron spectroscopy (XPS) for surface modifications. These analyses were performed before and after 15 days exposure tests in autoclave with a CO_2-laden hypersaline synthetic brine (0.5 wt.% $NaHCO_3$, 13wt% NaCl) at 200, 250 and 300 °C. Initial EIS tests on the PES/NMP systems of different weight ratios revealed that the highest resistance to corrosion was provided by the 15/85 system. This was related to the higher viscosity of the other formulations, which hindered a uniform substrate surface coverage and led to local paint delamination. Further exposure tests were therefore performed only on the 15/85 PES/NMP system. Post-exposure analysis showed a marked decline in the contact angle of 17.7, 39.4 and 53.5% at 200, 250 and 300 °C respectively compared to the unexposed paint system, thus suggesting that hydrothermal oxidation had taken place. This was confirmed by XPS analysis of the paint surface, which highlighted the possible pathway of hydrothermal degradation. According to the author, hydrothermal oxidation of the polymer took place during exposure, with the worst effects observed at the highest temperature tested, i.e. 300 °C: breakage of PES ether bonds, sulfone → benzosulfuric acid transformation and bond rupture in the phenyl rings (**Figure 17**). The adverse effect of this transformation was confirmed by EIS tests performed on the paint systems after exposure. The authors concluded that the PES system could only protect the substrate up to 200 °C temperature.

Polyimide: Six commercial polyimides systems were among several paint systems tested by Lorensen et al.,[63] in 250 and 300 °C geothermal brine. The weight loss results after 72 h exposure show that all the tested polyimide systems suffered significant degradation (≈100 wt.% weight loss for five out of six systems). The results were surprising as the authors expected a better performance from these systems. Additional details on the tests performed, revealed that most polyimide systems failed after only 21 h exposure. The authors concluded that the poor performance was due to the presence of hydrolyzable bonds within the polyimide molecular structure.

An interesting application of polyimide was identified by Reinsch et al.,[103] for coated fibers used in wellbore applications for high temperature geothermal areas. In the study, silica fibers were coated with four different commercial polyimides and two metals, aluminum, and gold. The performance of the paints and coatings was evaluated by exposing the fibers to different temperature cycles simulating the conditions of a wellbore cable. Temperatures in the range 90–385 °C, 269–400 °C and 269–700 °C for polyimides, aluminum and gold coated fibers respectively were selected for the tests, which were performed under both air and argon atmospheres. Attenuation was then calculated after the exposure tests via optical time-domain reflectometry. Results from the tests revealed that an application of polyimide-coated fibers might be possible at temperatures ≈350 °C for extended periods of time.

Polyphenylenesulfide (PPS): A commercial polyphenylenesulfide (PPS) material was already tested by Lorensen et al. in 1975,[63] combined with 40% glass fiber. According to the authors, the system was observed to "break into small pieces" during the exposure test in 300 °C brine for 72 h, which however was not necessarily linked to degradation. No further tests were reported for this system.

Although results from the tests were not presented in the paper, a commercial PPS Ryton paint was also tested by Borenstein,[104] together with other 21 coating and paint systems for corrosion mitigation of steam turbine blades in The Geysers (California, USA) geothermal area. The coatings/paint systems, applied onto ASTM A276, Type 403 stainless steel and ASTM A470 Class 8 steel, were tested in both simulated and field tests. Two types of simulated tests were performed, salt spray and erosion. A modified salt spray test was performed utilising condensate from real geothermal steam, while particles removed as sediment from the condensate were employed in the erosion test. Field tests were instead performed by fitting coupons to the raincatcher section of the turbine shell as well as by coating diaphragm nozzles. Unfortunately results from the tests were not presented in the paper.

Better performance was reported in a later study by Conrad et al.,[105] testing a PPS paint system commercialized as Ryton and a 40% graphite fiber/PPS composite in hypersaline brine from Magmamax No 1 geothermal well (Salton Sea Geothermal Resource Area). The paint system was applied on 316L stainless steel by first applying a ≈200 μm primer layer (CorroTherm

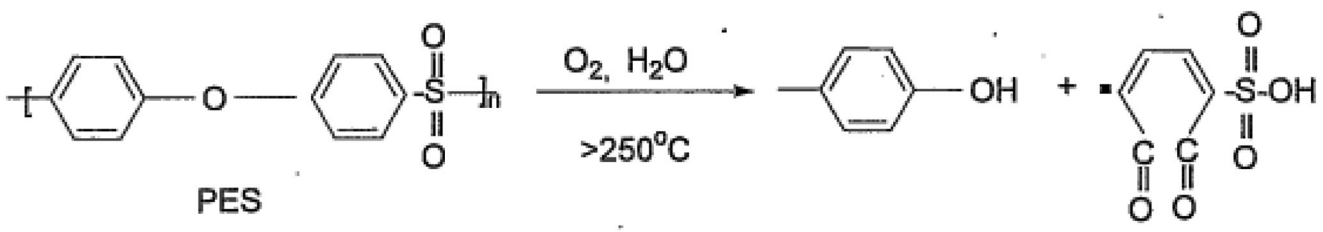


Figure 17. As suggested by Sugama,[102] hydrothermal oxidation of polyethersulfone (PES) exposed to artificial brine at temperatures >250 °C leads to the formation of hydroxyl and carbonyl groups, with consequent enhancement of moisture susceptibility. Reproduced with permission.[102] Copyright 2005, Brookhaven National Laboratory.

© 2023 The Authors. Advanced Materials Technologies published by Wiley-VCH GmbH

CT-33) and then spraying several layers of PPS to achieve a final thickness of ≈500 µm. Both the PPS paint system and graphite/PPS composite were exposed in field tests for 15 to 45 days to several medium compositions including wellhead brine and 1st–2nd separators output steam and brine. The variety of the exposure environments resulted in a temperature range between 180 and 215 °C, a pH between 5.3 and 6.9 and a Cl^- concentration between 0.17 to 12.9%. Post-exposure visual assessment revealed that the PPS paint system withstood the exposure conditions satisfactorily in all environments, with good adhesion and only occasional blistering and edge chipping. Cracking and general degradation was instead observed in the graphite fiber/PPS composite in all process environments. According to the authors, this was linked to the exposure to temperatures above the maximum recommended for the system, 150 °C.

SiC/PTFE Fillers: Several PPS-based paint systems were later evaluated by Gawlik et al. in three subsequent studies employing similar exposure and analysis techniques.[91,92,106] The aim was to develop cost-effective heat exchanger tubes by replacing titanium alloys with carbon steel covered with corrosion- and scaling-resistant paint for the Hoch power plant (Salton Sea geothermal area). To this aim, analytical techniques were used to evaluate the chemical changes on the paint surface after laboratory exposure tests. The growth of scale, and its influence on the scaling coefficient (R_f, km^2/W) was instead employed to evaluate the results of field tests on tube heat exchangers.[92] For all three studies, laboratory-based exposure tests were performed in low pH, 1wt% H_2SO_4, 13wt% NaCl hypersaline brine at 200 °C, while field tests were run in an ad-hoc designed skid to test several heat exchangers in parallel. The earlier study[106] aimed at evaluating the effect of a zinc phosphate (ZP) primer layer before application of PPS and the addition of SiC into the PPS matrix. The result of the laboratory exposure clearly demonstrated that the absence of a ZP primer led to PPS blistering already after 3 days of exposure, with complete delamination occurring after 14 days. A good resistance to oxidation for the ZP/PPS system was further confirmed by XPS analysis after the test. The beneficial effects and importance of successful preparation of a ZP primer layer on the durability of the ZP/PPS system was previously confirmed by Sugama et al.[107] and Gawlik et al.[108] The field tests then focused on comparing ZP/PPS and ZP/PPS/SiC systems (18 wt.% SiC). Results from these tests showed that, although the addition of SiC has no effect on the scaling rate, it has a large effect on the thermal conductivity, with the overall heat transfer coefficient of the ZP/PPS/SiC system being 55% higher than ZP/PPS. The addition of PTFE to the ZP/PPS and ZP/PPS/SiC system was then evaluated by the same group using similar testing and analysis techniques.[91,92] The analysis of the specimens after field exposure tests revealed that the scale formed on surface of the paint systems (measured thickness between 1.8 and 2.3 mm) could be easily removed by hydroblasting for all the PPS systems, without damage to the liner. This result suggested a weak interfacial adhesion for the scale/paint system, which was later confirmed by shear bond strength measurements. The lowest bond strength was measured in the ZP/PPS/PTFE system, which was attributed to the low surface energy of PTFE. The evolution of the scaling coefficient with exposure time was then evaluated.

Due to the nature of the skid testing apparatus, each tube was exposed to geothermal brine with different chemical-physical properties, thus making a result comparison challenging. The systems exposed to the hottest brines, i.e., PPS/PTFE (A1) and PPS/PTFE/SiC (A2) showed significant scaling compared to other systems, which required mechanical scale removal after ≈800 h of exposure. However, the authors report that the scale could be easily removed by hydroblasting at the lowest pressure used (41 MPa).

The improved resistance of the added PTFE phase was analyzed in depth by Sugama et al.[109] by chemical analysis of scale/paint interface for SP/PPS and ZP/PPS/PTFE systems after exposure to 110 °C hypersaline geothermal brine for 45 days. According to the authors, the observed hydrothermal oxidation of un-blended PPS is linked to its preferential reaction with $FeCl_2$ present in the geothermal brine. The reaction leads to the transformation of sulfide into polychloroaryl compounds and $FeSO_4$. Due to the water-soluble nature of this latter, the scale formed can be easily removed from the PPS surface, as experimentally proven. When PTFE was added to the PPS matrix, the PTFE was observed to mainly segregate at the paint surface, thereby creating a layer almost inert to scale formation.

The anti-oxidative properties of the PTFE were also confirmed by another study from the same author[110] by exposure of the paint systems in silica-rich brine. In the work, uncoated AISI 1008 carbon steel, ZP/PPS, and ZP/PPS/PTFE paints were tested for 7 days at 200 °C in hypersaline, silica-rich brine (2 wt.% $Na_2SiO_3 \cdot 5H_2O$, 14 wt.% NaCl). Microstructural analysis and surface energy measurements were performed on the systems. The results demonstrated that the formation of a surface oxide layer, Fe_2O_3 for carbon steel and sulfur oxide derivatives for unblended PPS, facilitates the initiation of silica scale deposits. In contrast, due to the low susceptibility to oxidation of the PTFE blended paint system, the surface successfully inhibited silica deposition as well as retained its hydrophobic characteristics. Therefore, the addition of SiC and PTFE to PPS was proven to enhance the thermal conductivity and scaling resistance of the paint systems respectively. However, heat exchangers, the components most targeted for application of these PPS-based systems, also suffer from abrasive wear mechanisms, both due to the passage of hard mineral particles naturally present within the geothermal brine and due to high-pressure hydroblasting. Thus, several studies attempted to incorporate hard mineral inorganic pigments within the PPS matrix and their effect on abrasive wear resistance.

Hydraulic Inorganic Fillers: Sugama et al.,[111] tested two PPS-based paint systems, among which one was a ZP/PPS with added hydraulic aluminum oxide-rich calcium aluminate (ACA) filler. The rationale is that when the paint system is damaged, the Cl^- and SO_4^{2-} anions contained in the brine react with the Ca^{2+} ions liberated from the ACA, therefore forming $CaCl_2$ and $CaSO_4$ products, which are water-soluble and thus leave behind Ca-depleted ACA. This latter is then transformed into crystalline bohemite (γ-AlOOH) phase, a very hard, tough, strong ceramic.[112] The ZP/PPS/ACA paint system was applied onto AISI 1008 carbon steel tubes and exposed to the Mammoth geothermal power plant brine for eleven months at 160 °C. The coating was tested alongside another carbon steel tube coated with a ZN/PPS/SIC-PPS/PTFE multilayer paint system and uncoated stainless steel AISI AL-6XN for reference. Results demonstrated that the ZP/PPS/ACA system suffered from increased surface oxidation compared to the ZP/PPS/ACA, which led to the formation

© 2023 The Authors. Advanced Materials Technologies published by Wiley-VCH GmbH

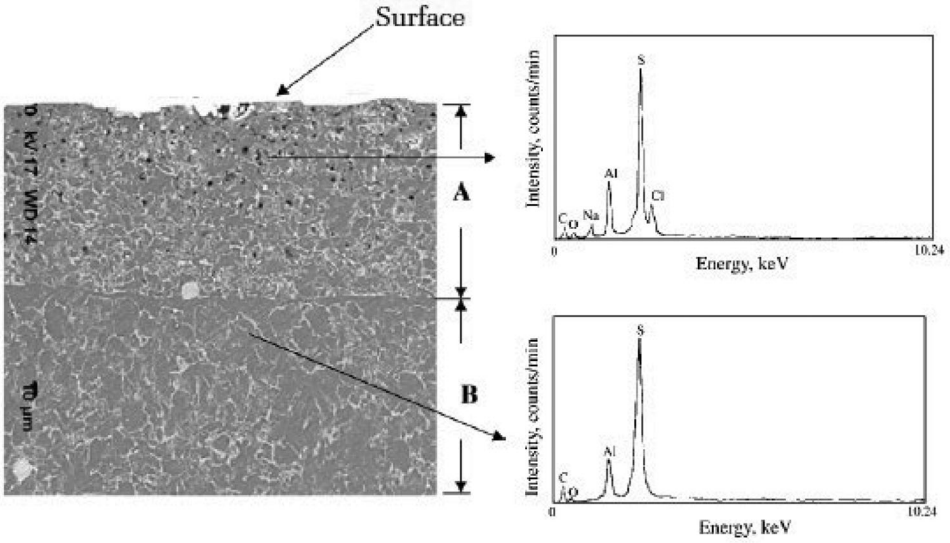


Figure 18. Backscattering SEM image and EDX spectra for the cross-sectional area of 15wt% boehmite-filled PPS paint system after exposure for 15 days in 300 °C brine. Porosity is generated within the paint layer in contact with the exposure medium, which was linked to an excessive amount of bohemite phase. Reproduced with permission.[113] Copyright 2004, SAGE Publications Inc.

of scale product in the former. However, the oxidation did not seem to be linked to hydrothermal oxidation, as both melting energy and crystallization energy measured by DSC were measured as being comparable before and after exposure. The authors concluded that PTFE is more effective in inhibiting scale formation than ACA.

Further studies from the same group[113,114] aimed at removing the step of ACA-to-bohemite transformation by incorporating nanoscale bohemite phase directly in the as-deposited paint system. The study focused on characterizing the resistance to erosion wear, thermal properties, and analysis of surface phases and morphology after exposure to CO_2-rich geothermal brine at 300 °C for 15 days. Results demonstrated a 6-fold improvement in resistance to erosion wear by adding 15 wt.% bohemite phase compared to pure PPS paint. Concerns however were raised by chemical analysis of the 15 wt.% bohemite/PPS paint system (**Figure 18**). The exposure caused in fact significant weight gain, possibly caused by the development of porosity within the paint and solution permeation. The authors therefore suggested the use of a maximum 5 wt.% bohemite phase. Further chemical structure modifications analysis suggested that although hydrothermal oxidation with sulfide to sulfite transformation could have occurred after the exposure to 300 °C, this however did not seem to have diminished the corrosion protection characteristics of ZP/PPS/bohemite paints when the boehmite loading was ≤5 wt.%.

Hydraulic inorganic grains of calcium aluminate (CA) fillers for PPS were employed by Sugama et al.,[115] to assess the self-repairing ability of the paint system. The authors suggested that the expanding CA crystals, due to contact with the hot geothermal brine, would densely fill cracks, thus reconstituting the damaged coatings. ZP/PPS/CA was therefore created, at different CA loading levels: 0, 2, 5, and 10 wt.%. The paints were prepared by forming, mechanically, cracks ≈5 μm wide and 8 to 17 μm deep prior to the exposure tests. The specimens were exposed for up to 20 days in simulated geothermal brine (200 °C, CO_2-laden brine, 13 wt.% NaCl). The corrosion performance of paint systems pre- and post-exposure was determined by EIS and the specimens were analyzed, post-exposure, for microstructural modifications. Results demonstrated that, already after 24 h exposure, the cracks resulted filled with ≈7 μm block-like crystals rich in Al oxide (**Figure 19**). The nature of the crystals was identified as being the bohemite phase. Their growth was demonstrated to occur already after only 2 h exposure by the authors, together with calcite phase, which is however transformed into water-soluble calcium bicarbonate, therefore leaching out from the grooves. The pore resistance measured on the self-repaired paints showed an increase of two orders of magnitude compared to the system without filler only after 24 h exposure, with the highest value measured with the 5 wt.% CA paint.

Montmorillonite (MMT) clay fillers were also tested later by Sugama,[116,117] dispersed in a PPS matrix, with three main aims: melting point increase, crystallization energy increase, and hydrothermal oxidation mitigation. The group aimed, in fact, at enhancing the protecting properties of the PPS system in environments containing 300 °C brine, thus a considerably higher temperature than what the group tested previously. MMT consists of one alumina octahedral sheet sandwiched between two silica tetrahedral sheets. The space between these sheets (≈1.1 nm) contains ions such as Na^+, K^+, Li^+, or Ca^+, which can easily exchange with long-chained organic alkyl amine cations. This leads to system expansion, which favors the exfoliation of silicate platelets and co-intercalation of further polymer (i.e., the PPS). In this work, the author used octadecylamine (ODA) as intercalating agent. The ≈150 μm ZP/PPS/MMT intercalated paint system, applied onto carbon steel, was tested for 20 days in simulated geothermal brine (300 °C, CO_2-laden brine, 13 wt.% NaCl). Electrochemical techniques were employed to quantify corrosion, with phase changes and microstructural modifications assessed pre- and post-exposure. The system demonstrated enhanced

© 2023 The Authors. Advanced Materials Technologies published by Wiley-VCH GmbH

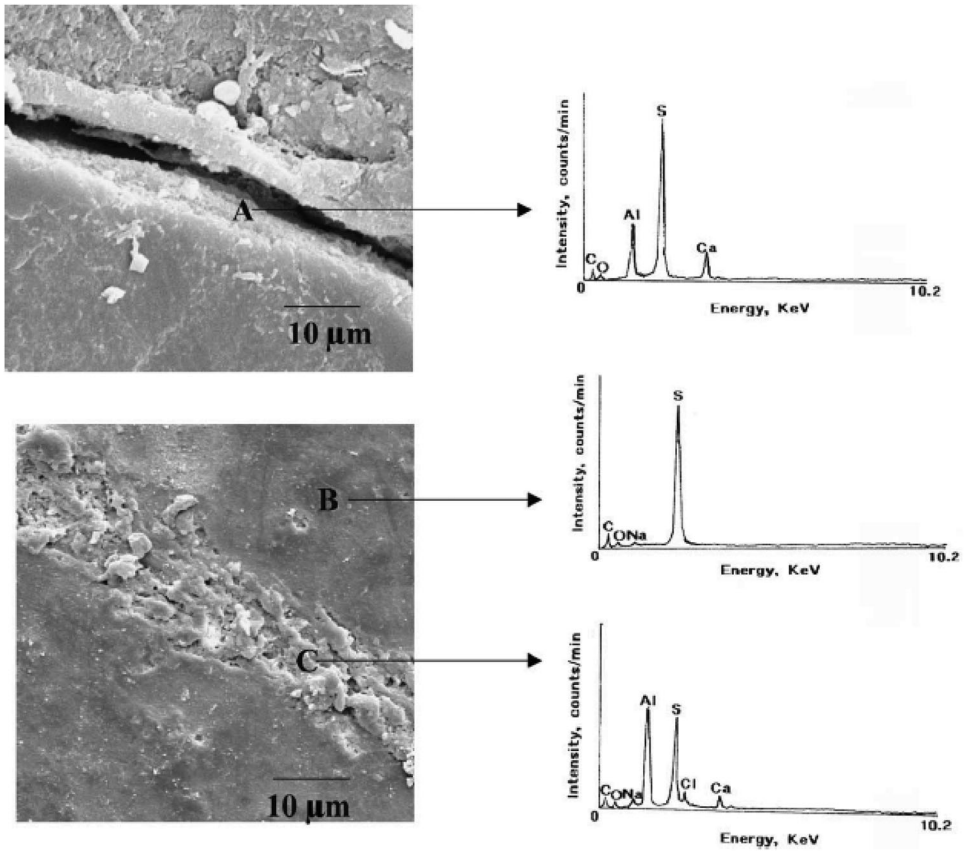


Figure 19. SEM images coupled with EDX spectra for cleaved PPS coatings with 5 wt.% CA fillers before (top) and after (bottom) exposure for 24 h to CO_2-laden brine at 200 °C, clearly indicating that crack filling with block-like crystals has occurred. Reproduced with permission.[115] Copyright 2003, Elsevier.

corrosion protection of the underlying steel for the whole 20 days experiment compared to a PPS-only paint. This was linked to three main factors: 1) an increase in melting temperature by almost 40 °C, 2) enhanced crystallization energy, driven by a good MMT/PPS interfacial bond, and 3) hydrothermal oxidation mitigation.

Carbon Fiber Fillers: Carbon fibers were also employed as a PPS filler, to enhance the thermal conductivity and mechanical properties of the paint system. As reported in two studies by Sugama et al.,[118,119] carbon fibers were tested to solve two main issues encountered with the use of SiC as a filler: susceptibility to hydrothermal oxidation and poor mechanical properties. In the study, ZP/PPS/carbon fibers paint systems were produced with polyacrylonitrile (PAN) precursor-derived carbon fibers of ≈7.4 µm diameter and ≈3 mm length, added to PPS at 0.0, 0.2, 0.5, 1.0 and 1.5 wt.% of the total mass of PPS and deposited onto AISI 1008 carbon steel material. The paint systems were exposed for 14 days in simulated geothermal brine (200 °C, 20 000 ppm CO_2, 13 wt.% NaCl) via EIS. Microstructural and phase changes, combined with thermal conductivity measurements were then employed to evaluate the results. Corrosion performance results showed an improvement compared to pure PPS up to 0.5 wt.% carbon fiber content, after which, an excessive porosity would develop in the film, promoting solution permeation. A ≈60% increase in thermal conductivity was also measured with the addition of 0.5 wt.% carbon fiber, together with 2.4, 2.6, and 1.5 times increase in tensile strength, tensile modulus, and elongation respectively compared to pure PPS. The improvement in mechanical properties was linked to a strong mechanical interlocking between the fibers, due to their porous surface, and the PPS matrix.

The same paint system was later tested by the same group[120] for protection of vaporizer and preheater heat exchangers at the Puna Geothermal Venture power plant. Carbon steel tubes and flat coupons were therefore coated and tested for four weeks in contact with 200 °C geothermal fluid within a test skid manufactured ad-hoc for the project. Different substrate preparation methods were employed prior to the PPS composite deposition for the tubes and flat coupons: zinc phosphate (ZP) layer application and galvanization respectively. Microstructural and phase changes were evaluated before and after the tests. The results demonstrated that the substrate preparation methodology has a significant impact on the exposure performance, since paint delamination was observed in the case of the galvanized tubes, but not in the flat coupons with a ZP layer. Because of delamination, the heat transfer performance of the coated tubes was measured to drop by 70% during the test, compared to 43–44% decline in the uncoated carbon steel tube.

More recently, Yang et al.,[121] tested a PPS/PTFE/MWCNT (multi-walled carbon nanotube) composite paint system onto

© 2023 The Authors. Advanced Materials Technologies published by Wiley-VCH GmbH

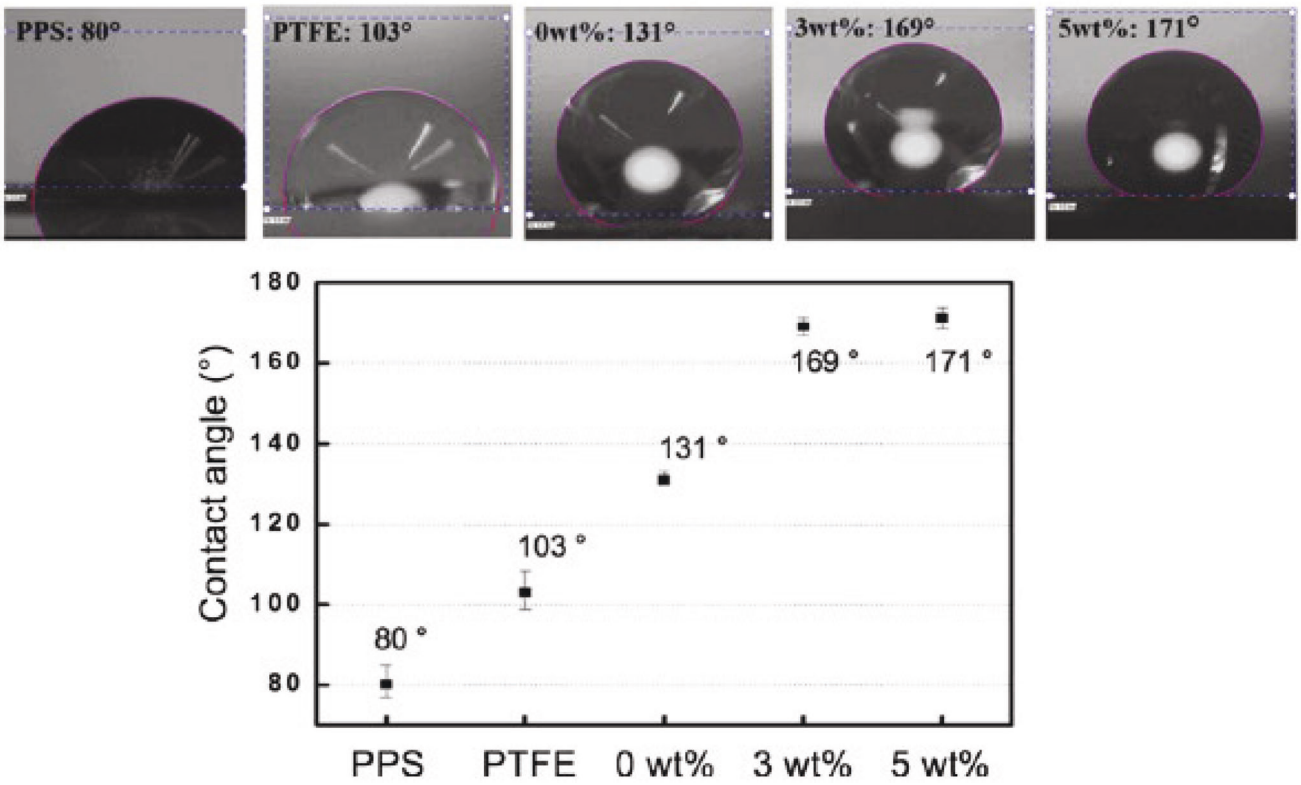


Figure 20. Water contact angle measured for PPS, PPS/PTFE and PPS/PTFE/MWCNT paint systems at different MWCNT loading levels. Reproduced with permission.[121] Copyright 2016, Wiley-VCH GmbH.

brass substrates, produced by melt compounding process using polyethylene glycol (PEG) surfactant as structure-directing template. Different load fractions of MWCNT were tested, from 0 to 5 wt.% and the microstructure, composition, and mechanical properties of the resulting paint systems were then analyzed. The results show that by adding MWCNT to the PPS and PPS/PTFE systems, a super-hydrophobic surface is generated (**Figure 20**). The water contact angle was in fact measured to increase to a maximum of 171° (for 5 wt.% MWCNT) from 80° and 103° for pure PPS and PPS/PTFE respectively, although only a 2° improvement was measured between the 3 and 5 wt.% PPS/PTFE/MWCNT systems.

Furthermore, the electrical resistance was measured to decrease with increasing MWCNT fraction, from 3×10^{16} Ωcm for PPS/PTFE to $\approx 3 \times 10^{3}$ Ωcm for PPS/PTFE/MWCNT with 3–10 wt.% MWCNT load. Interestingly, no further decrease in electrical resistance was measured by increasing the MWCNT load above the 3 wt.% level, which was ascribed to a tendency to increase aggregation between the MWCNTs at the highest concentrations tested. MWCNT aggregation at the highest loads was also considered detrimental to the system's mechanical properties.

Antioxidant Fillers: Antioxidants were also tested as filler materials for PPS by Sugama et al.,[42] to retard the degree of hydrothermal oxidation in the polymer. According to the authors in fact, oxidation of the PPS polymer occurs by breakage of the S-C bond in the PPS chain, generation of sulfide sulfur radical and its oxidation. Antioxidants would donate a hydrogen atom as radical scavenger to tie up with the sulfide sulfur radicals, effectively inhibiting the oxidation of the sulfide sulfur radical. In the work, three antioxidant: tetrakis [methylene-3,5,-di-*t*-butyl-4-hydroxyhydrocinnamate]methane (TMBHM), 4,4′-Bis(*α*,*α*-dimethylbenzl)diphenylamine (BDDA) and tris-2,4-di-tertiary-butylphenyl.phosphite (TTBH) were dispersed at 3 wt.% load into a PPS slurry and deposited onto a ZP-coated AISI 1008 carbon steel substrate material. The as-deposited paint systems, of 75–100 μm thickness, were exposed for up to 20 days in simulated geothermal brine (pH 1.6, 1 wt.% H_2SO_4, 13 wt.% NaCl, at 200 °C under a hydrothermal pressure of 1.6 MPa. Corrosion performance was quantified by EIS, and phase changes and surface energy properties were analyzed during the tests. Results demonstrated that TMBHM, among all the antioxidants tested, is the most effective in retarding hydrothermal oxidation of the PPS. In fact, contact angle measurements on the ZP/PPS/TMBHM system showed only a 1.3% drop in water contact angle during the 20 days exposure compared to the 17% drop of pure ZP/PPS. Moreover, although decreasing in all cases tested, the pore resistance R_p measured in the ZP/PPS/TMBHM system had a final value of 4.0×10^{6} Ωcm^2, one order of magnitude higher than the pure ZP/PPS.

Polysiloxane and Polysiloxane Organometallic Polymers: Polyaminopropylsiloxane (PAPS) polymers for scaling and corrosion mitigation in finned tubes of air-cooled condensers using geothermal fluid spray for heat transfer augmentation were first evaluated by Sugama et al. in 1994.[122] The paint system, applied to a ≈10 μm thickness, was synthesized by

© 2023 The Authors. Advanced Materials Technologies published by Wiley-VCH GmbH



Figure 21. Organometallic polymer-coated (left) and uncoated (right) aluminum fin after 30 days salt spray test in 3.5 wt.% NaCl and 35 °C. No corrosion products developed on the coated component. Reproduced with permission.[122] Copyright 2002, Geothermal Rising.

a heat-catalyzed condensation reaction using aminopropylsilanetrial (APST) as a network-forming monomer, water and HCl as the acid mineral catalyst. The system was applied onto aluminum fins and tested in 5 wt.% NaCl salt spray testing for 30 days at 35 °C. The specimens were visually examined post-exposure for presence of corrosion products and mineral scales (**Figure 21**).

The results showed no sign of corrosion products on the coated fin (Figure 21 left) compared to the uncoated one (Figure 21 right), thus suggesting promising performance for the tested paint system. It was later reported[123] that the useful lifetime of bare aluminum exposed in a 15 wt.% NaCl fog at 35 °C was considerably extended from only 40 h to more than 1400 h by PAPS deposition. However, a lower effectiveness was instead measured on bare steel, with the lifetime being only extended from 10 h to 216 h.

After these encouraging results, other polysiloxane organometallic polymers were later tested.[84,117,123-125] In the study by Sugama et al.,[123] a $Ce(OH)_3$-dispersed poly-acetamide-acetoxyl methyl-propylsiloxane (PAAMPA) was first created through three spontaneous reactions of condensation, amidation and acetoxylation at 150 °C between the Ce acetate dopant an aminopropylsilane triol (APST). The PAAMPA composite was then heat treated, leading to the transformation of $Ce(OH)_3$ into Ce_2O_3. Post heat treatments temperatures were tested from 150 °C to 250 °C, providing paint systems with different chemical and mechanical features. Corrosion performance of the films was evaluated by salt spray resistance (5 wt.% NaCl at 35 °C), with microstructural, phase, and surface energy changes measured throughout the tests. Results demonstrated that when the 150 °C made PAAMPA composite was heat treated at 200 °C, the transformation of $Ce(OH)_3$ into Ce_2O_3 took place. This however was combined with undesirable oxidation reactions of the Si-joined propyl groups when the heat treatment temperature was raised at 250 °C. Consequently, the film-forming performance was also affected, with the paints created at 150 and 200 °C showing no defects, while a high defects density was observed in the system heat treated at 250 °C. The system prepared at 200 °C then showed the best corrosion protection performance among the tested paints due to three main reasons: a more densified barrier layer, lower susceptibility to moisture, and formation of interfacial Ce_2O_3 passive film. The positive effect of the 200 °C-baked paint system was validated by salt spray resistance, where the useful lifetime of aluminum and steel substrates was prolonged from 40 h to 1800 and 800 h respectively.

The same PAAMPS/Ce oxide paint systems prepared in ref. [123] at 200 °C post-deposition heat treatment, were field-tested by Sugama et al.,[124] for protection of aluminum fin and carbon steel for air-cooled condensers applications. Uncoated, undoped PAPS and PAAMPS/Ce oxide coated substrates, with paints systems deposited at thicknesses from 3.5 to 10 μm, were tested in an ad-hoc manufactured testing equipment allowing 24,500 wet-dry 15 min exposure cycles for a total testing time of 8.5 months. The test was performed at the Mammoth Lakes binary plant. The exposed specimens were analyzed both by visual inspection and in depth-microstructural characterization techniques. Results showed that the uncoated substrates underwent severe corrosion, with complete disintegration of the aluminum fins and spallation of iron oxide-based scales on the carbon steel (**Figure 22**). The coated coupons performed considerably better, even though corrosion products were found.

The authors later found that an increase in paint thickness from 3.5 to 10 μm increases the overall protection. However, two issues were identified: a) poor paint coverage at the sharp aluminum edged, leading to corrosion initiation in these regions, and b) the need to develop more effective corrosion protection nanoparticle materials. On this latter point, the authors suggest the use of samarium oxide/PAAMPS-coated fins.

Three polysiloxanes: polydimethylsiloxane (PDMS, Sylgard 184), tetraethyl orthosilicate (TEOS), and a SmartCoat were also tested for scaling mitigation purposes in the work of Boersma et al.[84] In the study, the paint systems were applied over steel substrates prepared with different surface roughness and tested in environments rich in $CaCO_3$. The results demonstrated that the scaling rate depends on three parameters: surface energy, roughness, and bulk modulus. Among all the tested systems, the SmartCoat system performed best, likely due to its extremely low surface energy, while the TEOS and PDMS presented a performance in between that of the SmartCoat and the worst-performing paint system Araldite.

The corrosion resistance ability of a ferroferric oxide (Fe_3O_4)-polysiloxane-based composite paint systems was also tested by Xu et al.[125] in application to carbon steel pipelines for geothermal energy production. In the study, five paints obtained from precursor solutions with different molar ratio of Methyltriethoxysilane (MTES) and Glycidoxypropylthrimethoxysilane (GPTMS) were manufactured: Fe_3O_4-PGPTMS, Fe_3O_4-PMTES, Fe_3O_4-PMG-2:1, Fe_3O_4-PMG-1:1, and Fe_3O_4-PMG-1:2. The paint systems, deposited onto carbon steel, were tested by electrochemical techniques in 3.5 wt.% NaCl and simulated geothermal water for corrosion performance, while monitoring phase and microstructural changes.

Among the tested systems, the Fe_3O_4-PMG-2:1 exhibited the best corrosion performance in both 3.5 wt.%NaCl (see **Figure 23**) and simulated geothermal water. Superior performance was linked by the authors to the absence of defects, such as cracks, debonding, and scratches within the paint, as observed by SEM analysis. For the same reason, the authors concluded that thicker paints, probably as this would decrease defects density,

© 2023 The Authors. Advanced Materials Technologies published by Wiley-VCH GmbH

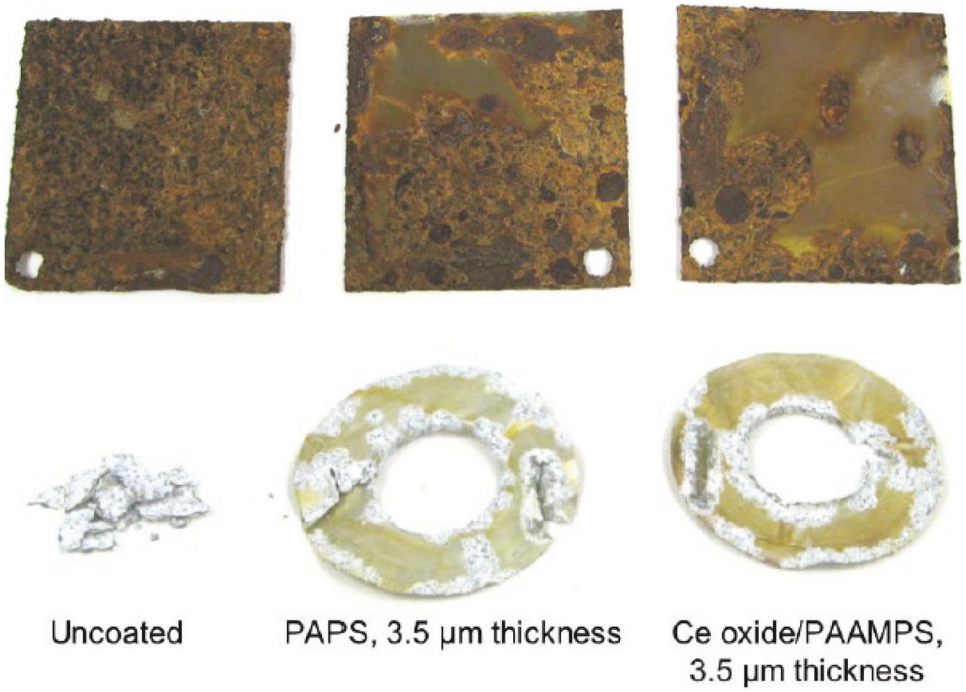


Figure 22. Uncoated, undoped PAPS and Ce oxide/PAAMPS-coated carbon steel coupons (top) and aluminum fins (bottom) after the 24 500-cycle test, showing significant improvements in corrosion performance for the latter. Reproduced with permission.[124] Copyright 2006, Geothermal Rising.

provide better corrosion protection. All the paints tested showed good thermal resistance and a <8% weight loss under 300 °C, with values as small as 3.40% and 3.80% for the PMTES and PMG-2:1 respectively. The authors also noted, however, that none of the paints tested presented long-term corrosion resistance.

Two paint systems, perfluoro ethyl trioxisylane $\{CF_3(CF_2)_5(CH_2)_2\text{-}Si(OCH_2CH_3)_3\}$ (PTES) deposited by dip technique and 3-glycyloxypropyltrimethoxysilane (GPTMS), deposited by spin-coating were tested by Covelo et al.[93] for hydrophobicity and corrosion resistance improvement for aluminum heat exchangers. The paints were tested alongside a commercial fluoride compound tetra deca-flouro hexane paint (TDFH, Chemguard, Sigma-Aldrich) paint deposited by spin-coating. The performance of the systems was evaluated by SEM, water contact angle measurement, thermal conductivity, and electrochemical impedance spectroscopy in simulated geothermal fluid (3580 ppm Na and 6693 ppm Cl) for 1000 h. Results demonstrated that the thicker PTES paint could improve hydrophobicity of the aluminum substrate, while retaining good corrosion resistance. This latter, however, was measured to decrease after ≈720 h of exposure time for all the paint systems.

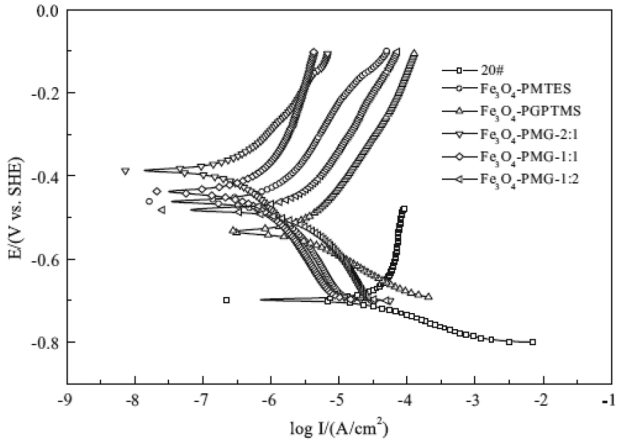


Figure 23. Potentiodynamic polarization curves of different ferric oxide polysiloxane-based composite coatings in 3.5 wt.% NaCl solution. The best performance was demonstrated by specimen Fe_3O_4-PMG-2:1. Reproduced with permission.[125] Copyright 2017, Elsevier.

Only one application of a carborane-siloxane polymer, commercialized as Dexsil-201 was also reported to be tested by Lorensen et al.[63] as part of their comprehensive material assessment campaign. This class of polymers was developed with the aim of enhancing the thermal and chemical resistance properties of conventional polymers by the introduction of, in this case of the work of Lorensen, a $C_2B_{10}H_{12}$ carborane. Unfortunately, the paint showed a >10% weight loss after exposure for 72 h in a 300 °C synthetic brine and therefore was not further investigated.

One silicone-based paint was also tested, alongside other paints and CVD coatings, by Belas-Dacillo et al.[65] for corrosion mitigation of carbon steel in acidic geothermal brine. The results from exposures, performed at different temperatures and pressures, showed a satisfactory corrosion protection performance for all coatings when tested at ambient conditions but not at more extreme conditions. In this latter case, only one of the CVD coatings was assessed as suitable for the environment.

Polyurethane: The only application of polyurethane paints was mentioned in the review paper by Reeber[16] in reference to tests performed at the Brookhaven National Laboratory. The

© 2023 The Authors. Advanced Materials Technologies published by Wiley-VCH GmbH

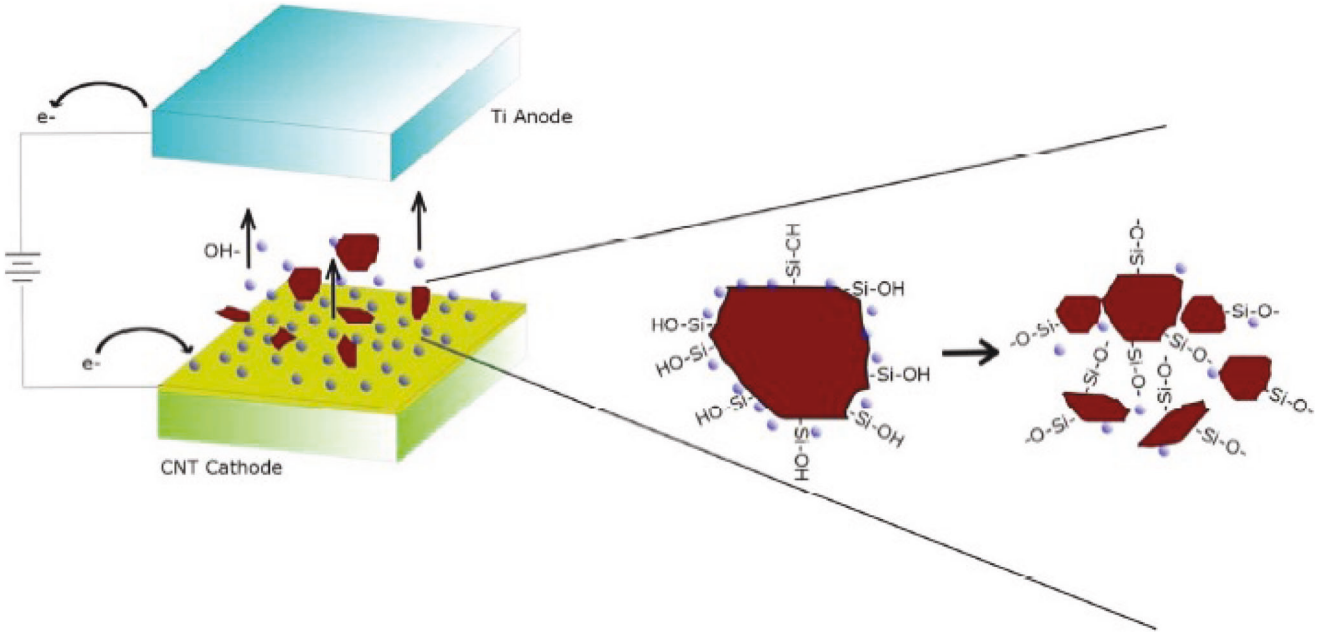


Figure 24. Graphical description of proposed electrochemically induced silicate dissolution cleaning mechanism provided by the carbon nanotubes(CNT)/polyvinylalcohol(PVA) paint for the membrane distillation (MD) process. Reproduced with permission.[126] Copyright 2017, American Chemical Society.

Tuboscope TK-33 polyurethane paint and a polymorphic resin were both tested for 30 days in a 25 wt.% NaCl geothermal brine at 238 °C. Both systems, however, performed poorly, with the polyurethane paint showing discoloration and flaking off the substrate.

Purethane, a commercial polyurethane paint, was also tested by Borenstein[104] among 21 other coating and paint systems for corrosion protection of turbine blades in The Geysers area (California USA). Although results from tests are not presented, tests performed involved modified salt spray an erosion tests and field tests within the turbine itself.

Polyvinylalcohol (PVA): Carbon nanotubes (CNT), cross-linked with hydrophilic poly(vinyl alcohol) (PVA), were applied onto an hydrophobic polypropylene (PP) membrane with the aim of enhancing the membrane distillation (MD) process of spent geothermal brines, thus recovering desalinated water. The rationale behind the application was that by applying an electrical potential to the CNT/PVA layer, water hydrolysis, and therefore hydroxide ions formation, would be facilitated. This in turn would locally increase the solution pH, increasing the silica dissolution rate (**Figure 24**).

The relative potential of the novel membrane was evaluated by electrochemical measurement in a geothermal brine containing up to six times the concentration of salts than what naturally found in brine from a geothermal region in Nevada, USA. Electrical conductivity, water flux measurements, surface energy, and microstructural characterization were measured on the specimens. Results demonstrated that, compared to an un-coated PP membrane, the novel system increases the water flux significantly, while at the same time allowing efficient removal of the silicate gel layer nucleated on the surface. The process was demonstrated for three cycles, and only residuals of barium and calcium sulfate were observed, these, latter considered being pH insensitive. This good performance was coupled to a significant system stability, with elimination of CNT release and therefore enhanced environmental safety. The scaling inhibition properties of PVA, together with other antiscalant systems, was also proven in the work of Topcu et al.,[127] although not in paint form.

Self-Assembled Monolayers (SAM): The possibility to improve dropwise condensation in geothermal steam condensation processes using SAM was evaluated by Vemuri et al.[128] In the study, ultra-thin hydrophobic films obtained from stearic acid (SAM-1) and *n*-octadecyl mercaptan (SAM-2) solutions were deposited onto copper condenser tubes. Their performance, in terms of heat flux and condensation heat transfer coefficient were then measured, by means of a custom-made apparatus, for up to 3600 hrs. Variations in surface energy during the tests were also recorded by means of contact angle measurement.

Remarkable results were obtained with the system SAM-2, with an enhancement in heat transfer coefficient up to 3 and 1.6 times after 100 and 3600 h of operation respectively. Although a high initial contact angle of 155° was also measured on the SAM-1 system, this was observed to drop to 61.1° during the tests, which was linked to its weak adhesion to the substrate surface (**Figure 25**). The authors therefore conclude that the bonding of the SAM layer to the condenser surface is essential to its performance.

Thiols: Although thiols are commonly employed as hardeners for two-pack epoxy resins, applications where these have been produced in the homopolymer form have been proposed for geothermal applications. The anti-scaling properties of an organometallic polymer, 2-(dioctylamino)−1,3,5-triazine-4,6-dithiol, deposited onto steam turbine rotor and tested in service environment, were assessed by Shimizu et al.[129] Details of the

© 2023 The Authors. Advanced Materials Technologies published by Wiley-VCH GmbH

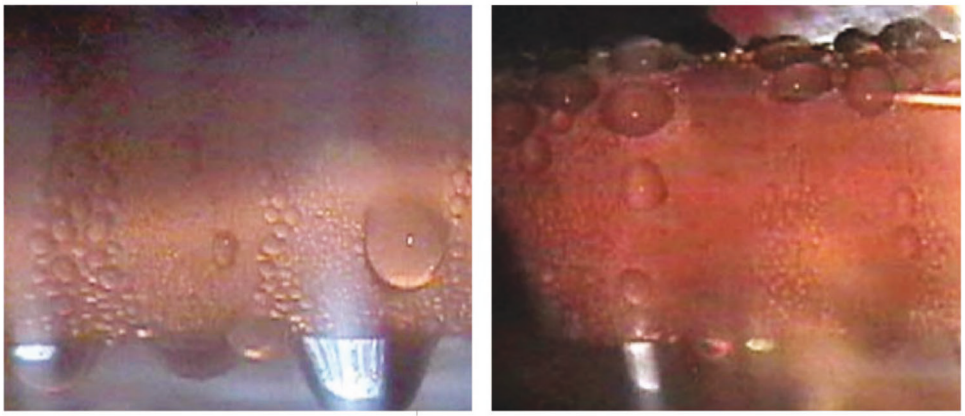


Figure 25. Surface photograph of condensation onto a self-assembled monolayer paint-coated tube (SAM-2) after 100 h (left) and 3600 h test (right), demonstrating an increase in drop size with exposure time. Reproduced with permission.[128] Copyright 2006, Geothermal Rising.

polymerization process, employed to deposit the paint, are reported in a previous study,[130] where the formation of disulfide polymer is proposed. The coating was deposited by electrochemical polymerization in Na_2CO_3 aqueous solution by preparing the rotor substrate (UNS S41000 stainless steel) surface by grit blasting prior to deposition. According to the authors, a final coating thickness of 0.3 μm was obtained, and the presence of coating was evaluated by water contact angle measurements (i.e. decrease in contact angle corresponding to a decrease in surface energy). The authors propose that, following voltage application, the negatively charged portion of monomer thiolate anion (forming as an intermediate step during the polymerization reaction) directs toward the cathode, in an electric bilayer fashion (**Figure 26**).

Both coated and un-coated rotors were tested at the same time for one year in service conditions. Only qualitative results were presented by visually comparing the amount of scale formed on the components after testing. The results showed a reduced amount of scale on the coated rotor compared to the un-coated one.

Trimethylpropane Trimethacrylate Cross-Linked Styrene/Methyl Methacrylate Copolymer (ST-TMP): The first reference to the use of a trimethylolpropane trimethacrylate cross-linked styrene/methyl methacrylate (ST-TMP) copolymer is found in the work of Fontana et al.,[131] for application as heat exchangers tube material. In the study, silicon carbide (SiC) aggregate phase was added to the polymer matrix, composed of 60 wt.% ST and 40 wt.% TMP and formed in tube shape. The tubes were found to provide excellent thermal conductivity at temperatures up to 150 °C, with an overall heat transfer coefficient only 9% less than more expensive stainless steels commonly used in geothermal power plants. A later study on the same material used as liner for carbon steel heat exchangers however, demonstrated that the polymer surface suffers from hot brine-induced oxidation through the formation of a carboxylate group.[132] The formation of this group eventually led to the reaction with Ba^+ ions present in the geothermal brine and degradation of the cross-linked matrix structure.

To minimize polymer oxidation and reduce scaling, the same group later tested the addition of 1,4-phenylene diamine (PDA) as an antioxidant to the ST-TMP/SiC system.[91,92,106] Moreover, to improve the adherence of the paint system to the substrate, a zinc phosphate inorganic coating was applied on the steel substrate before the paint system. The performance of the systems was compared to bare steel substrates and other paint systems including PPS/PTFE and phenolic materials. The paint systems were applied as liners to carbon steel tubes and tested both in accelerated laboratory conditions (low pH, 1wt% H_2SO_4, 13wt% NaCl hypersaline brine at 200 °C for up to 40 days) and field tests at the Hoch power plant in the Salton Sea geothermal area for 45 days. Results from initial field tests showed that the addition of PDA to the ST-TMP/SiC system reduced the rate of scaling from 15 to 19% compared to only ST-TMP/SiC.[106] Later results however, demonstrated that the scale formed presented a very strong adherence to the PDA/ST-TMP/SiC paint system (8.20 MPa bond strength) compared to other systems tested (e.g. 1.59MPa measured for the PPS/PTFE system).[91] The authors concluded therefore that the PDA antioxidant is inefficient in providing a chemically inert polymer surface. A similar result was obtained by Sugama et al.,[109] by testing the PDA/ST-TMP/SiC paint system in a brine of lower temperature (110 °C). The PDA was again proven unsuccessful in preventing the formation of strongly adhered scale.

Vinyl Ester: The only reference to the use of vinyl ester-type paint systems was found in the work of Jacobson et al.,[74] where the performance of six different such systems was assessed after exposure for 58 days to the Magnamax-1 Salton Sea brine. Although an in-depth post-exposure analysis is not provided, the authors describe that the vinyl ester paints Derakane 411 and 470 appeared warped and brittle, while no visible attack was observed on the 4000-series systems.

3.2.2. Coatings

Aluminum: The first reference to the use of a pure aluminum coating was identified in the work of Borenstein[104] on corrosion mitigation of steam turbine blades in The Geysers geothermal area (California, USA). In the reference, only the overview of the future work was presented, where commercial Ion Vapour Deposited (IVD) aluminum, together with other 21 coating and paint systems, was planned to be deposited onto stainless steels and tested both in simulated tests: salt spray and erosion tests

© 2023 The Authors. Advanced Materials Technologies published by Wiley-VCH GmbH

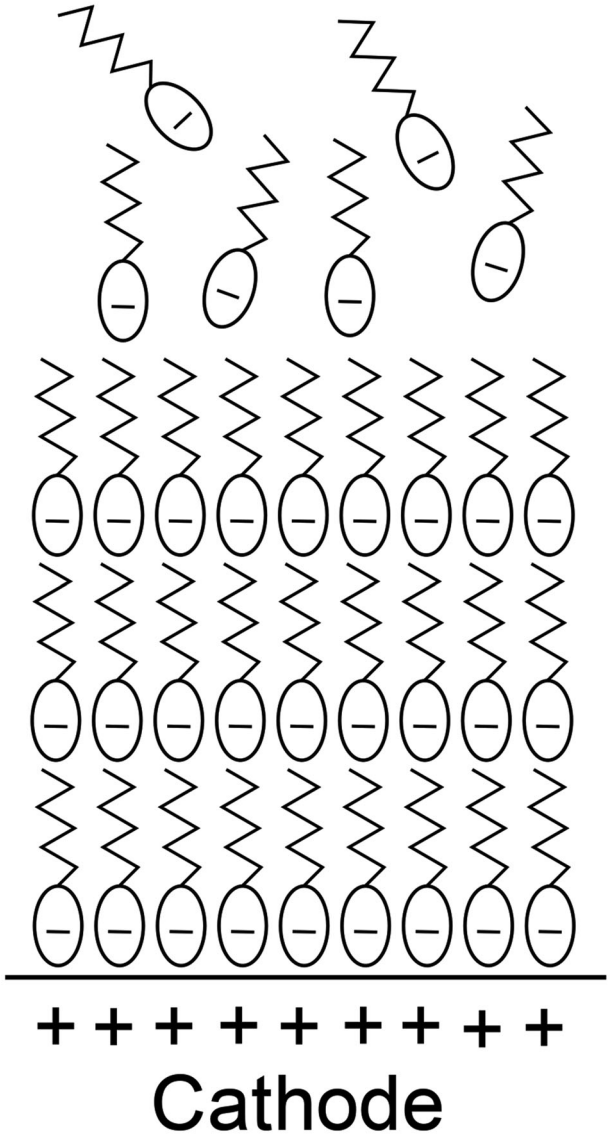


Figure 26. Monomer thiolate ions could arrange in an electric bilayer fashion after voltage application.

and field tests with coupons placed inside the steam turbine. No results from the tests were described in the reference.

Another interesting application of aluminum coating was presented in the work of Reinsch et al.,[103] for the protection of Raman-based distributed temperature sensing (DTS) silica fibers operating in hot geothermal wells in Iceland. Aluminum-coated fibers were tested alongside gold and polyimide-coated fibers at different heating/cooling cycles ranging from 65 to 700 °C and either in air and/or argon atmosphere. The performance was evaluated by microstructural analysis and measuring the attenuation. Results revealed an elevated attenuation for the metal-coated fibers (both aluminum and gold) below 200 °C that led the authors to select the polyimide-coated fibers for further tests.

Antimony/Arsenic: Arsenic and Antimony thin films (≈0.5 µm thick), deposited by ion beam sputtering on carbon steel, were used by Lichti et al.,[133] to simulate corrosion

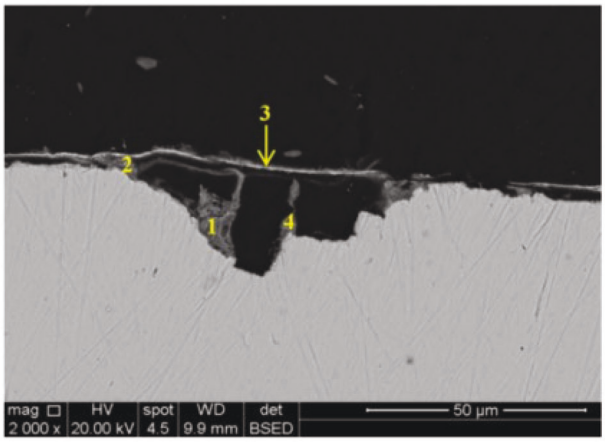


Figure 27. SEM micrograph of a corrosion pit formed under antimony-coated carbon steel coupon after exposure to aerated pH 5.4 solution. Reproduced with permission.[133] Copyright 2015, International Geothermal Association.

mechanisms occurring in heavy metal scales naturally forming in geothermal power plants in New Zealand. Both coated coupons and bulk materials were tested in the study, by using exposure tests and electrochemical methods and varying temperature, pH, and aeration level (i.e., aerated, and non-aerated). For the coated coupons, exposure tests were performed for 4 days in a solution containing 1000 ppm of chloride ions at 20 °C. The corrosion performance was evaluated by varying pH, between 3 and 4.5, and aeration levels on both scratched and unscratched coupons. Apart from evaluation of corrosion potentials and current densities, microstructural evaluation was also performed after the exposure tests. Results revealed the main corrosion mechanism as being chloride-induced pitting corrosion under the coating layer (**Figure 27**), accelerated by aerated conditions and initiated by defects in the coating. In every case, corrosion under the coating layers was always greater than both on uncoated steel and on scratched coatings.

To account for more realistic environmental conditions, the same coating materials were later deposited again by the same authors[134] and exposed for 5 days to higher temperature (i.e., 120 °C), pressure (i.e., 1.4 barg) and in an atmosphere containing H_2S and CO_2 gases (although de-aerated). Compared to the previous study by the same authors, thicker coatings (1–2 µm), deposited on both carbon (UNS G10050) and duplex stainless steel (UNS S32205) were produced. Specimens after exposure were analyzed by means of microstructural examination, both on the surface and ion cross-section. Results revealed a similar magnitude of corrosion of the carbon steel substrate for both arsenic and antimony coatings. For these carbon steel substrates, the preferential corrosion mechanism was evaluated as still of localized pitting corrosion type, while no corrosion damage was observed on the stainless-steel coupons, likely due to extensive coating delamination rather than material-specific performance. Due to possible contamination occurring from exposing together different substrate and coating materials, the authors conclude that new tests should follow where one material at a time is tested.

Boron Phosphide: Boron phosphide films deposited by plasma-enhanced chemical vapor deposition (PECVD) were

© 2023 The Authors. Advanced Materials Technologies published by Wiley-VCH GmbH

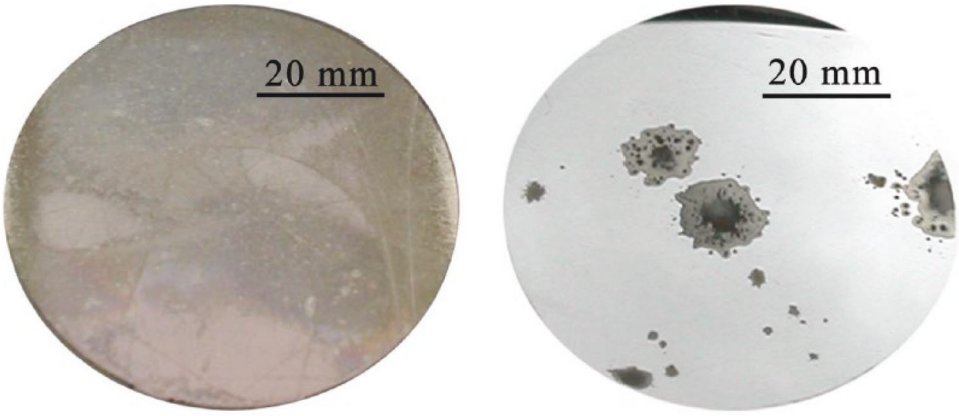


Figure 28. Surface photographs of (left) BP-coating and (right) 304 L stainless steel after potentiodynamic polarization test in 5.7 M NaCl solution at 25 °C. Pitting is observed on the un-coated stainless-steel substrate. Reproduced with permission.[135] Copyright 2014, Elsevier.

studied by Ogwu et al.[135] for corrosion protection of 304L stainless steel against hypersaline geothermal brine. Different coatings, deposited to a 7.1 to 9.7 μm thickness by varying deposition conditions, were analyzed for surface energy, corrosion resistance (via electrochemical methods), and morphology/microstructure. The electrochemical tests were carried out in 5.7 M NaCl aqueous solution at 25 °C. Results revealed a correlation between surface energy and corrosion rate for the tested materials, which allowed the authors to identify a specific set of deposition conditions providing the optimal corrosion resistance. All of the deposited coatings performed better than the un-coated stainless-steel substrate, this latter showing typical stainless steel passive layer formation and breakdown (i.e. pitting) behavior in Cl^- environment (**Figure 28**).

Bulk Metallic Glass: Although not many details are provided, the application of a nanocrystalline/amorphous coating for geothermal drilling tools, deposited by thermal spray, was reported by Zhang et al.[94] The coating was deposited together with other systems, including WCCoCr and CrC-NiCr cermets, self-fluxing NiCrFeSiB coating, HEA coating, a graphene oxide-PTFE paint, and electroless plated coatings. Only values of as-deposited coating porosities are reported: 3.6% for the nanocrystalline/amorphous coating, compared to 0.9%, 1.1%, 2.4%, and 1.6% for WCCoCr, CrC-NiCr, self-fluxing NiCrFeSiB, and HEA coating. Microhardness values in the range 558–1218$HV_{0.3}$ were also reported for these coatings, although these were not linked to specific coatings.

Calcium Carbonate: An interesting approach to producing superhydrophobic layers for corrosion and scaling protection of 304 stainless steel (UNS S30400) was employed by Wang et al.[136] In their work, a continuous cactus-like $CaCO_3$ coating with hierarchical nano- and micro-sized featured was prepared by self-assembly method inspired by scaling in geothermal water. The deposition approach involved pre-nucleation treatment, followed by immersion in simulated geothermal water at 50 °C for 48 h and a final surface modification with sodium stearate to impart the superhydrophobic character. Results from contact angle measurements reported a water contact angle of 158.9° and a sliding angle of 2°. Further microstructural examination revealed that the temperature of the geothermal water had a significant effect on the morphologies of the $CaCO_3$ crystals, but no quantification on actual corrosion or scaling protection was reported.

Ceramic Fused Basalt: The only reference to the testing of a ceramic fused basalt is found in the work of Jacobson,[74] where an Abresist coating with a thickness of ≈51 mm was exposed for 58 days in the Magnamax 1 geothermal well in the Salton Sea geothermal region. Cracking was however observed after the test.

Cermets: The first reference to the use of cermet coatings was identified in the work of Borenstein,[104] where three different electrospark deposited (ESD) systems: WC+TiC+TaC+Ni, WC+TiC+TaC+Co and Cr_3C_2+Ni were evaluated for corrosion mitigation in steam turbine blades operating in The Geysers geothermal area (California, USA). The coatings, deposited onto three different steel alloys, were tested both in simulated conditions: modified salt spray test and erosion test, and field tests. Unfortunately, results from the tests were not presented.

One thermally sprayed cermet material, WC-Co-Ni (METCO 5803), was evaluated by King et al.[137] as a replacement for high-temperature/high-pressure o-ring elastomer seals in deep geothermal applications. The coating system was evaluated alongside other alloys, including Shape Memory Alloys (SMA), deposited by High Velocity Oxygen Fuel (HVOF), Twin Wire Arc Spray, and Flame Spray Fusion processes. Several compositions and post-deposition processes were tested, including sealing the coatings and with a liquid sealer and fusing with an oxy-acetylene torch to reduce coating porosity. The coatings were applied onto both ID and OD tool joints made of AISI 304L stainless steel and tested in two steps: a pressurized water test (354 bar for 4 h to 10 days) and a pressurized/high-temperature silicon oil test (345 bar, 225° for 1000 h). A list of the seven coatings that passed both tests was reported by the authors, together with their deposition parameters and thickness characteristics. The WC-Co-Ni cermet, deposited by HVOF with a Ni/Al bondcoat and sealed with Diamant liquid sealer, was among the coatings that passed the pressure/temperature test. According to the test results, the HVOF technique was the one providing the best results. However, as the authors point out, the oxide and porosity content should be carefully tuned to avoid negative effects in the coating's mechanical properties.

© 2023 The Authors. Advanced Materials Technologies published by Wiley-VCH GmbH

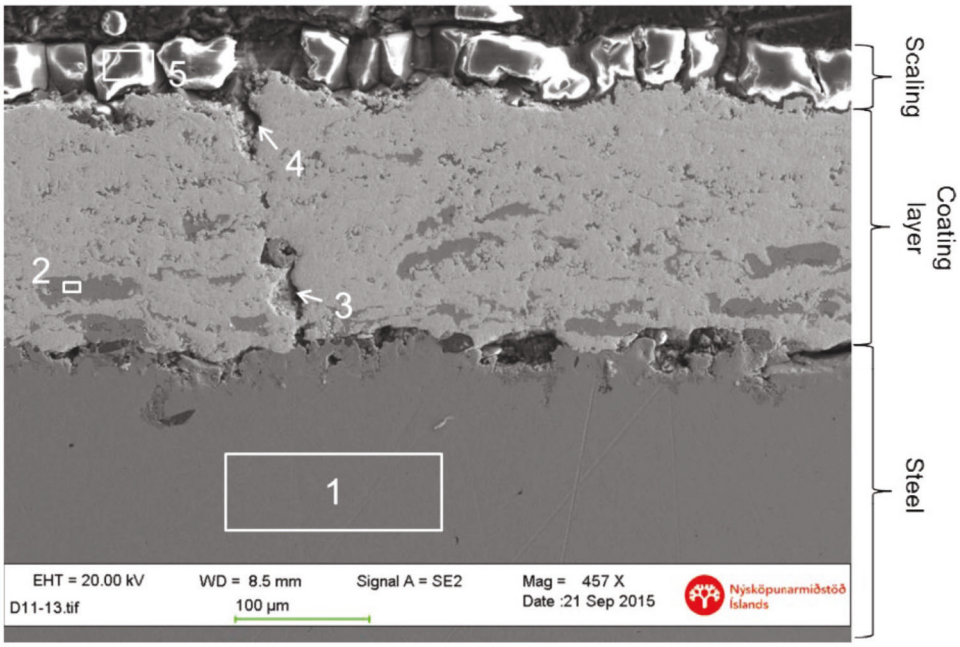


Figure 29. Cross-sectional SEM micrograph of HVOF WC-Co-Cr cermet coating deposited onto carbon steel, showing vertical cracks and voids at the interface after in-situ exposure test at the Hellisheiði geothermal power plant. Reproduced with permission.[141] Copyright 2017, Association for Materials Protection and Performance.

Cermets composed of NiCr/NiCoCr with added 5 wt.%Y_2O_3-X%ZrO_2 (Yttria Stabilised Zirconia) with X being either 3 or 5 wt.% were tested by Buzaianu et al.[138] for corrosion mitigation of geothermal steam turbine blades and rotor. The coatings were deposited by Atmospheric Plasma Spray (APS) onto 6%Cr-4%Ni and 1%CrMoNiV steel substrates for blade and rotor material respectively. The coatings were tested for corrosion resistance during exposure to a simulated geothermal environment (1.8% NaCl, 600 ppm CO_2, 50 ppm Na_2SO_4, and pH 7–8). Different temperature regimes were evaluated in the exposure tests: thermal cycling at 65 °C for 100 cycles of 1 h duration and isothermal heating at 400, 500, and 600 °C for 48 h. The performance post exposure was then evaluated by SEM-EDX analysis and microhardness test across the coating and substrate thickness. The results indicated the development of corrosion and thermal cycling-related cracks, which would hinder the application of the coating in the developed form.

Later, the same author[139] tested two WC-CoCr cermets, one deposited via HVOF (86WC10Co4Cr, METCO Andry 5843), and one by ESD (5WC9Co5Cr1Ni) for corrosion mitigation of geothermal steam turbine blade components. The coatings, deposited onto AISI 304 stainless steel, were tested for hot corrosion in contact with 10 wt.%NaCl-90 wt.%Na_2SO_4 salt during 10 heating-cooling cycles at 655 °C peak temperature and air cooling, with weight gain measured after exposure. Metallographic examination via standard analysis techniques and tribological characterization was also performed to evaluate surface roughness, friction coefficient, and wear rate in the as-deposited coatings. Results demonstrated that, although superior mechanical properties were measured in both cermet coatings compared to AISI 304 steel, the presence of defects in the coatings also led to their poor hot corrosion resistance.

Ti-based cermets, deposited by chemical and physical vapour deposition techniques were also evaluated for corrosion-erosion mitigation in geothermal environments. In a study by Sugama[140] titanium carbonitride Ti(CN) coating, 4 to 12 µm thick, was deposited by CVD for corrosion mitigation of AISI 1010 mild steel. Exposure tests were performed in acid-brine steam (1 wt.% H_2SO_4, 13 wt.% NaCl, 86 wt.% H_2O) at 200° under 1.45 MPa pressure for up to 28 days. Corrosion performance was evaluated by means of weight change measurements and surface characterization techniques. Results showed that although a general reduction in corrosion rate compared to the bare steel was observed by weight gain measurement, the coating was also susceptible to oxidation. In fact, dissolution of the coating was observed and linked to subsequent oxidation (TiO_2)→chlorination ($TiCl_4$)→dissolution reactions. Moreover, defects and pores discovered in the coatings were linked to the permeation of electrolyte through the coating, with development of Fe-corrosion products at the substrate/coating interface.

HVOF WC-Co-Cr coatings, deposited onto carbon steel for erosion-corrosion protection of geothermal steam turbine components in the Hellisheiði geothermal power plant (Reykjavik, Iceland), were tested by Ragnasdottir et al.[141] Large cracks were observed in the WC-Co-Cr coatings after in situ exposure test (**Figure 29**), however likely generated during the specimen preparation phase according to the authors.

More recently in the work of Houdkova et al.,[142] two types of cermets deposited by HVOF, WC-CoCr, and Cr_3C_2-NiCr, were tested for corrosion protection of carbon steel for geothermal steam turbine applications, alongside other Ni- and Fe-based alloys, also deposited by HVOF as well as TWAS methods. The coatings were exposed in autoclave for 105 days in a simulated

© 2023 The Authors. Advanced Materials Technologies published by Wiley-VCH GmbH

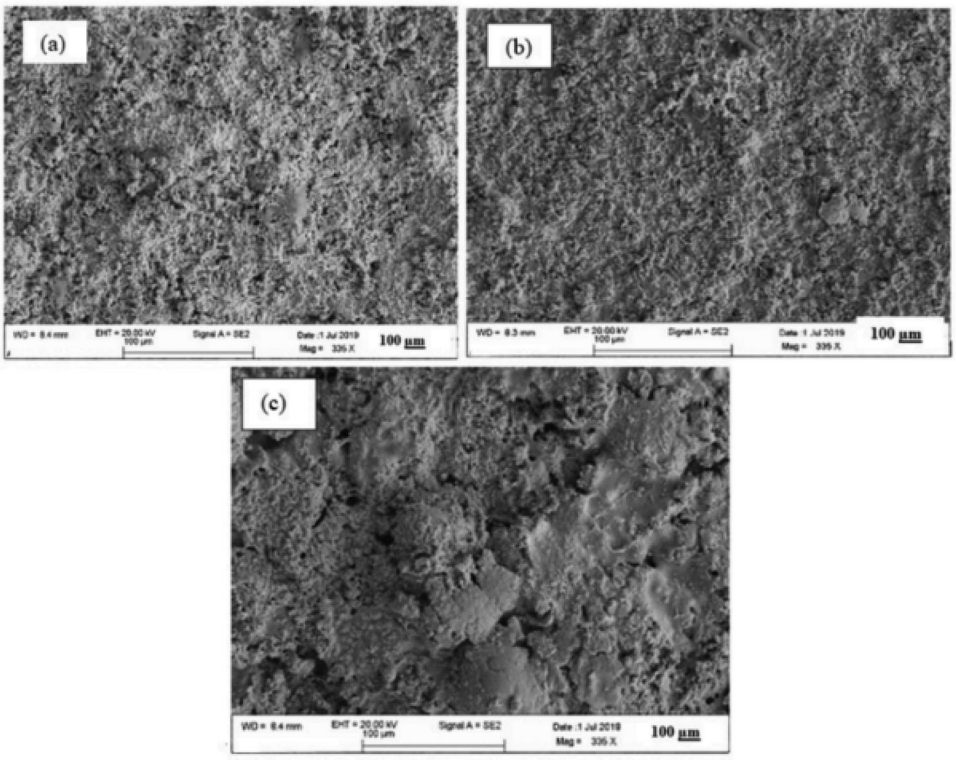


Figure 30. Surface SEM micrographs of the HVOF-deposited cermet coatings, tested against sliding wear behavior by Boakye et al.: a) WC-Co-Cr, b) Cr_3C_2-NiCr, and c) CA3 – Ni-Cr-Fe-Si-B-C. Reproduced with permission.[144] Copyright 2021, International Geothermal Association.

geothermal brine rich in chloride ions and CO_2, of pH 3.5–4, 250 °C temperature, and 12 bar pressure. Additional performance tests involved abrasive wear resistance and solid particle erosion resistance, together with standard microstructural examination and hardness tests. Results revealed that, in terms of wear and erosion resistance, the HVOF cermet coatings performed better, as expected than the other alloys. One of the cermet coatings, the HVOF Cr_3C_2-NiCr, also performed best among all coatings in corrosion resistance, with little evidence of developed corrosion products. Other coatings instead showed indication of corrosion degradation, on the coating surface and/or at the interface between coating and substrate in the form of crevice and pitting corrosion. According to the authors, the good corrosion performance of the HVOF Cr_3C_2-NiCr coating is linked to its low porosity compared to the other coatings.

More recently, HVOF-deposited cermets were tested, as part of the same European research program for corrosion and erosion mitigation, by Fanicchia et al.,[143] and Boakye et al.[144] Among other systems (i.e. HEAs, electroless plated Ni, etc.) three commercial coatings were tested, a WC-Co-Cr, a Cr_3C_2-NiCr, and a Ni-Cr-Fe-Si-B-C, deposited onto both carbon and stainless-steel substrates. In ref. [143], results are presented after corrosion and erosion wear tests. Pure corrosion tests were carried out with linear polarization resistance in 3.5 wt.% NaCl at 25 °C and pH 4 for 168 h, while erosion wear tests were performed with 220 mesh white alumina at 90° impact angle. Results from the corrosion tests show an overall poor performance of all the cermet coatings (corrosion rate >1 mm year^{-1}) compared to some of the other high-entropy-alloy and except for Cr_3C_2-NiCr, where a 0.1340 mm year^{-1} rate was measured. Conversely, the erosion wear performance was the lowest among all the systems tested in the project, with WC-Co-Cr performing best among all three cermets. In ref. [144], the sliding wear behavior of the same three cermet coatings was evaluated, together with bulk 304L and 630SS for comparison (**Figure 30**).

A WC ball of 6 mm diameter and 5 N applied load were used in the tests. Results showed a lower coefficient of friction of the cermet coatings compared to the bulk materials, with minimum surface damage and no penetration into the substrate material.

Chromium: The first reference to the use of chromium-based coatings can be found in the work of Borenstein[104] on corrosion mitigation of steam turbine blades in The Geysers geothermal area (California, USA). In the work, four different commercial chromium-containing coatings: one SermeTel, two SermaTel, and one high-velocity oxygen fuel sprayed Cr_3C_2 coatings, were deposited onto various steels and tested both in simulated conditions and field tests. Modified salt spray and erosion wear tests were employed, together with field tests involving specimens placed within a steam turbine. Results from the tests were not reported unfortunately.

Although not successful, Cr-plating was tested by Wiesner et al.,[145] alongside anodizing and electroless Ni-plating to mitigate erosion-corrosion of aluminum alloy AA7075-T6 steam turbine blades operating in the Salton Sea geothermal region. Preliminary deposition trials on wedges showed several challenges for this deposition technique, including likelihood of uneven coverage, poor adhesion, and accumulation of Cr on sharp edges and

© 2023 The Authors. Advanced Materials Technologies published by Wiley-VCH GmbH

corners. Cr-plating was therefore excluded as potential technique for the application.

Cobalt: To our knowledge, only one Co-based alloy, Ultimet UNS R31233 was tested for geothermal applications by Moore et al.,[146] together with other three Ni-based alloys (Inconel Alloy 625-UNS N06625, Hastelloy C276-UNS N10276, and AMS4777). The coatings, applied onto carbon steel, were evaluated for scaling and corrosion mitigation of pipelines in the Salton Sea geothermal region. The Ultimet-coated specimens were the only ones left on the custom-made test rig after the 1200 h wellhead exposure tests. A thick silicate scale was observed on the surface after the tests and metallographic analysis revealed coating spallation, likely due to stresses developed by the growth of corrosion products between coating and substrate. The authors therefore decided not to further employ the Ultimet alloy for further tests, in favor of Inconel Alloy 625.

Copper: Cu-plated carbon steel and bulk Cu materials, together with other plated coatings (Ni, Ni-P, Ni-W-P, and Zn) and surfaces (PVC, carbon steel, and Type 316 stainless steel), were part of a comprehensive investigation into scaling mitigation from calcium carbonate undertaken by Hashimoto et al.[147] The Cu surfaces showed large-scale adhesion (of calcite phase) values compared to Zn-, Ni-, Ni-P, and Ni-W-P-plated steel.

Gold: Gold-coated silica fibers were tested, alongside aluminum- and polyimide-coated ones, as a Raman-based distributed temperature sensing (DTS) system for hot geothermal wells in Iceland.[103] The gold-coated fibers were tested by heat treating them from 269 to 700 °C in four cycles and their performance was evaluated by measuring attenuation and microstructural evaluation after the test. Lower maximum heat treatment temperatures were used to test the other fibers. Results revealed a significant attenuation for both metal-coated fibers (gold and aluminum), which was linked to the micro-bending and different coefficient of metal expansion between silica and the metals.

With the same aim of developing temperature-resistant fibers for DTS systems, Jacobsen et al.,[148] used a thinner gold coating, 3–5 μm, compared to 15–25 μm typical of commercially available metal-coated fibers. Multiple heat treatment cycles from 25 to 500 °C showed consistent temperature sensing and a good mechanical integrity maintained throughout the test.

High Entropy Alloys (HEA): An AlCrFeNiMn HEA, manufactured by vacuum arc remelting as a preliminary step to application in coating form, was tested by Csaki et al.,[149] for corrosion in geothermal steam from the Reykjanes geothermal power plant (Iceland). Exposure was performed with steam at 200 °C and 1.65 MPa for 30 days, with corrosion performance evaluated by means of weight loss and SEM-EDX analysis. An average corrosion rate of ≈3 mm year^{-1} was measured after the exposure test, with the specimens' surface revealing a corrosion layer containing sulfur and oxygen. According to the authors, corrosion degradation in the alloy was driven by preferential dissolution of one of the two phases present in the alloy microstructure, defined of a spinodal nature. The alloy was therefore considered not suitable for the tested environment.

The same corrosion testing methodology, together with additional adhesion and tribological analyses performed on the coating in the as-deposited condition, was later used by the same authors[150] for a CoCrFeNiMo HEA, deposited in coating form by HVOF. In this case however, a much better corrosion performance was measured: 0.0001 mm year^{-1} corrosion rate. The good corrosion resistance of this alloy was attributed to the formation of a sulfur-free passive film. The alloy was therefore considered suitable for application in the environment as manufactured in coating form. Results from the mechanical tests also revealed satisfactory performance, with good adhesion, 12% increase in wear performance and 50% decrease in friction coefficient compared to the carbon steel plate.

The same group[151] therefore later prepared coatings of the same alloy composition, CoCrFeNiMo, by means of ESD deposition from an electrode produced by vacuum arc melting (VAM). Apart from standard microstructural and phase analysis (SEM-EDX and XRD) and mechanical analysis (Vickers hardness), corrosion behavior was investigated by means of linear polarization resistance (LPR) for 6 h and potentiodynamic polarization in 3.5 wt.% NaCl solution. The as-deposited coating showed an inhomogeneous distribution of elements, with a microstructure mainly composed of FCC phase and fractions of BCC and potentially σ. Performance results demonstrated a low corrosion rate of 0.0072 mm year^{-1} and a high hardness (593HV), together with good coating adhesion and density.

Six different compositional variations of the same alloy, with different amounts of elements Mo and Cu, were later investigated by Thorhallsson et al.,[152] as corrosion-resistant materials for geothermal casings exposed to superheated geothermal steam. The alloys were exposed in a flow-through testing facility used for to simulating the geothermal steam from the first flowing well in the Iceland Deep Drilling Project (IDDP1, Krafla region, Iceland), containing 250 ppm CO_2, 150 ppm H_2S, and 36.5 ppm HCl (pH 3) at 350 °C, 10 bar pressure, 0.3 mL min^{-1} flow rate for 240 h (10 days). Specimens after exposure were evaluated by metallographic examination and phase characterization methods to evaluate the nature of the surface deposits. Results from the tests revealed a variety of possible oxide chemistries on the surface of the four "non-Cu" containing HEAs, with the 10at%Mo (HEA2) alloy possibly identified as the most corrosion-resistant among them. Analysis of the Cu-containing HEAs revealed, in all cases, the presence of Cu_2S as main corrosion product. According to the authors, the Cu necessary for the formation of the Cu_2S layer would be provided by Cu intermetallics and combining with H_2S on the surface of the specimen (**Figure 31**). The authors suggested further exposure tests including HF, H_2, and SiO_2 species to resemble more closely the chemistry of the IDDP1 geothermal steam.

The same alloy composition, although with a reduced amount of Mo element, $CoCrFeMo_{0.85}Ni$, was produced in powder form, both by means of mechanical alloying and gas atomization and deposited by HVOF over carbon steel by Fanicchia et al.[153] for corrosion and erosion mitigation. Coatings were characterized for microstructure and phase composition and their corrosion performance was evaluated by means of linear polarization resistance in 3.5 wt.% NaCl at constant pH 4, 25 °C for 7 days. Results showed that the powder manufacturing technique has an impact on the corrosion performance of the coatings, with the mechanically alloyed powders providing coating of worse corrosion performance than the gas atomized powders. This was attributed to galvanic effects due to the nonhomogeneous phase distribution found in the coating obtained from mechanically alloyed powder.

© 2023 The Authors. Advanced Materials Technologies published by Wiley-VCH GmbH

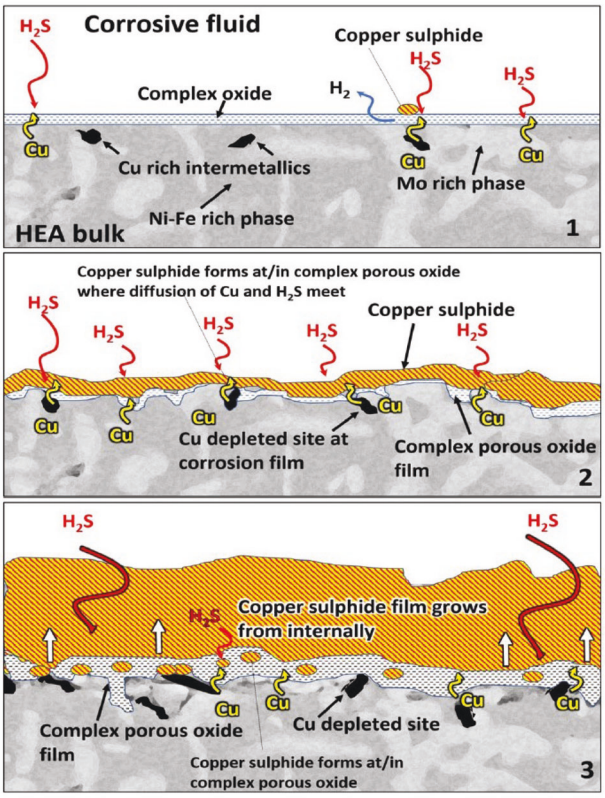


Figure 31. Cu_2S formation mechanism proposed by Thorhallsson et al., for Cu-containing HEAs after exposure to hot geothermal brine resembling the IDDP1 chemistry (Krafla region, Iceland). Reproduced with permission.[152] Copyright 2021, Elsevier.

The performance of the same $CoCrFeMo_{0.85}Ni$ alloy, together with another $Al_{0.5}CoCrFeNi$ alloy, both deposited by laser metal deposition, were later analyzed by Brownlie et al.,[154] and Thorhallsson et al.,[155] by means of laboratory and in-situ tests respectively. The two alloys were formulated to be composed, largely, of an FCC microstructure, as well as secondary phases to improve their mechanical properties. In the work of Brownlie et al.,[154] the two alloys, deposited onto stainless steel 304L (UNS S30403, $CoCrFeMo_{0.85}Ni$) and stainless-steel Type 316 (UNS S31600, $Al_{0.5}CoCrFeNi$) were analyzed for their erosion-corrosion performance against wrought carbon steel P265GH (EN10028) and stainless-steel Type 304 (UNS S30403). Erosion-corrosion testing was performed by using a custom-made submerged impingement jet test rig, using a slurry of angular silica sand in a 3.5wt.%NaCl solution of pH = 4 at a 90° impingement angle. Pure corrosion performance was also evaluated by using cathodic protection with quiescent and flowing (non-slurry) solution. Additional analyses included microhardness and microstructural examination by means of SEM and XRD. Results demonstrated that, in slurry conditions, all materials showed comparable pure corrosion and erosion-corrosion rates, likely the result of a depassivation/re-passivation mechanism. Corrosion-enhanced erosion appeared to represent the most prevalent attack in all alloys. For the two HEAs, the damage mechanism appeared to involve sliding abrasion in the outer regions (i.e., low-angle impingement), as well as plastic deformation and micro-cracking at high-angle impingement.

In the work by Thorhallsson et al.,[155] the same two HEAs, deposited by laser metal deposition onto carbon steel S235JR (EN 1.0038) and the two stainless-steel Types 316L (UNS S31603) and 304L (UNS S30403), were tested by in-situ exposure at the Hellisheiði geothermal power plant (Reykjavik, Iceland). Custom-made rigs were manufactured for tests, which were performed in three different environments: wellhead test at 194 °C, 14 bar pressure for 90 days, erosion test at 198 °C, 15 bar pressure for 60 days, and aerated test at 90 °C, 1 bar pressure for 90 days. All tests were performed in custom-made test rigs. Post exposure microstructural characterization was performed by standard techniques. Results suggested that cracks, observed in the $CoCrFeMo_{0.85}Ni$ coating deposited onto carbon steel and assumed being present in the as-deposited state, locally enhanced erosion damage (**Figure 32**).

The same cracks were not present in the same coating deposited onto stainless-steel, which suggested the need for future improvements in the $CoCrFeMo_{0.85}Ni$ alloy composition for use onto carbon steel. Moreover, results for the $Al_{0.5}CoCrFeNi$ coating revealed a greater susceptibility to corrosion and erosion damage compared to the $CoCrFeMo_{0.85}Ni$ alloy. For this alloy, both uniform and localized corrosion damage was observed, with an oxygen-rich layer measured after the aerated tests and >100 µm-deep erosion pits observed after the erosion test.

Three HEA coating compositions: $CoCrFeMo_xNi$, $Co_xCrFeMoNi$, and $Al_xCoCrFeNi$, deposited by laser cladding, high-velocity oxygen fuel spray, and electrospark deposition onto both carbon and stainless steel, were also assessed by Fanicchia et al.,[143] for corrosion and erosion wear resistance and compared to other cermets and electroless plated coatings and bulk alloys. For corrosion, linear polarization resistance was performed in 3.5 wt.% NaCl at 25 °C and pH 4 for 168 h, while erosion wear tests were performed with 220 mesh white alumina at 90° impact angle. Results showed that both the HEA material and technique have a significant influence on the final coating performance, both in corrosion and erosion wear. The best corrosion results were obtained with the laser-cladded $CoCrFeMo_xNi$ HEA, which was comparable to the performance of even the best-performing bulk alloys. It is worth noting that all the electrospark- and HVOF-deposited HEAs showed corrosion rates >1 mm $year^{-1}$. Two alloys, $CoCrFeMo_xNi$ and $Al_xCoCrFeNi$ also performed satisfactorily in erosion wear, with performances comparable, or even better than some of the cermet coatings.

Iron: The first reference to the use of an iron-based alloy coating (FeCrAl, Kanthal) was identified in the work of Borenstein[104] for corrosion mitigation of steam turbine blades in The Geysers geothermal area (California, USA). In the work, the alloy was electrospark deposited onto different steel substrates and tested in a modified salt spray test, erosion wear test, and field tests. No results were presented.

Explosive-cladded coatings of austenitic stainless steel 254SMO (UNS S31254) and Hastelloy C276 (UNS N10276), prepared both in the as-deposited and heat-treated conditions, were tested by Ragnasdottir et al.[156] for corrosion mitigation of carbon steel. Metallographic examination was performed on the specimens after in-situ exposure testing for 10 weeks in the Krafla geothermal region. Cracks were identified in both

© 2023 The Authors. Advanced Materials Technologies published by Wiley-VCH GmbH

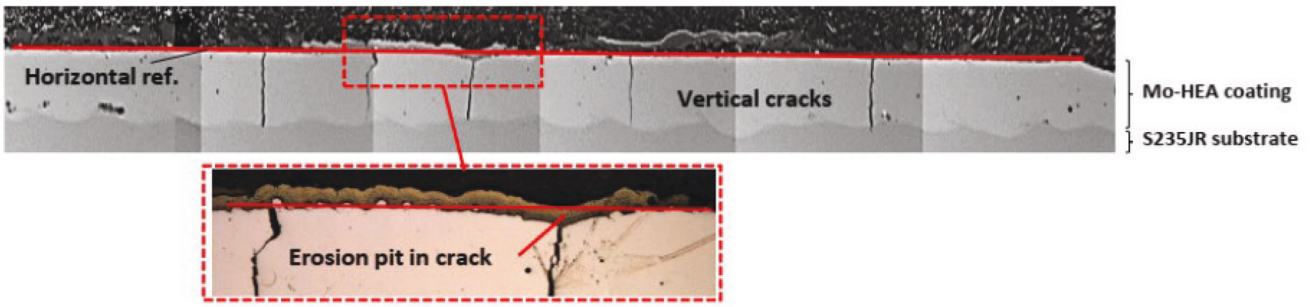


Figure 32. The laser metal deposited $CoCrFeMo_{0.85}Ni$ coating onto carbon steel revealed manufacturing cracks, which were considered responsible for a locally enhanced erosion damage after erosion in-situ exposure at the Hellisheiði geothermal power plant. Reproduced under the term of CC-BY license.[155] Copyright 2021, The Authors, published by MDPI.

coatings in the heat-treated form, although in higher density within the steel coating. Moreover, galvanic corrosion in exposed substrate/coating regions were identified in both coating systems, with the worst effect being recorded in this case on the Hastelloy specimen.

A series of stainless-steel weld overlays and plates, together with another Ni-based alloy, were evaluated by Amend et al.,[157] as repair solution for carbon steel in the Kawerau geothermal power plant (New Zealand). The focus of the study was to mitigate the harsh corrosive-erosive conditions experienced in acid-dosing areas of the power plant. To this aim, both circular weld beads and U-bend specimens of several weld overlays including 22%Cr and other grades of duplex stainless steel, Type 304L stainless steel, and carbon steel for comparison, were exposed for 5 months in a pH-modified brine and two-phase flow environments upstream and downstream of the acid injection location. The performance was evaluated by visual examination, weight loss, and measurement of pit depth. Results showed a significantly thinner scale and no pitting on any of the stainless-steel samples compared to carbon steel, therefore triggering a re-design of some of the affected power plant components to include stainless steel.

More recently, a study by Medvedoski et al.,[158,159] investigated iron boride coatings deposited by pack CVD technology, for corrosion mitigation of carbon steel in downhole tubing equipment. In the work, coated specimens of 155–220 μm thickness and control carbon and stainless steel coupons, were exposed to six different environments: a) 1.5% NaCl, 1.5% CaCl, 0.3% H_2S, 12.6% hydrocarbons, 17.7% CO, 69.4% CO_2 at 280 °C, 28 MPa, for 168 h, b) 15% HCl at 100 °C for 168 h, c) 70% H_2SO_4 at 100 °C for 168 h, d) mixture of alkali and earth-alkali chloride salts at 370–416 °C for 672 h, e) partial immersion into salt mixes solution (to obtain steam), heated to 370 °C for 168 h, and f) salt mixes solution under boiling conditions at 110 °C for 4 to 7 h. Specimens after exposure were analyzed by visual examination, weight loss, and microstructural examination. Results revealed no signs of corrosion-induced damage such as thickness reduction, cracking, delamination, or scale growth. The encouraging results, according to the authors, were linked to the inertness of the iron boride layer, given by its high crystalline lattice energy and consolidated, well-adhered microstructure.

Three Fe-based alloys, $Cr_{18.09}Ni_{17.9}C_{4.62}Al_{2.06}V_2Si_{0.25}Fe_{55.05}$, $Cr_{13}Fe_{87}$, and $Cr_{24}Al_8Y_{0.5}Fe_{67.5}$, were also deposited by TWAS and HVOF for corrosion mitigation of carbon steel in steam turbines by Houdkova et al.[142] The coatings, deposited to thicknesses in the range 369–537 μm, were subjected to 105 days exposure in a simulated geothermal brine containing Cl^- ions and CO_2, of pH-3.5–4, 250 °C, and 12 bar. Mechanical performance tests were also performed, together with standard microstructural examination. Results showed a limited oxidation and spallation evidence for all coatings, except the $Cr_{13}Fe_{87}$, which suffered the most corrosion damage, both at the coating/substrate interface and on the coating surface itself (**Figure 33**).

The best result, among all the tested coatings, was obtained with the $Cr_{18.09}Ni_{17.9}C_{4.62}Al_{2.06}V_2Si_{0.25}Fe_{55.05}$ TWAS coating, possibly linked to its high Ni and Cr content.

Nickel: Seven Ni-containing commercial alloy coatings, deposited onto various grades of steel, were evaluated already by Borenstein[104] for corrosion mitigation of steam turbine blades in The Geysers geothermal area (California, USA). Three electroless plated alloys, one plasma-sprayed Ni-Al alloy, two electroplated systems, and one nickel aluminide diffusion coating were manufactured in the study, among a total of 22 coating and paint systems. Both simulated and field tests were performed, as modified salt spray, erosion wear, and field tests in a real steam turbine. Unfortunately, however, results from the tests were not reported.

Electroless Ni-1 wt.% Cu-plated coatings were tested by Wiesner et al.,[145] on aluminum alloy AA7075-T6 substrates as erosion-resistant coatings for steam turbine blades in the Salton Sea geothermal region. The coating was tested alongside anodized and Cr electroplated coatings and was proven to perform best among the different coating solutions tested. The electroless Ni-plated coating was applied both on wedges at lab scale, as well as on a large (1.1 m diameter) mock-up turbine component to test the scalability of the deposition technology. The wedges were proven to withstand water droplets impinging at 457 m s^{-1} for 3 h, providing the minimum hardness of the coating was in the range 525–545 $DPH_{100\,g}$. Tests on plating of the mock-up turbine component showed poor adhesion, measured by bend test and vibratory marking pen, demonstrating the importance of deposition parameters optimization in the transition from lab-scale to production-scale processing. Nevertheless, the group successfully plated the whole component with a 0.075 mm coating layer.

Several electroplated Ni-based coatings were applied by Salvago et al.,[160] onto AISI 4137-H steel for sulfide stress corrosion cracking (SSC) mitigation of drill tool joints in the Larderello geothermal area (Italy). Different coating compositions: Ni, Ni-S,

© 2023 The Authors. Advanced Materials Technologies published by Wiley-VCH GmbH

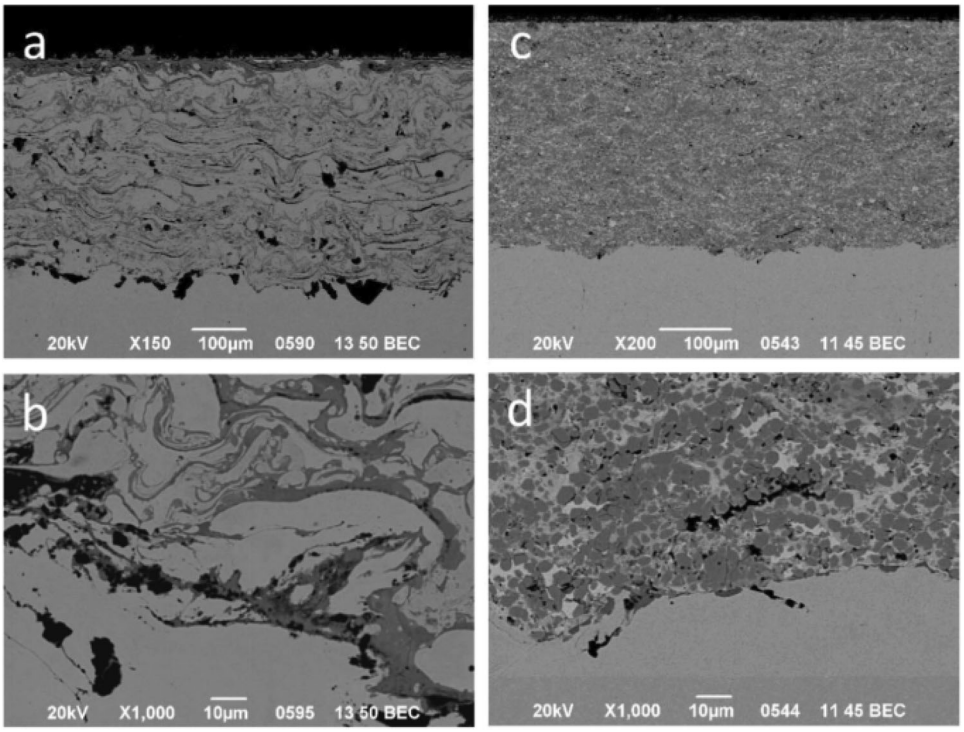


Figure 33. Cross-sectional SEM micrograph of a,b) TWAS-deposited $Cr_{13}Fe_{87}$ and c,d) HVOF-deposited Ce_2C_3-NiCr (cermet) coatings after 3 months exposure to simulated geothermal fluid. Corrosion damage is observed, particularly with the Fe-based alloy. Reproduced with permission.[142] Copyright 2021, Tanger Ltd.

Ni-P (chemical), Ni-P (electrolytic), and Zn-Ni were tested both by electrochemical and stress corrosion test methods in the presence of coating damages. For the electrochemical method, three solutions were used: a) 5% NaCl, 0.5% CH_3COOH at room temperature, b) 5% NaCl, 0.5% CH_3COOH at room temperature with H_2S bubbling, and c) a mixture simulating the geothermal fluid composition at Larderello, maintained at 80 °C and atmospheric pressure. For stress corrosion, tests were carried out both in laboratory and in a geothermal well. Laboratory tests were carried out in continuously circulating, simulated geothermal fluid (the same employed for the electrochemical tests) and in two operating conditions: d) 80 °C, 0.1 MPa pressure and e) 200 °C, 6 MPa pressure. Tests in the well were instead performed by exposing the specimens at a depth of 2000 m in the well Casaglia 2 (Ferrara, Italy) for 1000 h. Results showed that, in general, all coatings provided an improvement in SSC behavior compared to uncoated steel, due to galvanic coupling effects between steel and corrosion products. The authors note however that protection can only be provided when the corrosion product is made up of nickel sulfide (NiS) as demonstrated by the poor performance, in some of the tested conditions of the Zn-Ni coating, where ZnS was observed to form.

The same group, in a later study[161] addressed the advantages and dizadvantages of electroless Ni-based coatings, i.e., Ni and Ni-P, for corrosion protection of high-strength steels in geothermal environments (for drill pipes) and aluminum brasses (for power plant condensers) in river waters. In the work, some examples are presented in an attempt to highlight the benefits of the coatings deposited at different process parameters levels (e.g. pH) and exposed to three different environments ((a) i.e. 3.5% NaCl de-aerated solution at pH 4.5 and 25 °C, b) 0.4 mM NaCl, 0.2 mM Na_2SO_4, 2 mM $(NH_4)_2SO_4$, 11.5 mM H_3BO_3, 26.5 mM NaOH, 8.6 mM NH_4OH, pH 6.5, and 80 °C and c) 0.1 M Na_2SO_4, 0.5 mM $CuSO_4$, 5 mM NaCl, pH 3, and 25 °C). The results, generally demonstrating beneficial corrosion protection properties of the coatings in all environments, also highlighted the necessity to always test the corrosion behavior of the coating applied on the substrate, as opposed to testing the behavior of coating and substrate separately. Moreover, the authors also note the necessity of developing accelerated types of corrosion performance tests and the importance of including defects in the coatings for testing.

Plated Ni, Ni-P, and Ni-W-P-coated carbon steel sheets, together with other plated coatings Cu, Zn, and bare metallic and non-metallic surfaces PVC, carbon steel, Type 316 stainless steel, and Cu, were later tested by Hashimoto et al.[147] for calcium carbonate scaling mitigation in geothermal power plants components (i.e., cooling tower and heat exchanger). Scaling tests were performed by immersing the specimens, washed, and degreased with acetone, in a solution containing dissolved $NaHCO_3$ and $CaCl_2 \cdot 2H_2O$ at a 25 °C for 10 min, followed by an increase to 90 °C for ≈2 h. After the test, specimens were then air dried and the surface products analyzed. Results revealed a significant effect of metallic ions (Fe^{2+}, Cu^{2+}, Zn^{2+}, Ni^{2+}, and PO_4^{3-}) on the amount of scale adhered onto the surface with all coated specimens (expect the Cu-coated one), showing reduced scaling compared to the bare surfaces. The Ni-plated specimens resulted particularly successful with Ni-P and Ni-W-P showing the least amount of scale amongst all tested coupons. The specific nature

© 2023 The Authors. Advanced Materials Technologies published by Wiley-VCH GmbH

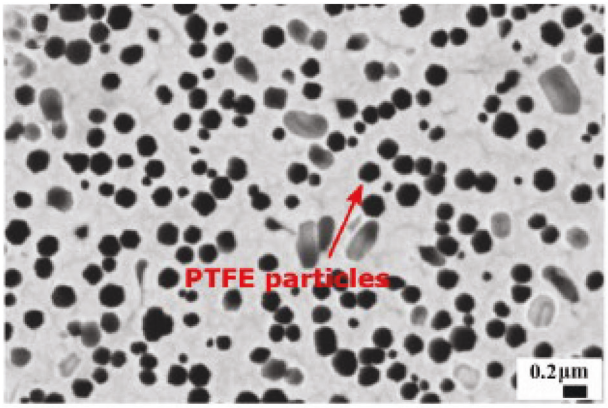


Figure 34. Sem micrograph of electroless plated Ni-P-PTFE layer as reported by Fanicchia et al. Reproduced with permission.[143] Copyright 2021, International Geothermal Association.

of the metallic ion was also observed to determine the specific polymorph of calcium carbonate deposited onto the surface, with primary phase being calcite (on PVC, carbon steel, Type 316 stainless steel, Cu and Cu-coated steel) and aragonite (on Zn, Ni, Ni-P, and Ni-W-P coated carbon steel).

The beneficial effect of electroless Ni and Ni-P coatings (i.e. Ni-5 wt.% P, Ni-8 wt.% P, Ni-12 wt.% P, and Ni-14 wt.% P) on calcium carbonate scaling mitigation was later further proven by the same group.[162]

Electroless plated Ni-P/Ni-P-PTFE coatings deposited onto carbon steel for corrosion and scaling protection in geothermal heat exchangers were also evaluated by Fanicchia et al.,[143] (**Figure 34**). In the published work, the project consortium evaluated the corrosion performance of the coating systems, together with other coatings including high-entropy alloys and cermets, in simulated geothermal environment by means of electrochemical test in 3.5 wt.% NaCl, 25 °C, and constant pH 4. Results demonstrated an excellent performance of the Ni-P/Ni-P-PTFE coatings, with the lowest corrosion rate measured among all the coatings and comparable to the 254SMO bulk alloy. This promising performance was not matched in exposure tests in real environments, as later published by the same group.

The microstructural, mechanical, and tribological properties of duplex Ni-P/Ni-P-PTFE electroless plated coatings, deposited onto carbon steel, was more recently evaluated by Boakye et al.[163] In the study, the effect of a variation in PTFE content in the coating (i.e., corresponding to concentrations of 5 g L^{-1}, 10 g L^{-1}, 15 g L^{-1} in solution) was evaluated against microstructural changes, hardness and sliding wear performance and surface energy variations, also in comparison to a reference 304L stainless steel alloy (UNS S30403). Results demonstrated an improved performance of all the coatings, irrespective of PTFE content, compared to the reference 304L. In particular, the coating with 10 g L^{-1} PTFE was found to perform best for low friction and wear applications at low contact load, while the coating with 15 g L^{-1} PTFE had good wear resistance performance but limited lubrication performance under dry contact sliding. This latter reduced lubrication performance was linked by the authors to a non-uniform dispersion of PTFE particles in the coating, suggesting the existence of a maximum PTFE concentration for enhanced performance.

Ni-P/Ni-P-PTFE electroless plated coatings, with low (≈4wt.%) and high (>11wt.%) P content, were studied by Davidsdottir et al.[164] for corrosion protection of carbon steel exposed to geothermal brine at the Hellisheiði geothermal power plant. Two different 3-months exposure tests were conducted: an in-situ exposure in wellhead HE-23 (15017 ppm CO_2, 1363.4 ppm H_2S, 62.1 ppm Cl^-, 58.44 ppmSO_4^{2-}, 194 °C, 12.6 bar) and exposure in aerated fluid connected to separator water (acidic pH, 90 °C, 1 bar, 492 L kg^{-1} air). Both flat-coated coupons and U-bend samples (to evaluate stress corrosion cracking behavior) were tested, the latter only exposed in the in situ wellhead test. Specimens were analyzed after exposure by metallographic examination, both on the surface and in cross-section. Results revealed pinholes and galvanic corrosion at the coating/substrate interface in specimens exposed to the aerated conditions. For the wellhead exposure, the formation of NiS on the surface of the specimens was instead the main feature observed, possibly generated by the interaction of H_2S in the brine and Ni from the coating. Cracks were identified in most specimens, generated according to the authors by hydrogen absorption and entrapment close to the PTFE particles. Functionalization of the PTFE particles to improve adhesion with the coating Ni-P matrix is therefore suggested by the authors as further improvement methodology.

A variety of thermally sprayed Ni alloys: Inconel (Ni 328), Ni-Al, Bondarc Wire-75B (95% Ni-5%Al), Nickel Wire-06T (99% Nickel), and Colmonoy 69 SC (70%Ni-17%Cr) were tested by King et al.,[137] alongside other thermally sprayed coatings, as metal-to-metal sealing systems for replacement of elastomer seals in deep geothermal applications. The coatings were applied onto internal and external diameters of AISI 304L tool joints to thicknesses varying between 0.254 and 1.52 mm and tested first by a pressurized water test (354 bar for 4 h to 10 days) and then by a pressurized/high-temperature silicon oil test (345 bar, 225° for 1000 h). Successful specimens were defined as those which did not leak (water/oil) by the end of the tests. Seven coatings successfully passed both tests, including all the Ni-based alloys, except for the Bondarc Wire-75B. However, as noted by the authors, no consistent results could be obtained thus suggesting the need to improve the control on spray parameters.

Thermally sprayed (arc spray) Ni-based alloy coatings were also tested by Moore et al.,[146] for scaling and corrosion mitigation of carbon steel pipelines used in the Salton Sea geothermal region. The coatings were seen as potentially able to replace expensive cement-lined and Ni-alloy piping currently employed to process the hypersaline, high-temperature brine found in the region. Carbon steel coupons were coated by means of four different alloys: a Co-based alloy (Ultimet, UNS R31233), and three Ni-based alloys (Inconel Alloy 625-UNS N06625, Hastelloy C276-UNS N10276, and AMS4777) to a thickness to approximately 380 µm. The coupons were mounted onto an ad-hoc manufactured holder and exposed in situ within a wellhead for 1200 h. Geothermal brine conditions were pH 5.5, temperature ≈250 °C, pressure ≈25.5 bar, and a flow of ≈3 m s^{-1}. Surprisingly the authors report that at the end of the test, only the Ultimet coupons were left on the sample holder, with the other specimens being lost likely due to a vibration of the wellhead piping. The

© 2023 The Authors. Advanced Materials Technologies published by Wiley-VCH GmbH

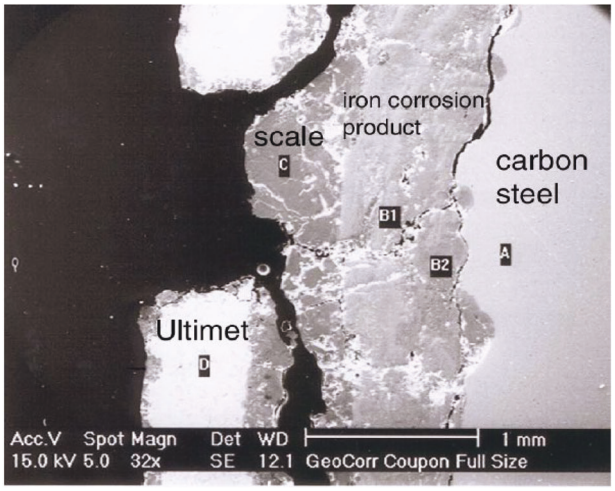


Figure 35. SEM micrograph of Ultimet-coated (Co-based alloy) carbon steel coupons after exposure for 1200 h within a wellhead in the Salton Sea geothermal area. Scale and corrosion products are observed at the interface between coating and substrate because of brine permeation through defects in the coating. Reproduced with permission.[146] Copyright 2002, Geothermal Rising.

remaining Ultimet coupons visually showed a thick adhered silicate scale on the surface of the coupons (**Figure 35**).

Further metallographic analysis revealed spallation of the coating due to brine permeation through defects in the coating, which caused the growth of corrosion products at the substrate/coating interface. After the first test, a second 5000 field test was also run by using a carbon steel pipeline internally coated with Inconel Alloy 625. However, results from this exposure test were not presented in the paper.

A NiCrMo alloy, applied onto carbon steel both by weld overlay and HVOF methods was also tested, among other stainless-steel solutions by Amend et al.[157] The aim of the work was to identify material solutions to very corrosive-erosive brine in acid-dosing carbon steel components. To this aim, both circular weld beads and U-bend specimens of several weld overlay materials, were exposed for 5 months in a pH-modified brine and two-phase flow environments upstream and downstream of the acid injection location. Visual inspection, weight loss, and pit depth analysis were used to evaluate the specimens' performance. Results showed no significant difference between the performance of specimens welded with NiCrMo and stainless steel, therefore suggesting no significant galvanic effect with the materials studied.

Berndt et al.,[165] also tested HVOF-sprayed Inconel Alloy 625 (UNS N06625) coatings, deposited onto carbon steel substrates to two final thicknesses 330 and 560 μm, for corrosion mitigation in a hypersaline synthetic brine of pH = 4.15 and ambient pressure and temperature. The coatings were tested alongside wrought and clad Incoloy Alloy 825 (UNS N08825) and Hastelloy C276 (UNS N10276) specimens. The different manufacturing methods were employed to evaluate the potential effect that defects, and surface preparation have on the corrosion performance. The cyclic potentiodynamic polarization method was employed to test the different systems. Analysis of the polarization curves showed a general absence of distinct features such as primary passivation, pitting, and repassivation potential and therefore only corrosion potential corrosion current density and the general form of the curves could be compared. Nevertheless, results showed that wrought Inconel 625 performed best among the alloys tested, while passivity is only observed in both wrought and clad Hastelloy C276 specimens. Moreover, the corrosion behaviour of the HVOF coatings (Inconel Alloy 625) appeared to differ from the one of the wrought and clad specimens, with a more active potential and lower current density measured in the former.

Several Ni-based coatings were also tested by Ragnarsdottir et al.,[141] as deposited onto carbon steel for mitigation of erosion-corrosion damage in geothermal steam turbines of the Hellisheiði geothermal power plant (Reykjavik, Iceland). Results showed that, among the Ni-based coatings tested, the HVOF NiCrBSiFeC was the best performing, with the least number of cracks identified. This coating also resulted the best among the remaining coatings tested in the work.

Coatings of Hastelloy C276 (UNS N10276) and 264SMO (UNS S31254), deposited by explosive cladding, were also employed by Ragnarsdottir et al.,[156] for corrosion mitigation of carbon steel in geothermal steam from the Krafla geothermal region (Iceland). In the work, both flat (for corrosion only) and U-bend coupons (for Stress Corrosion Cracking, SCC) were exposed, in situ, to CO_2 and H_2S-rich geothermal steam directly within one of the wellheads for 10 weeks. Measured steam properties at the test location were a 190 °C temperature, 14 bar pressure, pH 8.57, and an 18.42 kg s^{-1} flow rate. Both visual inspection and metallographic examination were performed after the tests to characterize the results. Results showed that heat treatment post-coating operation has a significant effect on performance as cracks were observed only in the heat-treated specimens. Heat treatment seemed however beneficial in mitigating cracking and pitting at the substrate/coating interface, which triggered the authors to suggest future improvement in the heat treatment parameters. Furthermore, no cracking typical to SCC degradation was observed in any of the specimens and scales mainly composed of elements S and Cl were detected on the exposed surfaces. According to the authors, the Hastelloy C276 coating showed the best performance among the ones tested.

In another study by Csaki et al.,[166] a NiCrBSi (Ni ≈82 wt.%) HVOF thermally sprayed coating was tested for erosion-corrosion protection of carbon steel through in-situ exposure at the Hellisheiði geothermal power plant (Reykjavik, Iceland). In the work, coated coupons and un-coated carbon steel specimens were exposed for 30 days to steam at 210° temperature, 18 bar pressure, and 31 m s^{-1} velocity in an ad-hoc testing apparatus built to simulate conditions of the fluid entering the steam turbine in the power plant. Analysis included microstructural analysis, adhesion, cohesion and wear resistance for the as-deposited coating, and microstructural analysis after exposure. Results demonstrated that, although the adhesion and wear resistance of the as-deposited coating were superior to those of the carbon steel material, its exposure led to coating delamination, vertical cracking in the coating and formation of corrosion products at the substrate/coating interface. The authors therefore suggest the possibility to include a bondcoat between substrate and coating in future studies.

More recently, in the study of Houdkova et al.,[142] two Ni-based alloys, both of the $Cr_{20}Ni_{80}$ type, were deposited by Twin wire arc

© 2023 The Authors. Advanced Materials Technologies published by Wiley-VCH GmbH

spray (TWAS) and HVOF over carbon steel for corrosion mitigation of steam turbine components.[142] The coatings were tested in simulated geothermal brine containing Cl^- ions and CO_2 for 105 days, followed by standard microstructural and visual examination and further mechanical tests. Among the tested coatings, the two Ni alloy specimens performed satisfactorily, with no indicative signs of corrosion damage, although the alloys were not listed as the best-performing ones.

Oxides (Al, Si, Ti, Y, Zr): Although not successful, a hard anodized layer of aluminum alloy AA7075-T6 was tested against water droplet erosion for mitigation of geothermal steam turbines used in the Salton Sea area (USA) by Wiesner et al.[145] The coating was tested alongside Cr electroplating and electroless Ni plating, deposited onto substrates with a wedge geometry. Although details of the anodizing procedure are not reported by the authors, the measured 0.05 mm hard-anodized layer was observed to fail in 10 to 15 min the water droplet impingement test. The failure was also linked to coating spallation at the sharp tip of the wedge-shaped substrate. The coating was therefore discarded from the options in the work.

A comprehensive testing campaign was then reported by Ragnarsdottir et al,[141] who analyzed the erosion-corrosion behaviour of plasma sprayed Al_2O_3/TiO_2 coatings, together with Ni-based alloy, Ti, and WC-Co-Cr coatings deposited onto carbon steel substrates. The coatings were tested in a custom-made rig manufactured to simulate the erosion-corrosion environment experienced by the steam turbine components. The rig was connected directly to one of the wellheads at the Hellisheiði power plant and two test exposure durations were performed (on repetitions of each coating) to evaluate the repeatability of the test: 38 and 31 days. The measured steam properties were 210° temperature, 18 bar pressure, 31 m s^{-1} velocity, and pH 8.24, with a significant concentration of NCGs CO_2 and H_2S. Visual inspection, surface profilometry, and microstructural examination were employed to analyze the specimens after exposure. Results showed that, among the Ni-based alloys, only one specimen (HVOF NiCrBSiFeC) showed satisfactory results, while cracks were observed in all other Ni-based coatings. For the Al_2O_3/TiO_2 coating, although no cracks or delamination was observed, a significant erosion rate was measured, with coating completely absent in some areas (**Figure 36**).

Large cracks were observed on the Ti- and WC-Co-Cr-coated specimens, however these were likely generated during specimen preparation for analysis according to the authors. The erosion-corrosion behavior of these later coatings however resulted generally satisfactory according to the authors.

Coatings of Al_2O_3, deposited by sol–gel method to a thickness of 8.4 ± 0.3 µm (with a three-layer application), were evaluated by Aristia et al.[167] for corrosion protection of martensitic steel (X20Cr13, UNS S42000). In the work, the corrosion resistance of the coatings was evaluated by exposure to simulated geothermal water resembling the North German Basin (166 g L^{-1} Cl^-, 0.05 g L^{-1} SO_4^{2-}, 56.5 g L^{-1} Ca^{2+}, 0.5 g L^{-1} Mg^{2+}, 3.1 g L^{-1} K^+, 38.7 g L^{-1} Na^+, 0.2 g L^{-1} NH_4^+, and 1.55 g L^{-1} Sr^{2+}) at 150 °C, 1 MPa for 168 h and EIS at 150 °C for 24 h. Microstructural examination, both on the exposed surface and in cross-section, was employed to characterize the specimens after exposure. Results from the exposure tests revalued that already after 1 h the Al_2O_3 was transformed into AlOOH, which resulted stable until up to

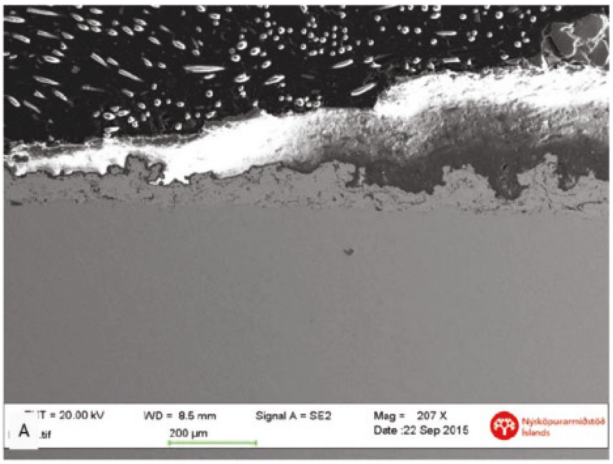


Figure 36. Cross-sectional SEM micrograph of Al_2O_3/TiO_2 coating after 38 days in-situ exposure at the Hellisheiði power plant (Iceland), showing no cracks nor delamination, but significant erosion wear. Reproduced with permission.[141] Copyright 2017, Association for Materials Protection and Performance.

3 months of exposure. The absence of Fe and Cr elements on the surface of the specimens after three months confirmed the protective nature of the coating, especially when compared to a corroded uncoated steel sample. The protective nature of the coating was also confirmed by the high absolute impedance values measured in the EIS test. Further tests to evaluate the mechanical performance, adhesion, and other corrosive properties were however suggested by the authors before the use of the coatings in geothermal applications.

The performance of SiO_2 coating systems, deposited via liquid phase deposition, was tested by Chen et al.[168] with the aim of developing a fouling- and corrosion-mitigation solution for copper components. In the study, after an initial study on deposition parameters optimization, where the coating roughness, thickness, morphology, and chemical composition were assessed by standard characterization techniques, fouling and corrosion experiments were performed. Fouling experiments were conducted in saturated $CaCO_3$ solution, while real geothermal water from the well No. 2 at the Tianjin University was employed for the corrosion tests. In both cases, tests were run at different temperatures from 40 to 90 °C and for up to 360 h, followed by microstructural characterization and surface roughness and energy analysis. Results indicated significantly improved fouling performance of the coating system compared to the bare copper substrates (see **Figure 37** left). However, although the new system was able to inhibit corrosion after a short exposure time, a decrease in coating mechanical performance led to a corresponding decrease in corrosion mitigation after long-term exposure (see Figure 37 right).

SiO_2 coatings, deposited by liquid phase deposition method to thicknesses of hundreds of nm for fouling and corrosion mitigation of copper, were also tested by Ning et al.[169] In the work, the effect of varying deposition parameters onto the thickness, roughness, surface free energy, surface morphology and composition of the coatings was tested. Moreover, fouling and corrosion performance was measured by exposure to saturated $CaCO_3$ solution and geothermal water at No. 2 geothermal well

© 2023 The Authors. Advanced Materials Technologies published by Wiley-VCH GmbH

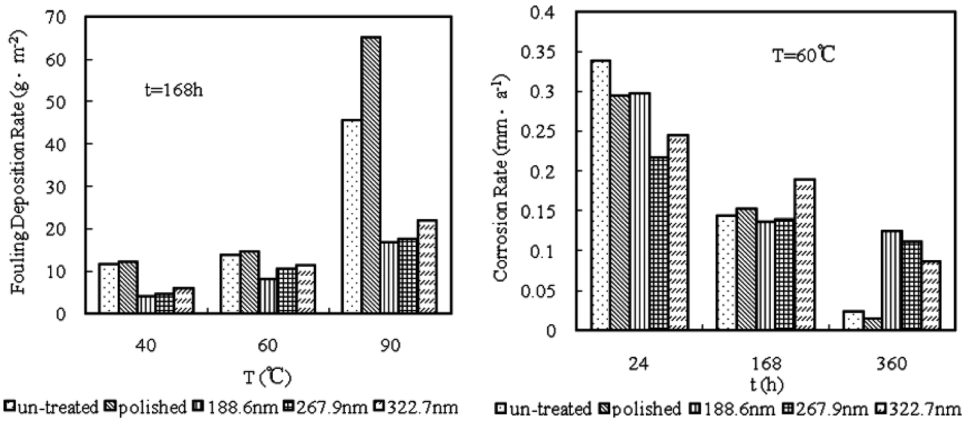


Figure 37. The performance of bare and SiO_2 coated copper substrates, at different coating thicknesses, was assessed against (left) fouling and (right) corrosion performance by Chen et al. Results showed improved fouling performance but corrosion mitigation only at short exposure times, due to worsening of the coating mechanical properties. Reproduced with permission.[168] Copyright 2021, American Chemical Society.

in Tianjin University (90 °C temperature, 1993.2 ppm SO_4^{2-}, 815.4 ppm Cl^-, 776.0 ppm Na^+, 621.2 ppm Ca^{2+}, 375.3 ppm HCO_3^-, 57.8 ppm Mg^{2+}, 39.0 ppm K^+, 24.5 ppm SiO_2) respectively. In this latter case, specimens were removed after different exposure times and tested by electrochemical impedance spectroscopy experiments. Results indicated reduction in scaling by the application of the SiO_2 coating compared to the bare Cu substrate. Moreover, corrosion inhibition was clearly observed after a short immersion time, even though this decreased after longer exposure times due to coating delamination. The authors conclude that the systems can represent a valid alternative to organic coatings in geothermal applications.

Another interesting application of SiO_2 coatings obtained from geothermal waste can be found in the work of Silviana et al.[170] In the study, SiO_2 coatings were prepared by sol-gel method and applied by spraying onto glass substrate, targeting a maximization in contact angle. The effect of a variation in manufacturing parameters, determined by a design of experiment statistical approach, was correlated to changes in surface morphology, phases, and microstructural features. Results demonstrated hydrophobicity of the coated surfaces, with a maximum contact angle value of 130.9° obtained by using 2% sodium silicate and 2% methyltrimethoxysilane (MTMS) concentrations.

TiO_2, SiO_2, and SiO_2-FPS (3,3,4,4,5,5,6,6,7,7,8,8,9,9,10,10,10-heptadecafluorodecyltri-isopropoxysilane, $C_{19}H_{25}F_{17}O_3Si$), deposited by sol-gel and liquid phase deposition (LPD) methods onto AISI 304 stainless steel, were tested by Song et al.[171] for scaling and corrosion mitigation in heat exchangers in contact with hot-dry-rock (HDR) geothermal water. A custom-made experimental equipment utilizing two types of simulated geothermal fluid from the Yingshen area (Daqing of China), one rich in calcium carbonate for scaling experiments and one resembling the real water (which is rich in HCO_3 and Cl^-/Na^+ ions), were employed for the experiments. The temperature of the fluid was maintained at 150 °C at the inlet of the heat exchanger during the exposure experiments, which were run for up to 21 days. The coatings were analyzed for surface morphology, roughness, static contact angle and surface free energy, scaling performance, and corrosion performance. This latter was performed by using electrochemical methods potentiodynamic polarization and electrochemical impedance spectroscopy methods. Results demonstrated that in the scaling-specific fluid, a 48% reduction of fouling was obtained by using LPD TiO_2 and sol-gel TiO_2 coatings compared to bare 304 alloy. Moreover, in the simulated real geothermal fluid, the sol-gel SiO_2 and SiO_2-FPS coatings were proven to reduce fouling by over 30% compared to the bare substrate. Electrochemical tests performed on the same coatings further demonstrated a reduction in corrosion rate in the order of 60% compared to the Type 304 stainless-steel substrate, which was considered promising for real application by the authors. The authors however suggested that further work would be needed in increasing exposure times and performing the tests in geothermal fluids of different chemistries.

TiO_2 and TiO_2-FPS (3,3,4,4,5,5,6,6,7,7,8,8,9,9,10,10,10-heptadecafluorodecyltri-isopropoxysilane, $C_{19}H_{25}F_{17}O_3Si$), deposited by liquid phase deposition and sol–gel methods respectively onto AISI 304 stainless steel, were also tested by Lv et al.[172] for scaling and corrosion mitigation in pipeline and heat exchanger applications (**Figure 38**). In the study, the surface free energy, surface morphology and chemistry and corrosion performance (measured by electrochemical methods) were assessed while exposing the samples to simulated geothermal water and crude oil at different ratios (V_{oil}:V_{water} = 0:1, 1:15, 1:25, 1:35, 1:45, and 1:55). The 80 °C water chemistry was selected to simulate the one from the Huabei oilfield geothermal water (China) and the tests were run for 720 h.

Results from tests in geothermal water (V_{oil}:V_{water} = 0:1) demonstrated that the TiO_2-FPS coating provided superior scaling and corrosion protection compared to TiO_2 and bare stainless steel, mainly due to its superior hydrophobic properties. Tests in geothermal water containing oil indicated that when V_{oil}:V_{water} = 0:25, the lowest fouling rate is again measured in the TiO_2-FPS system. These tests also demonstrated that oil and minerals contained in the water phase both contribute to the scaling behaviour. The authors specified how further tests would be needed to separate the contribution of water and oil scaling and fundamental mechanisms of oil adhesion.

A Y_2O_3–based system, deposited by sol–gel method onto Inconel 625 alloy substrate, was manufactured by Sugama[173] for oxidation and corrosion mitigation. The coating was deposited

© 2023 The Authors. Advanced Materials Technologies published by Wiley-VCH GmbH

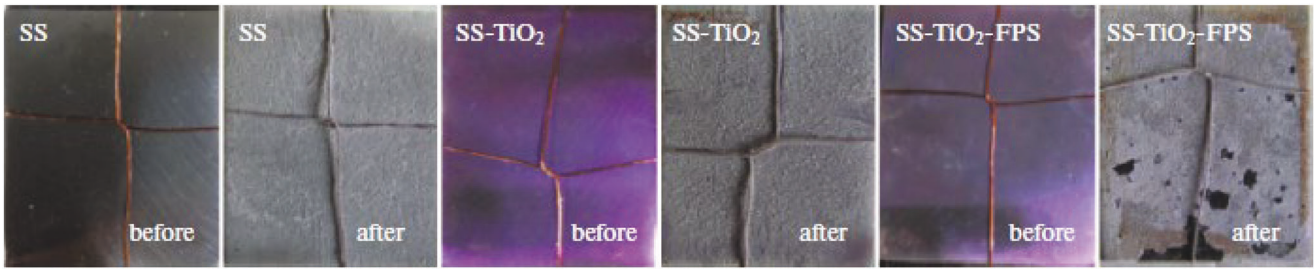


Figure 38. Surface photographs of the un-coated 304 stainless steel coupons and coated coupons before and after immersion for 720 h in simulated geothermal water at 80 °C. Reproduced with permission.[172] Copyright 2018, Springer.

by sol-gel method from yttrium acetate tetrahydrate as precursor powder and tested for oxidation resistance by weight gain measurement after exposure to atmospheric oxygen at 900 °C for up to 8 days and corrosion resistance by potentiodynamic polarization in 0.5 M NaCl solution at 25 °C. The 0.5 to 1.5 μm thick coatings were later analyzed for surface morphology and phase composition pre- and post-exposure tests to evaluate the evolution of the coating chemistry. Results from the oxidation tests revealed that at temperatures >700 °C, yttrium carbonate originally present in the coating, is transformed into Y_2O_3, while at the same time, the Inconel 625 substrate oxidation led to the growth of Cr_2O_3. The interaction between Y_2O_3 and Cr_2O_3 eventually yielded chromium yttrium oxide $YCrO_3$, which was observed to promote densification in the coating. This optimal coating density, together with the strong affinity of Y_2O_3 with oxygen, was therefore linked to the observed superior corrosion resistance of the coated system compared to bare Inconel 625.

A composite ZrO_2–TiO_2 coating, deposited by LPD onto AISI 304 stainless steel was tested for corrosion protection by Cai et al.[174] In the study, coating morphology and phase characterization was performed before and after corrosion performance tests evaluated by electrochemical methods in simulated geothermal water resembling the composition characteristic of central China (NaCl rich). The tests were run for up to 720 h and the water was maintained at 50 °C during the experiments. Results demonstrated that the as-deposited pants consist of nanoparticles of a 20–30 nm size range, which vary from amorphous to a crystalline state with increasing sintering temperature from 500 to 800 °C. Electrochemical experiments also demonstrated a superior corrosion performance of the coatings compared to the bare stainless steel, although an increase in corrosion rate is observed at prolonged exposure time (>360 h). This performance degradation is associated with a combined pitting and scaling mechanism, which the authors claim to promote each other (**Figure 39**).

Polymer Concrete: Polymer concrete (PC) is a type of concrete in which part, or all the cement binder is replaced with polymers. In geothermal applications, PCs have been employed in coating form as corrosion protection liner with thicknesses in the range 6–13 mm, for components such as pipelines, vessels, and heat exchangers.

The promising performance of PC mortars coatings were already mentioned in the review by Reeber.[16] The author refers to several recent and ongoing tests on novel PC compositions developed at the Brookhaven National Laboratory. A PC mortar applied to carbon steel material and tested in autoclaves for

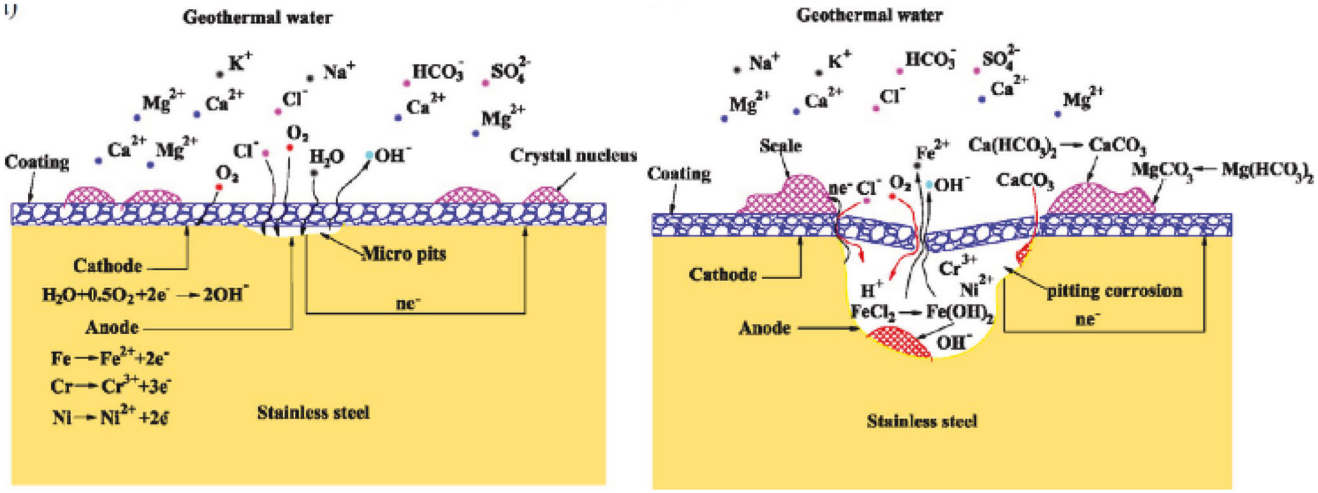


Figure 39. Schematic representation of corrosion and scaling mechanisms proposed by Cai et al. involving composite ZrO_2-TiO_2 coatings deposited onto AISI 304 stainless steel and exposed to NaCl-rich simulated geothermal water at 20 °C. a) The tortuous path of O_2 and Cl^- through the protected coating at the initial stage and b) coating damage and scale formation processes after prolonged immersion time. Reproduced with permission.[174] Copyright 2016, American Chemical Society.

© 2023 The Authors. Advanced Materials Technologies published by Wiley-VCH GmbH

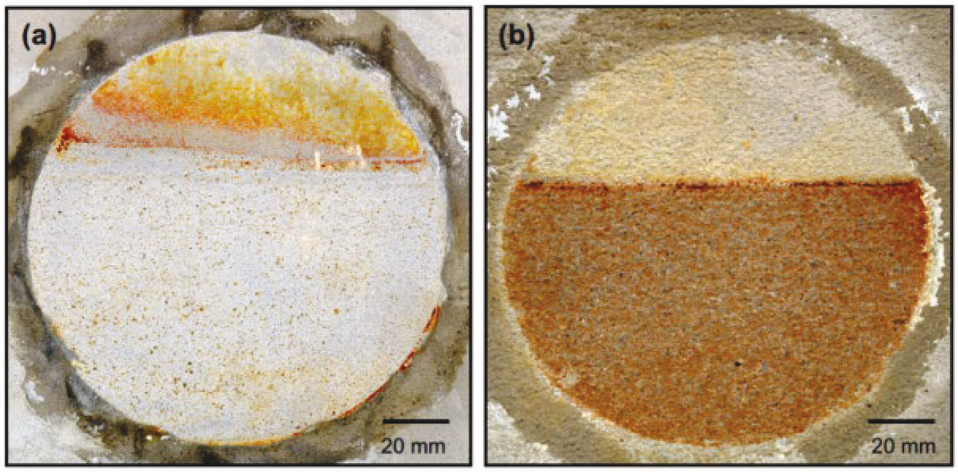


Figure 40. Surface photograph of a) Sikagard 75 EpoCem mortar and b) latex-modified mortar after exposure to *Thibacillus. ferrooxidans* showing very slight etching in immersed zone. Reproduced with permission.[80] Copyright 2011, Elsevier.

2 years at 238 °C in a geothermal brine containing 28% of dissolved salts was measured to retain more than 80% of its strength and impermeability to water after the test. Several tests were then also reported of PC mortars containing monomers such as styrene, acrylonitrile, and trimethylopropane trimethacrylate (TMPTMA) with a 9:1 sand:Portland cement mixture. Moreover, PC coatings were applied to several steel pipes to thicknesses of ≈9.5 to 19 mm and installed in four geothermal regions in the USA: China Lake (California), East Mesa (California), Raft River (Idaho), and Niland (California). Visual examination after extended period of exposure (>1 year) shows in all cases limited scale build-up and no apparent development of corrosion damage. The same was reported true for a PC using a high-temperature resistant monomer, exposed both in simulated and field tests to a 220° brine containing 28% of dissolved salts. More details on these tests can be found in the earlier reports by Kukacka et al.[175,176]

Later work from the same group, in collaboration with the Idaho National Engineering Laboratory, evaluated the application of the same class of PCs onto counterflow heat exchangers.[177] Field tests in aggressive geothermal brine had to be terminated after only 30 h due to plugging of the tubes. An examination of the tubes revealed that the plugging was caused by non-uniform application of the PC coating. Further tests were then resumed later by the same group after devising a method for uniform application of the PC coating to a thickness of ≈0.8 mm. The exposure test was then run for 75 days, by comparing the PC-coated heat exchanger tubes with a control AL-6XN (UNS N08367).[178] Results identified comparable heat transfer and pressure drop performance for the PC-coated and control tubes, suggesting a similar fouling rate. However, further analysis[179] of the same tubes revealed instead a significantly thicker (≈8.5% more) and more strongly adhered (>6 times) scale layer in the PC-coated tubes compared to the control AL-6XN ones. The authors therefore suggested the use, in future tests, of a novel PC formulation to reduce the adhesion strength between scale and PC.[180]

More recently, other PC mortar chemistries were evaluated by Berndt,[80,81] to improve resistance of concrete to microbiologically influenced corrosion induced by *Thiobacillus ferrooxidans* sulfur oxidizing bacteria in geothermal cooling tower basins. Three PC mortars were evaluated: an epoxy-modified cementitious mortar (Sikagard 75 EpoCem, Sika) a custom-made latex-modified mortar and a commercial calcium aluminate cement mortar designed for use in sewers (SewperCoat, Lafarge) (**Figure 40**).

The PCs were tested alongside other three epoxy coatings. Only for the custom latex-modified mortar, a bondcoat composed of a slurry mix of cement and latex was applied on the concrete surface prior to PC application. The coatings were exposed both in a lab environment (40° for 60 days) and field tests within a cooling tower of a geothermal power plant in Indonesia (38°, pH 7.8–8.0, <40 ppm $CaCO_3$, for 8 months). Results showed improved resistance compared to the control concrete for all three PCs, with the SewperCoat calcium aluminate cement mortar being virtually unaffected after both lab and field tests. The good performance was attributed to the stability of the alumina hydrate phase forming in low pH conditions, and to the inhibiting effect on acid formation provided by Al^{3+} ions. Additionally, none of the epoxy paints or PC mortars subjected to lab exposure showed a statistically significant reduction of bond strength, which is promising for long-term protection capability.

Later, a polymer-modified foaming cement, with added corrosion inhibitor, was developed and tested By Sugama et al.,[181] for corrosion protection of carbon steel casings in Enhanced Geothermal Systems (EGS). The cement consisted of Secar #80, Class F fly ash, and sodium silicate treated with cocamidopropyl dimethylamine oxide-based compound as a foaming agent and modified with acrylic polymer emulsion as corrosion inhibitor. These modifications were performed with the aim of producing a low-density (<1.3 g cm^{-3}), corrosion-, and thermal-shock-resistant cement. Performance tests involved exposure to a hydrothermal temperature of 200 °C for 24 h, followed by electrochemical corrosion tests at 25 °C in a 1.0 M NaCl solution. The density, compressive strength and toughness, and microstructural examination were performed on the specimens prior, and post hydrothermal exposure. Results showed that the performance of the coating depended on the concentration of the foaming agent and acrylic polymer in the initial cement

© 2023 The Authors. Advanced Materials Technologies published by Wiley-VCH GmbH

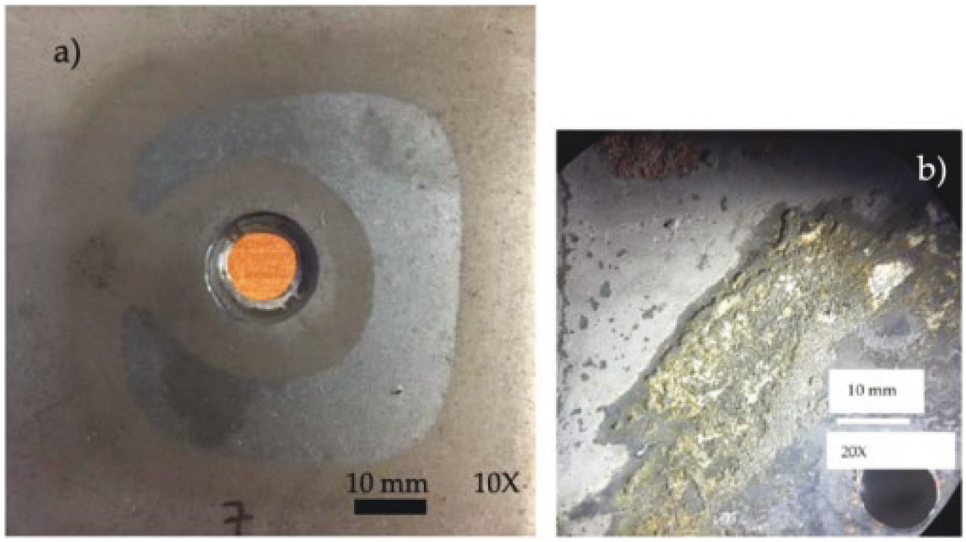


Figure 41. Surface photographs of a) TiB_2-Ni_3B nanocomposite coating and b) uncoated stainless-steel type 304 specimens after 1 month in situ exposure to geothermal fluid at the Geothermal Unit Los Humeros (Mexico); no clear corrosion products are visible on the coated coupon as opposed to the steel substrate. Reproduced with permission.[183] Copyright 2021, Institute of Physics.

mix. The authors report an optimum concentration of 1 wt.% foaming agent and 2 wt.% acrylic polymer providing a density <1.3 g cm^{-3}, a compressive strength >3.44 MPa, and a corrosion rate <1.78 mm $year^{-1}$. The improved performances were linked to reduced permeation of electrolyte, inhibition of cathodic reactions on the carbon steel surface, improved adherence of the cement to the substrate and extended coverage of the coating over the carbon steel substrate.

Titanium: Two TiN alloys, one deposited by PVD and one by CVD, were already tested for corrosion mitigation of steam turbine blades in The Geysers area (California, USA) by Borenstein.[104] In the work, the coatings, deposited over three different steel grades were tested in a modified salt spray test, an erosion wear test, and a field test. No results were reported.

Titanium coatings deposited by electric arc spray onto carbon steel substrates with a NiAl bondcoat, were among the coatings tested by Ragnarsdottir et al.[141] for erosion-corrosion mitigation in geothermal steam turbines. In-situ exposure tests in a custom-built rig at the Hellisheidi (Reykjavik, Iceland) geothermal power plant revealed a generally good erosion resistance of the Ti coatings. However, large cracks were observed in the coatings, although according to the authors, these developed during the specimen preparation for microstructural examination.

Pure Ti coatings deposited onto both carbon and stainless steel (UNS S17400), were also examined by Haralsdottir et al.[182] for erosion-corrosion mitigation of steam turbine components. The coatings were deposited by electric arc spray, with a bondcoat layer of NiAl and tested for 2 months in situ via a custom-built rig connected to one of the wellheads of the Hellisheiði geothermal power plant (Reykjavik, Iceland). Wrought carbon steel and stainless-steel specimens were also tested alongside the coated coupons. After the tests, visual inspection of the coupons' exposed surface was performed by polarized light microscopy and optical profilometry, while metallographic examination was performed by means of SEM-EDX. Results revealed different scaling levels on the two coated specimens, although this was likely due to asymmetries in the geothermal steam flow within the testing rig. However, no thickness reduction was measured in any of the coatings, a promising indicator of good erosion-corrosion performance. Analysis of the coating cross-section revealed a porous microstructure typical of thermally sprayed coatings infiltrated with silica scale products down to the bondcoat layer, indicating permeation of the geothermal steam. Oxygen and Nitrogen elements were also measured in the coating, suggesting the formation of Ti-oxide and Ti-nitrate compounds, possibly during the coating process.

More recently TiB_2-Ni_3B nanocomposite coatings were deposited by DC magnetron sputtering PVD method onto stainless-steel type 304 (UNS S30400) for corrosion-erosion protection of geothermal steam turbine components.[183] The target material for the PVD deposition was prepared by mechanical alloying followed by hot pressing. In the work, corrosion rate was quantified by linear polarization resistance method by using an electrolyte containing 0.28 M and 0.01 M of NaCl and Na_2SO_4 respectively, at 25 and 80 °C for 24 h. Additional characterization involved microstructural and phase examination, surface morphology, hardness, and wear testing. Results revealed very low corrosion rates of 0.0008 and 0.001 mm $year^{-1}$ at 25 and 80 °C respectively, which stayed constant throughout the testing time with no apparent coating degradation (**Figure 41**).

Moreover, a hardness of 537.4HV was measured on the coating, lower than typical hardness values for only TiB_2 (≈1000 HV) due to the presence of the Ni_3B phase but higher than the uncoated steel substrate (256HV). A similar trend as observed in wear resistance, with a wear coefficient for the coating of 2.552×10^{-10} m^2 N^{-1}, compared to 1×10^{-14} m^2 N^{-1} for a nitride hard coating and 3.47×10^{-3} m^2 N^{-1} for the uncoated steel substrate.

Tungsten and Tantalum: An innovative approach to WSi and TaSi alloy coating design was proposed by Tryggvason et al.[184] In the study, a combinatorial DC magnetron sputtering PVD method was used to deposit graded compositions of WSi

© 2023 The Authors. Advanced Materials Technologies published by Wiley-VCH GmbH

(4–60at.% W) and TaSi (12–80at.% Ta) coatings over both single crystal silicon Si(100) and stainless-steel type 304 (UNS S30400). The amorphous/crystalline nature of the as-deposited coatings was evaluated, together with microstructural examination and compositional analyses. Graded coatings deposited onto steel substrates were exposed for 30 days to geothermal steam in the Reykjanes geothermal power plant (6600 ppm CO_2, 220 ppm H_2S, 66 ppm N_2, 1.9 ppm H_2, 0.9 ppm CH_4, 200 °C, 17 bar) and their corrosion performance evaluated by microstructural examination of the exposed surface. Results revealed the amorphous nature of the coatings, which was retained in a wide compositional range up to approximately 500 and 800 °C annealing temperature for WSi and TaSi respectively. Results from the exposure tests revealed very poor performance for the WSi coating, with no remanence of the amorphous metallic phase. Conversely, TaSi coatings remained largely unaffected by the exposure, therefore showing great potential for application in geothermal environment.

Zinc: Zn, Zn-alloy, or $Zn_3(PO_4)_2$ (zinc phosphate) coatings are often used in paint systems as an intermediate layer as a primer pigment (see for instance[106] or[111]). To the authors' knowledge, the only studies looking into the utilization of zinc phosphate coatings for direct mitigation of geothermal water can be found in works of Xu et al.[185] and Sun et al.[186]

In the work of Xu et al.[185] corrosion mitigation of carbon steel by using modified zinc phosphate coatings, using hydroxylamine sulfate (HAS) as main accelerator, with and without sol-gel SiO_2 topcoat, is evaluated in hot-dry-rock geothermal water. Specimens were analyzed by microstructural examination and phase analysis (in the as-deposited condition) and electrochemical methods for corrosion analysis (i.e., potentiodynamic polarization and electrochemical impedance spectroscopy) in temperatures up to 150°. Different electrolytes were employed for the electrochemical and immersion experiments, from 3.5wt.%NaCl solution to simulated hot-dry-rock geothermal water containing different amounts of total dissolved solids (TDS) up to a maximum of 11,300. Results demonstrated a significant improvement in corrosion resistance for the new coatings compared to both traditional zinc phosphate coatings (using harmful chemicals as reagents) and ultrasonically assisted industrial coatings. The beneficial effect was also observed to improve after application of the sol-gel SiO_2 topcoat. Effectively, the authors could conclude that the newly developed coatings could provide an effective corrosion protection in geothermal water at 150° for 336 h, albeit also suggesting some further improvements in the toxicity of the phosphating solution and reducing small cracks identified in the SiO_2-sealed coatings. Similar positive results were obtained in an earlier work on deposition parameters optimization for ultrasonically assisted zinc phosphate coatings (although with no sol-gel SiO_2 topcoat) by the same group.[186,187]

Plated Zn was also tested, applied onto carbon steel, for calcium carbonate scaling mitigation together with other plated systems (Ni, Ni-P, Ni-W-P, and Cu) and bare metallic and non-metallic surfaces (PVC, carbon steel, Type 316 stainless steel, and Cu) by Hashimoto et al.[147] Results from the scaling tests revealed that the Zn-coated specimen could provide advantages in terms of scale mitigation compared to any of the tested bare surfaces, although the best performance was measured in the Ni-P and Ni-W-P plated coupons.

4. Conclusions

In this review paper, a comprehensive list of 103 works performed on paints and coatings for geothermal applications is reported, with studies identified in the period 1975–2021. Due to the chemical/architectural complexity of identified systems, the subdivision between paints and coatings was made, where the former refers to polymeric materials and the latter to metals, ceramics, or their combination (i.e., cermets). The study was subdivided into three sections, an introductory chapter describing types of power plants, brine chemistries, and degradation mechanisms and two review chapters analyzing research work on paints and coatings respectively.

The research highlighted the following main findings:

- The specific degradation mechanism observed on a component of a geothermal power plant is a combination of corrosion, erosion, and scaling phenomena. This is dictated by three main factors: plant configuration, geothermal brine chemistry, and component. This is because the chemical and thermo-mechanical properties of a brine entering the plant are modified at each component, depending on the configuration of the plant. As summarized in Figure 5, erosion and scaling are prevalent in steam production, due to elevated steam flows and extreme variations in temperature and phase (condensation). In steam transmission, where a steady state of steam is transported without significant fluctuation in temperature, scaling phenomena are mainly replaced by corrosion phenomena. Scaling becomes again an issue then in reinjection, due to fluctuations in temperature and the sole degradation mechanism in cooling, due to the low temperature and flows of the brine in this last stage.
- Paints and coatings have very different chemical-physical and microstructural properties, which makes them suitable for different degradation mechanisms (and therefore components). *Paints* are dense layers with limited mechanical properties on their own, but that can be improved by the addition of hard phases. They find application in temperatures up to a maximum of 300 °C due to both their intrinsic low melting point (compared to coatings) and strong hydrothermal oxidation degradation, which increases with temperature. Thus, paints are mainly employed and have the most potential in applications where corrosion (at low temperature) and scaling are of concern, such as heat exchangers, pipelines, and condensers. On the other hand, coatings can withstand higher mechanical and thermal (have been tested up to 500 °C) loads than paints, but suffer from corrosion degradation, including galvanic effects if different phases are present. Moreover porosity, often present depending on the deposition method, causes brine permeation, leading to corrosion in the substrate. Porosity and other defects, such as microcracks, must be therefore reduced. They are therefore mostly studied to prevent erosion and corrosion degradation at higher temperatures such as the steam turbine, wellhead components, and downhole tools.

This review paper is intended to give a good overview and insight into the work that has been done in developing and testing coatings for the application in geothermal environment. The performance of paints and coatings researched and tested in real or

© 2023 The Authors. Advanced Materials Technologies published by Wiley-VCH GmbH

simulated geothermal environment in the last 50 years varies as much as they are many, but the results and effort have given us valuable knowledge and input for further development and research. It has also led in some cases to the real application of paints and coatings in geothermal power plants. There is a clear need for further development and research of coating systems for different geothermal energy systems with increased demand in the world for renewable energy. Further utilization of geothermal energy has opened new areas of exploration such as deep geothermal systems with harsher conditions, requiring the development of new materials and methods. Also, there is a large potential for direct utilization of geothermal energy for district heating for lower temperatures geothermal areas, which will also require corrosion and scaling prevention methods. Paints and coatings will therefore play a significant role in the production of clean geothermal energy and our sustainable future.

Supporting Information

Supporting Information is available from the Wiley Online Library or from the author.

Acknowledgements

The authors would also like to acknowledge the resources and collaborative efforts provided by the consortium of the Geo-Coat project (H2020 EU project no. 764086), Geo-Drill project (H2020 EU project no. 815319) and GEO-HEX project (H2020 EU project no. 851917).

Conflict of Interest

The authors declare no conflict of interest.

Keywords

energy generation, energy harvesting, fabrication

Received: November 30, 2022
Revised: February 17, 2023
Published online: August 15, 2023

[1] J. Shere, *Renewable: The World-Changing Power of Alternative Energy*, St Martin's Press, New York **2013**.
[2] B. Goldstein, G. Hiriart, J. Tester, L. Gutierrez-Negrin, R. Bertani, C. Bromley, E. Huenges, A. Ragnarsson, M. Mongillo, J. W. Lund, L. Rybach, V. Zui, H. Muraoka, in *Power Stations Using Locally Available Energy Sources*, Springer, New York **2012**, pp. 4190–4201.
[3] IEA, Geothermal Power, **2021**, https://www.iea.org/reports/geothermal-power.
[4] F. V. Hackstein, R. Madlener, *Geotherm. Energy* **2021**, *9*.
[5] S. K. Sanyal, *Cost of Geothermal Power and Factors that Affect It*, World Geothermal Congress, Antalya, Turkey **2005**.
[6] P. F. Ellis, M. F. Conover, *Materials Selection Guidelines for Geothermal Energy Utilisation*, Radian Corporation, Austin, Texas **1981**.
[7] P. Iberl, N. S. A. Alt, E. Schluecker, *Mater. Corros.* **2015**, *66*, 733.
[8] U.S. Energy Information Administration, *Capital Cost and Performance Characteristics Estimates for Utility Scale Electric Power Generating Tehnologies*, U.S. Department of Energy, Washington, DC **2020**.
[9] S. N. Karlsdottir, in *Comprehensive Renewable Energy*, Elsevier, **2012**, pp. 241–259.
[10] J. Nogara, J. Zarrouk, *Renewable Sustainable Energy Rev.* **2018**, *82*, 1333.
[11] J. Nogara, S. J. Zarrouk, *Renewable Sustainable Energy Rev.* **2018**, *82*, 1347.
[12] N. Mundhenk, P. Huttenloch, B. Sanjuan, T. Kohl, H. Steger, R. Zorn, *Corros. Sci.* **2013**, *70*, 17.
[13] R. S. Atlason, G. V. Odsson, R. Unnthorsson, *Energies* **2014**, *7*, 4169.
[14] T. Sugama, *High-Performance Coating Materials (BNL-77900-2007-IR)*, Brookhaven National Laboratory, Upton, New York **2006**.
[15] M. A. Hoque, M. A. H. Chowdhury, A. K. M. Asaduzzaman, F. Fanicchia, M. A. Rahman, F. Chowdhury, *Study of Levelised Cost of Energy (LCOE) for Innovative Coating Materials for Geothermal Plant Components*, World Geothermal Congress, Reykjavik, Iceland **2021**.
[16] R. R. Reeber, *Thin Solid Films* **1980**, *72*, 33.
[17] E. Gunnlaugsson, H. Armannsson, S. Thorhallsson, B. Steingrimsson, *Short Course VI on Utilisation of Low- and Medium-Enthalpy Geothermal Resources and Financial Aspects of Utilisation*, Santa Tecla, El Salvador **2014**.
[18] G. Allegrini, G. Benvenuti, *Geothermics* **1970**, *2*, 865.
[19] S. Thorhallsson, *Short Course on Geothermal Development and Geothermal Wells*, Santa Tecla, El Salvador **2012**.
[20] N. Sanada, Y. Kurata, H. Nanjo, H.-S. Kim, J. Ikeuchi, K. A. Lichti, *IEA Deep Geothermal Resources Subtask C: Materials, Progress with a Database for Materials Performance in Deep and Acidic Geothermal Wells*, World Geothermal Congress, Kyushu, Japan **2000**.
[21] N. Sanada, Y. Kurata, K. A. Lichti, *Valuation and Development of Deep Geothermal Resources-Materials Subtask Update of IEA Research Collaboration Program*, Geothermal Resources Council, California **1997**.
[22] R. DiPippo, *GHC Bullettin*, **1999**, pp. 1–8.
[23] P. Valdimarsson, *Short Course on Geothermal Drilling, Resource Development and Power Plants*, Santa Tecla, El Salvador **2011**.
[24] R. DiPippo, *Geothermal Power Plants (4th Ed.). Principles, Applications, Case Studies and Environmental Impact*, Elsevier, Oxford, UK **2015**.
[25] R. DiPippo, in *Standard Handbook of Powerplant Engineering*, 2nd ed., McGraw-Hill, New York **1998**, pp. 827–860.
[26] R. DiPippo, *Fourth Annual Geothermal Conference and Workshop*, Palo Alto, CA **1987**.
[27] J. Jimenez Gibson, *Ninth Annual Geothermal Conference and Workshop*, Palo Alto, CA **1987**.
[28] H. E. Khalifa, R. DiPippo, J. K., *13th Intersociety Energy Conversion Engineering Conference*, **1978**.
[29] *Deliverable D1.1 – State of the Art of Material Selection for Geothermal Applications*, TWI Ltd, Cambridge, UK **2018**.
[30] E. T. Eliasson, S. Thorhallsson, B. Steingrimsson, *Short Course on Geothermal Drilling, Resource Development and Power Plants*, Santa Tecla, El Salvador **2011**.
[31] J. R. Scully, in *Corrosion Testing and Evaluation: Silver Anniversary Volume*, ASTM International, West Conshohocken, PA **1990**, pp. 351–378.
[32] *Deliverable D1.2: FMEA Worksheet to Prioritize Corrosion, Erosion and Scaling Impact on Geothermal Components*, Gerosion, Reykjavik, Iceland **2018**.
[33] L. S. Van Delinder, *Corrosion Basics. An Introduction*, NACE, Houston **1984**.
[34] J. C. Scully, *The Fundamentals of Corrosion*, 2nd ed., Pergamon Press, New York **1975**.
[35] D. Jones, *Principles and Prevention of Corrosion*, MacMillan Publishing Company, New York **1991**.
[36] W. Faes, S. Lecompte, J. Van Bael, R. Salenbien, R. Bassler, I. Bellemans, P. Cools, N. De Geyter, R. Morent, K. Verbeken, M. De Paepe, *Geothermics* **2019**, *82*, 182.

© 2023 The Authors. Advanced Materials Technologies published by Wiley-VCH GmbH

[37] A. Stoljarova, S. Regenspurg, R. Bassler, T. Mathiesen, J. Brauner Nielsen, *Geothermics* **2021**, *91*, 102024.
[38] M. Madirisha, R. Hack, F. Van der Meer, *Energy Rep.* **2022**, *8*, 2964.
[39] U. Citernesi, G. Benvenuti, G. C. Ferrara, *Geothermics* **1985**, *14*, 315.
[40] T. Sugama, B. Sullivan, *J. Mater. Sci. Lett.* **2001**, *20*, 1737.
[41] T. Sugama, *Mater. Lett.* **2001**, *50*, 66.
[42] T. Sugama, *Mater. Lett.* **2000**, *43*, 185.
[43] W. F. Bogaerts, I. Winstons, *Geothermal Corrosion: High-temperature Pitting of Stainless steels and Ni-alloys*, NACE Corrosion, New Orleans, Louisiana, USA **2017**.
[44] R. Thomas, *Geothermics* **2003**, *32*, 679.
[45] A. Keserovic, R. Bassler, *Geothermics* **2015**, *53*, 479.
[46] F. Brownlie, T. Hodgkiess, A. Pearson, A. M. Galloway, *Wear* **2021**, *477*, 203821.
[47] M. Wolf, R. Afanasiev, T. Bollinghaus, A. Pfennig, *Energy Procedia* **2017**, *114*, 5337.
[48] A. Pfennig, R. Wiegand, M. Wolf, C.-P. Bork, *Corros. Sci.* **2013**, *68*, 134.
[49] W. Qi, Q. Gao, Y. Zhao, T. Zhang, F. Wang, *Corros. Sci.* **2021**, *190*, 109699.
[50] M. F. Hurley, C. R. Olson, L. J. Ward, B. J. Jaques, K. A. Johnson, J. K. Gunnerson, D. P. Butt, *Eng. Failure Anal.* **2013**, *33*, 336.
[51] K. A. Lichti, D. M. Firth, A. D. Karstensen, *Hydrogen Induced Cracking of Low Strength Steels in Geothermal Fluids*, World Geothermal Congress, Antalya, Turkey **2005**.
[52] S. N. Karlsdottir, I. O. Thorbjornsson, *Embrittlement And Corrosion In High Temperature Geothermal Well*, NACE Corrosion, Salt Lake City, Utah, USA **2012**.
[53] M. Liu, Z. Ni, C. Du, Z. Liu, M. Sun, M. Fan, Q. Wang, X. Yang, X. Li, *Eng. Failure Anal.* **2021**, *129*, 105694.
[54] D. Van der Heuvel, E. Gunnlaugsson, I. Gunnarsson, T. M. Stawski, C. L. Peacock, L. G. Benning, *Geothermics* **2018**, *76*, 231.
[55] D. L. Gallup, *Geothermics* **1989**, *18*, 97.
[56] R. De Paula Cosmo, F. De Assis Ressel Pereira, E. J. Soares, E. Guasti Ferreira, *Geothermics* **2022**, *98*, 102272.
[57] A. Criaud, C. Fouillac, *Geothermics* **1989**, *18*, 73.
[58] H. L. J. Grant, M. D. Hannington, V. Hardardottir, S. H. Fuchs, D. Schumann, *Ore Geol. Rev.* **2020**, *116*, 103145.
[59] D. Kristanto, L. P. Kusumo, D. Abdassah, *Corrosion Managament Technology for Achieving Best Practice Application on Geothermal Industry*, World Geothermal Congress, Antalya, Turkey **2005**.
[60] IUPAC, *Pure Appl. Chem.* **2012**, *84*, 2167.
[61] G. Batis, N. Kouloumbi, K. Kotsakou, *Geothermics* **1997**, *26*, 65.
[62] M. L. Allan, C. C. Berndt, D. Otterson, *Geothermal Resources Council Meeting*, Davis, California **1998**.
[63] L. E. Lorensen, C. M. Walkup, E. T. Mones, *Present Status of The Polymeric Materials Screening Program for the LLL Geothermal Project – UCRL-51843*, Lawrence Livermore Laboratory, Livermore, California **1975**.
[64] T. Sugama, *Hydrothermally Self-Advancing Hybrid Coatings for Mitigating Corrosion of Carbon Steel (BNL-77335-2006)*, Brookhaven National Laboratory, Upton, NY **2006**.
[65] K. Belas-Dacillo, A. C. De Leon, A. C. R. Panopio, R. C. Advincula, *Evaluating Protective Coatings and Metal Alloys in Acidic Geothermal Fluids Using Laboratory Techniques*, World Geothermal Congress, Melbourne, Australia **2015**.
[66] G. Aristia, C. Roth, R. Bassler, *Polyaniline/Silicon Dioxide Containing Coating for Use in Artificial Geothermal Brines*, NACE Corrosion, Pheonix, Arizona, USA **2018**.
[67] G. Aristia, L. Q. Hoa, C. Roth, R. Bassler, *The Effect of Different Polyaniline Types in Silicon Dioxide Containing Coatings for Carbon Steel Protection in Artificial Geothermal Brines*, NACE Corrosion, Nashville, Texas, USA **2019**.
[68] G. Aristia, L. Q. Hoa, R. Baessler, *Mater. Sci. Forum* **2019**, *966*, 107.
[69] G. Aristia, L. Q. Hoa, R. Bäßler, *Study of Polyaniline/Silicon Dioxide Based Coating on Carbon Steel in Artificial Geothermal Brine*, World Geothermal Congress, Reykjavik, Iceland **2021**.
[70] A. Kaufman, *Geothermal Power: An Economic Evaluation, United States Departmentof the Interior*, Bureau of Mines, Washington, USA **1964**.
[71] B. J. Merten, *Corrosion Protection of Steel Structures by Coal Tar Enamel: 80 Years of Performance, ST-2017-1546-01*, U.S. Department of the Interior, Bureau of Reclamation, Denver, CO, USA **2017**.
[72] G. Cadelano, A. Bortolin, G. Ferrarini, P. Bison, G. Della Santa, E. Di Sipio, A. Bernardi, A. Galgaro, *Energies* **2021**, *14*.
[73] A. L. Austin, G. H. Higgins, J. H. Howard, *The Total Flow Concept for Recovery of Energy from Geothermal Hot Brine Deposits – UCRL-51366*, Lawrence Livermore Laboratory, Livermore, California **1973**.
[74] W. O. Jacobson, P. M. Henry, A. N. Rogers, F. Schoeflin, *J. Test Eval.* **1981**, *9*, 82.
[75] L. Bai, X. Meng, *12th New Zealand Geothermal Workshop*, Auckland **1990**.
[76] J. Suzuki, *Corrosion-Resistant Coatings Technology*, Marcel Decker, New York **1989**.
[77] G. Batis, N. Kouloumbi, E. Soulis, *Anti-Corros. Methods Mater.* **1998**, *45*, 222.
[78] H. A. Videla, *Manual of Biocorrosion*, Lewis Publishers, Boca Raton **1996**.
[79] A. Grandclerc, P. Dangla, M. Gueben-Minerbe, T. Chaussadent, *Cem. Concr. Res.* **2018**, *105*, 126.
[80] M. L. Berndt, *Constr. Build. Mater.* **2011**, *25*, 3893.
[81] M. L. Berndt, *Protection of Concrete in Cooling Towers from Microbiologically Influenced Corrosion*, Geothermal Reseources Council, Davis, California **2001**.
[82] S. Knudsen, *Conformal Coatings for 225 °C Applications*, Geothermal Resource Council, Reno, Nevada **2005**.
[83] G. G. Wang, L. Q. Zhu, H. C. Liu, W. P. Li, *Surf. Coat. Technol.* **2012**, *206*, 3728.
[84] A. Boersma, F. Vercauteren, H. Fisher, F. Pizzocolo, *43rd Workshop on Geothermal Reservoir Engineering*, Stanford, California **2018**.
[85] J. Scheiber, G. Ravier, O. Sontot, H. Christina, A. Genter, *Thirty-Eighth Workshop on Geothermal Reservoir Engineering*, Stanford, California **2013**.
[86] R. Losada, S. Holberg, L. Freire, J. Van Bael, *Heat Exchanger Fouling and Cleaning XIII*, Warsaw, Poland **2019**.
[87] L. Freire, J. Sanchez, A. Fernandez, R. Castro, R. Losada, S. Holberg, J. Van Bael, *Performance of Coatings Developed for Protecting Steel Pipes in Geothermal Power Plants: In-Situ Corrosion Monitoring by EIS-Based Sensor*, Eurocorr, Seville, Spain **2019**.
[88] R. Losada, S. Holberg, J. M. D. Bennedsen, K. Kamuk, F. Nielsen, *J. Coat. Technol. Res.* **2016**, *13*, 645.
[89] S. Bratt, M. Shirmohamadi, *Protecting Blade-Fit Areas of Geothermal Turbine Rotors Against Stress Corrosion Cracking Using an Isolation Coating (Sealant)*, Geothermal Resources Council, Davis, California **2000**.
[90] T. Sugama, K. Gawlik, *Prog. Org. Coat.* **2001**, *42*, 202.
[91] K. Gawlik, S. Kelley, T. Sugama, R. Webster, W. Reams, *Geothermal Resources Council Transactions*, **1999**.
[92] K. Gawlik, S. Kelley, *Development and Field Testing of Polymer Based Heat Exchanger Coatings*, World Geothermal Congress, Kyushu-Tohoku, Japan **2000**.
[93] A. Covelo, C. Menchaca, M. Flores, P. Rodrigues-Rojas, M. Hennandez-Gallegos, E. Martinez Mesa, R. Jaimes-Ramirez, J. Uruchurtu, in *New Technologies in Protective Coatings*, IntechOpen, London, UK **2017**, pp. 87–98.
[94] F. Zhang, H. Begg, N. . I. S. Kale, K. Franklin, K. Mallin, V. Wittig, S. Hahn, B. Alonso Rodriguez, F. Chowdhury, M. A. Hoque, S. N. Karlsdottir, G. Oppong Boakye, P. Kjellgren, P. Obene, K. F.

© 2023 The Authors. Advanced Materials Technologies published by Wiley-VCH GmbH

Alexandersson, S. O. Wallevik, *Geo-Drill: Development of Novel and Cost-Effective Drilling Technology for Geothermal Systems*, World Geothermal Congress, Reykjavik, Iceland **2021**.
[95] E. O. Straume, G. O. Boakye, B. A. Rodriguez, S. N. Karlsdottir, *High Temperature Testing of Materials and Corrosion Resistant Coatings for Geothermal Drilling Applications*, World Geothermal Congress, Reykjavik, Iceland **2021**.
[96] T. Sugama, S. S. Kelley, K. Gawlik, *J. Coat. Technol.* **2001**, *73*, 65.
[97] J. C. Espartero, A. C. De Leon, R. C. Advincula, *Nace International Corrosion 2019*, Nashville, Tennessee, USA **2019**.
[98] E. Caldona, A. de Leon, J. Mangadlao, K. Lim, B. Pajarito, R. Advincula, *React. Funct. Polym.* **2018**, *123*, 10.
[99] E. Caldona, A. de Leon, B. Pajarito, R. Advincula, *Appl. Surf. Sci.* **2017**, *422*, 162.
[100] E. Caldona, A. de Leon, P. Thomas, D. Naylor III, B. Pajarito, R. Advincula, *Ind. Eng. Chem. Res* **2017**, *56*, 1485.
[101] T. Sugama, *Mater. Lett.* **2004**, *58*, 1307.
[102] T. Sugama, *Polyethersulfone Coating for Mitigating Corrosion of Steel in Geothermal Environment (BNL-75362-2006-IR)*, Brookhaven National Laboratory, Upton, New York **2005**.
[103] T. Reinsch, J. Henninges, *20th International Conference on Optical Fibre Sensors*, Edinburgh, UK **2009**.
[104] S. W. Borenstein, *Protective Coatings to Reduce Corrosion Problems of Turbine Rotors*, Geothermal Resources Council, Davis, California, USA **1989**.
[105] R. K. Conrad, J. P. Carter, S. D. Cramer, *Report of Investigation 8792 – Corrosion of Selected Metals and a High-Temperature Thermoplastic in Hypersaline Geothermal Brine*, United States Department of the Interior, Avondale, MD **1983**.
[106] K. Gawlik, T. Sugama, R. Webster, W. Reams, *Field Testing of Heat Exchanger Tube Coatings*, Geothermal Resources Council, San Diego, California, USA **1998**.
[107] T. Sugama, N. R. Carciello, *J. Appl. Polym. Sci.* **1992**, *45*, 1291.
[108] K. Gawlik, T. Sugama, P. Hirtz, *Field Testing and Analysis of Polyphenylenesulphide (PPS) Composite Coatings Exposed to High Temperature, PH-Modified Brine*, Geothermal Resources Council, Reno, Nevada **2005**.
[109] T. Sugama, R. Webster, W. Reams, K. Gawlik, *J. Mater. Sci.* **2000**, *35*, 2145.
[110] T. Sugama, K. Gawlik, *Mater. Lett.* **2002**, *57*, 666.
[111] T. Sugama, D. Elling, K. Gawlik, *J. Mater. Sci.* **2002**, *37*, 4871.
[112] T. Sugama, P. Hayenge, *Polym. Polym. Compos.* **2000**, *8*, 307.
[113] T. Sugama, K. Gawlik, *Polym. Polym. Compos.* **2004**, *12*, 153.
[114] T. Sugama, *Nanoscale Bohemite Filler for Corrosion and Wear-resistant Polyphenylenesulfide Coatings (BNL-71395-2003-IR)*, Brookhaven National Laboratory, Upton, New York **2003**.
[115] T. Sugama, K. Gawlik, *Mater. Lett.* **2003**, *57*, 4282.
[116] T. Sugama, *Mater. Lett.* **2006**, *60*, 2700.
[117] T. Sugama, T. Butcher, L. Ecker, in *Materials Challenges in Alternative and Renewable Energy*, The American Ceramic Society, **2010**, pp. 389–401.
[118] T. Sugama, K. Gawlik, *Polym. Polym. Compos.* **2001**, *9*, 377.
[119] T. Sugama, K. Gawlik, *Geothermal Resource Council (GRC) Annual Meeting*, San Diego, California **2001**.
[120] T. Sugama, P. Hirtz, K. Gawlik, *High Temperature Field Testing of Polyphenylenesulphide Composite Coatings*, Geothermal Resources Council, Indian Wells, California, USA **2004**.
[121] E. Yang, T. Hwang, A. Kumar, K. Kim, *Adv. Polym. Technol.* **2016**, *37*, 843.
[122] K. Gawlik, T. Sugama, D. Jung, *Geothermal Resources Council Annual Meeeting*, Reno, Nevada, USA **2002**.
[123] T. Sugama, R. Sabatini, K. Gawlik, *Self-assembly Ce oxide/Organopolysiloxane Composite Coatings (BNL-73602-2005-IR)*, Brookhaven National Laboratory, Upton, New York **2005**.
[124] T. Sugama, K. Gawlik, B. Sullivan, *Field Testing and Analysis of Air-Cooled Condenser Components Coated with Cerium Oxide-Doped PAAMPS Polymer Nanocomposite Material*, Geothermal Resources Council, San Diego, California **2006**.
[125] Y. Xu, M. Liu, *Geothermics* **2017**, *70*, 339.
[126] L. Tang, A. Iddya, X. Zhu, A. V. Dudchenko, W. Duan, C. Turchi, J. Vanneste, T. Y. Cath, D. Jassby, *ACS Appl. Mater. Interfaces* **2017**, *9*, 38594.
[127] G. Topcu, A. Celik, A. Kandemir, A. Baba, H. Sahin, M. M. Demir, *Geothermics* **2019**, *77*, 106.
[128] S. Vemuri, K. J. Kim, T. W. Bell, *The Longevity of Self Assembled Monolayer Coatings for Enhanced Steam Condensation and Their Applications in Geothermal Power Plants*, Geothermal Resource Council, San Diego, California, USA **2006**.
[129] K. Shimizu, E. Suzuki, Y. Mitobe, H. Hirahara, H. Nakazawa, T. Saito, K. Oyama, R. Hirata, *Prevention of Scale Adhesion Using Surface Treatment of Coating with Organic Compound at Geothermal Power Station*, World Geothermal Congress, Kyushu-Tohoku, Japan **2000**.
[130] K. Mori, Y. Sasaki, S. Sai, S. Kaneda, H. Hirahara, Y. Oishi, *Langmuir* **1995**, *11*, 1431.
[131] J. J. Fontana, W. Reams, H. C. Cheng, *5th International Congress on Polymers in Concrete*, Brighton, United Kingdom **1987**.
[132] T. Sugama, *Geothermics* **1998**, *27*, 387.
[133] K. A. Lichti, L. Wallis, M. Ko, J. Kennedy, *Kinetics of Galvanic Corrosion of Carbon Steel to Arsenic and Antimony Couples*, World Geothermal Congress, Melbourne, Australia **2015**.
[134] K. Lichti, M. Ko, J. Kennedy, *Heavy Metal Galvanic Corrosion of Carbon Steel in Geothermal Brines*, NACE Corrosion, Vancouver, British Columbia, Canada **2016**.
[135] A. A. Ogwu, T. Hellwig, *Int. J. Electrochem. Sci.* **2014**, *9*, 8299.
[136] G. G. Wang, L. Q. Zhu, H. C. Liu, W. P. Li, *Langmuir* **2011**, *27*, 12275.
[137] K. King, J. Henfling, *Evaluation of Thermal Spray Coatings and Shape Memory Alloys as Pressure Seals for Downhole Tools*, Geothermal Resources Council, Las Vegas, Nevada, USA **2013**.
[138] A. Buzaianu, P. Motoiu, I. Csaki, G. Popescu, K. Ragnarsdottir, S. Guðlaugsson, D. Guðmundsson, A. Arnbjornsson, *Geothermics* **2015**, *57*, 1.
[139] A. Buzaianu, R. Trusca, P. Motoiu, I. Csaki, A. Ioncea, V. Motoiu, *IOP Conf. Ser.: Mater. Sci. Eng.* **2019**, *572*, 012044.
[140] T. Sugama, *Mater. Lett.* **1999**, *38*, 227.
[141] K. R. Ragnarsdottir, S. N. Karlsdottir, K. Leosson, A. Arnbjornsson, S. Guðlaugsson, H. O. Haraldsdottir, A. Buzaianu, I. Csaki, G. Popescu, *Corrosion Testing of Coating Materials for Geothermal Turbine Application*, NACE Corrosion, New Orleans, Louisiana, USA **2017**.
[142] S. Houdkova, M. Vostrak, K. Lencova, P. Sulkova, J. Duliskovic, *Resistance of Thermally Sprayed Coatings in an Environment Simulating a Turbine of Geothermal Power Plant*, Metal, Brno, Czech Republic **2021**.
[143] F. Fanicchia, N. Kale, S. Paul, R. Khan, S. Irukuvarghula, E. Davison, J. Barras, C. Leahy, H. Begg, D. Watson, A. Pearson, F. Brownlie, T. Hodgkiess, S. Gudlaugsson, S. N. Karlsdottir, G. B. Oppong, D. Kovalov, I. Csaki, L. E. Geambazu, *Development of Novel and Cost Effective Corrosion and Erosion Resistant Coatings for High*, World Geothermal Congress, Reykjavik, Iceland **2021**.
[144] G. O. Boakye, D. Kovalov, A. I. Thorhallsson, S. N. Karlsdottir, V. Motoiu, *Friction and Wear Behaviour of Surface Coatings for Geothermal Applications*, World Geothermal Congress, Reykjavik, Iceland **2021**.
[145] H. J. Wiesner, W. J. Comfort, W. P. Frey, C. Gardiner, W. Kelley, *Electroless-Nickel Plating of a Large Turbine Rotor for the Geothermal Program – UCID-17253*, Lawrence Livermore Laboratory **1976**.
[146] K. A. Moore, R. E. Mizia, R. A. Zatorski, *Geothermal Resources Council: 2002 Annual Meeting*, Reno, NV, USA **2002**.

© 2023 The Authors. Advanced Materials Technologies published by Wiley-VCH GmbH

[147] R. Hashimoto, M. Morita, O. Umezawa, S. Motoda, *J. Japan Inst. Met. Mater.* **2017**, *81*, 89.
[148] W. Jacobsen, R. Vanegas, J. D'Urso, A. Soufiane, D. Payne, D. Dutoit, G. Cedilinik, F. Zaidi, *Geothermal Reseources Council Meeting*, Salt Lake City, Utah, USA **2017**.
[149] I. Csaki, S. N. Karlsdottir, C. A. Manea, R. Stefanoiu, R. Trusca, V. Geanta, *Microstructural Study of the Corrosion Effect on AlCrFeNiMn Multicomponent Alloy Tested in Geothermal Environment*, NACE Corrosion, New Orleans, Louisiana, USA **2017**.
[150] I. Csaki, R. Stefanoiu, S. N. Karlsdottir, L. E. Geambazu, *Corrosion Behavior in Geothermal Steam of CoCrFeNiMo High Entropy Alloy*, NACE Corrosion, Phoenix, Arizona, USA **2018**.
[151] S. N. Karlsdottir, L. E. Geambazu, I. Csaki, A. I. Thorhallsson, R. Stefanoiu, F. Magnus, C. Cotrut, *Coatings* **2019**, *9*.
[152] A. I. Thorhallsson, I. Csaki, L. E. Geambazu, F. Magnus, S. N. Karlsdottir, *Corros. Sci.* **2021**, *178*.
[153] F. Fanicchia, I. Csaki, L. E. Geambazu, H. Begg, S. Paul, *Coatings* **2019**, *9*.
[154] F. Brownlie, T. Hodgkiess, F. Fanicchia, *Surf. Coat. Technol.* **2021**, *423*, 127634.
[155] A. I. Thorhallsson, F. Fanicchia, E. Davison, S. Paul, S. Davidsdottir, D. I. Olafsson, *Materials* **2021**, 14.
[156] K. R. Ragnarsdottir, A. Arnbjornsson, S. N. Karlsdottir, H. O. Haraldsdottir, *Preliminary Corrosion Testing of Explosive Clad Materials in Geothermal Environment*, NACE Corrosion, Phoenix, Arizona, USA **2018**.
[157] B. Amend, J. Yee, *Selective Application of Corrosion Resistant Alloys Mitigates Corrosion in pH-Modified Geothermal Fuids*, NACE Corrosion, Orlando, Florida, USA **2013**.
[158] E. Medvedovski, *Adv. Appl. Ceram.* **2020**, *119*, 462.
[159] E. Medvedovski, *Protective Iron Boride Coatings against Corrosion in Geothermal Wells*, World Geothermal Congress, Reykjavik, Iceland **2021**.
[160] G. Salvago, G. Fumagalli, A. Cigada, P. Scolari, *Corros. Sci.* **1987**, *27*, 1205.
[161] G. Salvago, G. Fumagalli, *Considerations on the Corrosion Resistance of Metallic Materials Coated with Electroless Nickel*, **1988**, pp. 20–28.
[162] M. Morita, A. Yamaguchi, S. Motoda, *Effect of Phosphate Ion Eluted from Ni-P Coated Steel on $CaCO_3$ Scale*, Vol. *53*, **2018**, pp. 368–373.
[163] G. O. Boakye, A. M. Ormsdottir, B. G. Gunnarsson, S. Irukuvarghula, R. Khan, S. N. Karlsdottir, *Coatings* **2021**, *11*.
[164] S. Daviðsdottir, K. R. Ragnarsdottir, S. Irukuvarghula, S. Guðlaugsson, D. I. Olafsson, R. Khan, A. I. Thorhallsson, *NACE Corrosion 2021, Virtual Conference*, **2021**.
[165] M. L. Berndt, D. M. Otterson, *Cyclic Polarization Studies on Clad and Thermal Sprayed Ni-Base Alloys In Synthetic Geothermal Brine*, Geothermal Resources Council Transactions, Davis, California, USA **2000**.
[166] I. Csaki, K. R. Ragnarsdottir, A. Buzaianu, K. Leosson, V. Motoiu, S. Guðlaugsson, M. V. Lungu, H. O. Haraldsdottir, S. N. Karlsdottir, *Surf. Coat. Technol.* **2018**, *350*, 531.
[167] G. Aristia, L. Q. Hoa, M. Nofz, R. Sojref, R. Bassler, *Coatings* **2021**, *11*.
[168] N. Chen, M. Liu, W. Zhou, *Ind. Eng. Chem. Res.* **2012**, *51*, 6001.
[169] C. Ning, L. Mingyan, Z. Weidong, *Ind. Eng. Chem. Res.* **2012**, *51*, 6001.
[170] S. Silviana, G. J. Sanyoto, A. Darmawan, *J. Teknol. Lab.* **2020**, *83*, 41.
[171] J. Song, M. Liu, X. Sun, J. Wang, J. Zhu, *Appl. Therm. Eng.* **2018**, *132*, 740.
[172] Y. Lv, M. Liu, Y. Xu, *Prot. Met. Phys. Chem. Surf.* **2018**, *54*, 526.
[173] T. Sugama, *J. Sol-Gel Sci. Technol.* **1998**, *12*, 35.
[174] Y. Cai, X. Quan, G. Li, N. Gao, *Ind. Eng. Chem. Res.* **2016**, *55*, 11480.
[175] L. E. Kukacka, J. Fontana, T. Sugama, W. Horn, *Alternate Materials of Constructions for Geothermal Applications – BNL50699*, Brookhaven National Laboratory, Upton, New York, USA **1977**.
[176] L. E. Kukacka, *Geothermal Materials Symposium*, Austin, Texas, USA **1978**.
[177] C. G. Bliem, Mines Miller, L. G., *Results of Field Investigations Conducted with The Polymer-Concrete Lined Heat Exchanger Tubes*, Idaho National Engineering Laboratory, **1993**.
[178] V. Hassani, E. Hoo, *Results of Field Testing on Heat Exchanger Tubes with Polymer Concrete Lining*, National Renewable Energy Laboratory, **1995**.
[179] R. P. Webster, L. E. Kukacka, *Evaluation of Field-Tested Thermally Conductive Polymer Concrete-Lined Heat Exchanger Tubing*, Brookhaven National Laboratory, Upton, NY **1995**.
[180] E. Hoo, V. Hassani, *Field Testing of Thermally Conductive, Corrosion-Resistant Liners*, National Renewable Energy Laboratory (NREL), Golden, CO **1996**.
[181] T. Sugama, S. K. Gill, A. Muraca, T. Pyatina, *Corrosion-Resistant Foamed Cements for Carbon Steels in Enhanced Geothermal Systems*, Geothermal Resources Council, Las Vegas, Nevada, USA **2013**.
[182] H. O. Haralsdottir, K. R. Ragnasdottir, S. N. Karlsdottir, D. I. Olafsson, S. Gudlaugsson, *In-Situ Erosion-Corrosion Testing Equipment for Geothermal Environment and Comparative Results for Tested Electric Arc Sprayed Titanium*, NACE Corrosion, Nashville, Tennessee, USA **2019**.
[183] J. M. Hernandez, J. M. J. Garcia, H. H. Hernandez, H. J. D. Rosales, R. H Basurto, *Mater. Res. Express* **2021**, *8*.
[184] T. K. Tryggvason, A. Tryggvason, S. N. Karlsdottir, A. S. Ingason, U. B. Arnalds, F. Magnus, *Geothermics* **2020**, *88*.
[185] Y. Xu, M. Li, X. Sun, M. Liu, *Surf. Coat. Technol.* **2019**, *370*, 340.
[186] X. Sun, M. Liu, J. Song, *Fushi Kexue Yu Fanghu Jishu* **2016**, *28*, 435.
[187] X. Sun, M. Liu, J. Song, Y. Xu, *Geothermics* **2020**, *86*, 101807.

© 2023 The Authors. Advanced Materials Technologies published by Wiley-VCH GmbH



Francesco Fanicchia received his M.Sc. in Materials Science from the University of Rome Tor Vergata and Ph.D. on ceramic Thermal Barrier Coatings (TBC) design from The University of Nottingham. From 2018 to 2021 he was senior project leader at TWI Ltd (Cambridge, UK), where he technically coordinated large (>$4 m) research programs on design of novel coatings for geothermal environments. In 2022 he joined Cranfield University as Senior Lecturer in High Temperature Surface Engineering. His research interests are in sustainable surface engineering for transport (aerospace, automotive), energy production (geothermal, nuclear), and energy-intensive industries (steel, cement, ceramic manufacturing).



Sigrun N. Karlsdottir received her B.Sc. degree in Mechanical and Industrial Engineering in 2003 from the University of Iceland and her Ph.D. degree in Materials Science and Engineering from the University of Michigan in December 2007. She worked as a researcher and a project manager at Innovation Center Iceland in the Department of Materials, Energy and Biotechnology from 2008 to 2013. Dr. Karlsdottir is now a Professor in Mechanical Engineering at the University of Iceland. The focus of her research is on the performance of materials in harsh environments, scaling, and corrosion in geothermal environment, including material testing in extreme conditions such as in superheated geothermal steam in situ and in a simulated environment. Her recent involvement in projects in national and international collaboration includes corrosion studies of cladding materials and coatings for high-temperature geothermal environment.

© 2023 The Authors. Advanced Materials Technologies published by Wiley-VCH GmbH



https://dspace.org/

Research and development on coatings and paints for geothermal environments: a review

Fanicchia, Francesco; Karlsdóttir, Sigrún N.

2023-09-01
Wiley
https://doi.org/10.1002/admt.202202031
Fanicchia F, Karlsdottir SN. (2023) Research and development on coatings and paints for geothermal environments: a review. Advanced Materials Technologies, Volume 8, Issue 18, September 2023, Article number 2202031

Downloaded from a DSpace repository. https://dspace.org/